Федеральное государственное автономное образовательное учреждение
высшего образования «Южно-Уральский государственный университет»
(национальный исследовательский университет)

На правах рукописи

Ян Юйсун

Повышение эффективности работы ветроэнергетической установки путем использования комбинации интеллектуальных алгоритмов ориентации и отбора мощности

2.4.5. Энергетические системы и комплексы

ДИССЕРТАЦИЯ

на соискание учёной степени
кандидата технических наук

Научный руководитель:
д.т.н., профессор
Соломин Е. В.

Челябинск – 2023

Federal State Autonomous Educational Institution of Higher Education
«South Ural State University (National Research University) »

As a manuscript

Yang Yusong

Improving the efficiency of the wind turbine using a combination of smart yawing and power control algorithms

2.4.5. Energy Systems and Complexes

DISSERTATION

Degree of candidate of technical sciences

Scientific supervisor:
Doctor of Technical Sciences, Professor,
Evgeny V. Solomin

Chelyabinsk – 2023

Content

INTRODUCTION

Relevance of work: with the increase of human needs and the rapid growth of national economies, the use of various energy sources is also gradually increasing the lack of resources of traditional energy sources and the pollution problems caused to the ecological environment began to gradually appear. The most used energy sources in the world today are mainly coal, oil and natural gas, which we call fossil fuels. While fossil fuels were formed millions of years ago, we've only been using them for fuel for a fairly short period of time – just over 200 years, and we've consumed a huge amount of fossil fuels since. If we keep burning fossil fuels at our current rate, it is generally estimated that we will run out of available oil within the next 50 years, natural gas within the next 60 years, and there are enough coal reserves to last the next 150 years. They are primary energy sources with non-renewable characteristics, and substances. After burning, fossil fuels will release CO_2 and toxic gasses, which will not only warm the climate and affect the global environment but also cause harm to our own health. Therefore, based on protecting the environment and ourselves, it is necessary to find other renewable and non-polluting energy sources to meet the needs of our own survival and development.

In the 21 century many countries have developed and used wind energy as a sustainable development strategy. Wind energy is an abundant, clean and renewable energy source that governments around the world have highly valued. The global wind power installed capacity reached 74.653 GW in 2022; by the end of 2021, the cumulative installed capacity of global wind power had reached 898.824 GW, with a cumulative annual growth rate of 9%. Wind power's position in the power industry is growing. Integrating wind power into the grid not only reduces traditional fossil energy consumption and environmental pollution, but also takes on some of the load of conventional units, thus bringing significant economic benefits to the grid.

Since wind resources are highly stochastic, the control system of the wind turbine (WT) and the yaw mechanism itself have a certain lag. When the wind direction and speed change frequently, the windward side of the turbine blade cannot be

accurately aligned with the wind direction, and the consequent system tracking failure of the wind will affect the WT. The wind turbine's efficiency will be affected by the tracking failure of the system. Frequent changes in wind direction and speed will also cause the yaw mechanism to the frequent changes in wind direction and wind speed will also cause the yaw mechanism to operate frequently, resulting in faster mechanical losses and thus affecting the life of the yaw mechanism. In addition, the controller cannot be easily parameterised. Also, the controller cannot be easily set, and someone cannot easily monitor the operating condition of the wind turbine in real-time. Finally, the deviation of onrushing air flow by the rotating blades causes extra differential yawing error which wasn't fixed so far and continue collecting losses on megawatt-class wind turbines. This series of problems are impacting the wind power plant (WPP). The research and solution to these problems are of profound significance.

The yaw error is mainly caused by two reasons: (1) The wake impacts on downstream wind turbine performance and yaw alignment. Studies have shown yaw misalignment of up to 35° for turbines operating in the wakes of aligned upstream turbines based on field measurements. Furthermore, it was shown that the yaw misalignment was accentuated further downstream for turbines affected by multiple wakes. The probability of a turbine affected by wakes to be yaw misaligned ±25° was more than 25 % [1]. (2) Yaw error comes from the wind vane installed on the nacelle behind the rotor. Hence, the data is lagging and affected by the wake comes from rotor rotation. According to one wind farm's SCADA data, the wind turbine yaw misalignment was concentrated between −20° and 5°, and the mean error was approximately 9.57°. With a mean yaw error of 9.57°, the power loss due to yaw misalignment accounted for approximately 2.76 % of the total loss. For a 100 MW wind farm, assuming the average available time to be 6 h per day for 365 days per year, the annual loss of power due to yaw misalignment is 6.03×10^6 kWh. The annual economic loss of power due to yaw misalignment is 0.9045 million dollars per year, when calculated at a price of 0.15 dollar per kWh [2].

In order to better reduce the impact of wind uncertainty on the efficiency of wind turbines, and to capture the maximum wind energy while solving the "under-yaw" and

"over-yaw" problems, it is necessary to optimize the wind turbine yaw system (such as using more accurate measurement sensor, adjusting yaw control strategy), so that the wind turbine can be more accurate and timelier to the wind, to achieve the improvement of wind turbine efficiency and power plant efficiency.

However, because the yaw system is highly nonlinear and uncertain, it is difficult to establish an accurate mathematical model, and its working performance is poor because of the uncertainty of wind changes, and there are problems such as untimely tracking of wind direction, poor accuracy of wind alignment, and frequent action of yaw mechanism, so it will affect the effectiveness of WTs and wind farm benefits. Modern megawatt WTs adopt the yaw strategy with uniform control parameters, i.e., the parameter values of fixed allowable yaw error and yaw time delay. This yaw strategy is poorly adapted and cannot be fully applied to different wind conditions. So the existing yaw strategy needs to be improved to a more suitable yaw strategy for the local wind conditions by optimizing the yaw parameters. Using a neural network prediction model to predict future wind conditions and establish an optimized yaw strategy with predictable yaw control parameters, as well as the use of a hill climbing search algorithm to accurately track the wind direction in a small area, will cause more accurate wind alignment and more timely yaw for the WT, which will bring a great improvement to the overall comprehensive economic efficiency of the wind farm.

At present, many scholars at home and abroad are mainly interested in studying the effects of yawing wind turbines by two methods: simulation and experimental research. In simulation research, researchers mostly extract one or more factors from the natural wind conditions to investigate the performance indexes of wind turbines in this condition, and most of the related studies also focus on how to improve the power characteristics of large wind turbine units.

In the experimental research, in order to simulate the real external working environment, based on the wind tunnel incoming wind speed controlled conditions, the construction and commissioning of small wind turbine rotating platform, can simulate the incoming wind direction and the wind wheel plane angle between the continuous change over time, and then explore the wind turbine dynamic changes in the impact of

changes related to the wind turbine aerodynamic performance research, which is to reveal the wind turbine blade force mechanism and explore ways to extend the blade life. This is of great academic significance and realistic application background.

The degree of elaboration of the research topic: there has been a large amount of literature, including scientific papers and technical reports, on capturing yaw angles, reducing yaw errors, and improving the efficiency of wind power generation. First, N.Y. Zhukovsky, L. Prandtl and A. Betz created the theoretical foundations that explain the basic principles and patterns of operation of wind. The Betz limit substantiates the maximum limits for the use of wind energy by WTs, which are target values. It is these fundamental theories of wind power technology that have enabled scientists to develop different control technologies to improve the efficiency of power generation, such as pitch angle control, MPPT, yaw control, generator control. In Russian publications we should particularly highlight the work of leading scientists in wind energy: N. Y. Zhukovsky, N. V. Krasovsky, G. K. Sabinin, E. M. Fateyev, V. N. Andrianov, P. P. Bezrukikh, V. V. Elistratov, V. G. Nikolaev, E. V. Solomin, V. M. Lyatcher, V. I. Velkin, V. L. Okulov, B. V. Lukutin and others. They studied various methods of controlling WTs to improve wind energy utilization at different levels of aerodynamics, transfer efficiency, power conversion, etc. Foreign scientists H. Bindner, A. Rebsdorf, R. Hoffmann, O. Carlson, TG. Wang, Z. Chen, WZ. Shen and others, who also studied various methods of controlling WTs. In addition, Risø DTU National Laboratory for Sustainable Energy (RISØ DTU), National Renewable Energy Laboratory (NERC), Energy Research Centre of the Netherlands (ECN), the National Renewable Energy Centre (CENER) and the German Wind Energy Institute (DEWI) are among the large research institutions where different research groups exist, all of which have an in-depth study of WTs. Obviously, the reduction of yaw errors and the improvement of the efficiency of wind power generation have been the focus of relevant scientific research fields, and the solutions are of theoretical and practical importance.

The purpose and tasks of the study. Purpose - to develop an accelerated, accurate and efficient method and algorithm for determining and eliminating the yaw error, in which the yaw control principle is based on the combination of wind direction

prediction model (artificial neural network (ANN)) and wind turbine power control model (hill climbing search (HCS)).

To achieve this goal, the following tasks have been formulated:

1. Research and analysis of experimental SCADA data of operating wind turbines and wind farms in terms of wind speed and direction, rotor position (nacelle), as well as output power. (SCADA – Supervisory Control And Data Acquisition - data collection and operational management system);

2. Development of a computer simulation model of the SWT-3.6-120 WT manufactured by Siemens in the MATLAB/Simulink package based on the factory technical characteristics of the WT. Testing (verification) of the simulation model for operability and adequacy by conducting a comparative analysis of the operation of the model and the real WT based on experimental data obtained from SCADA;

3. Development of a new combined algorithm for real-time control of the orientation of the WT rotor based on the data predicted by the ANN and a method for controlling the power of wind turbines based on HCS;

4. Conducting research on the verified simulation model of SWT-3.6-120 WT in terms of the influence of orientation error on the performance characteristics of the WT.

The object of research - is the wind turbine yaw system, which includes a wind turbine, an electric generator, a yaw system and a control system.

The subject of the research - is the influence of methods and algorithms for controlling the wind power plant operating in conditions of variable wind direction and speed on its performance.

Scientific novelty of dissertation research:

1. The results of the analysis of experimental SCADA data of operating WTs and wind farms in terms of graphs of wind speed and direction, the position of the rotor (nacelle), as well as output power are obtained;

2. Using the MATLAB/Simulink package, a new computer simulation model of the SWT-3.6-120 WPP has been developed, including computer models of an asynchronous generator and an orientation system with a new virtual orientation controller and an MPPT controller. The adequacy of the model was verified by

comparison with experimental data obtained from the SCADA system for various operating conditions;

3. A new combined algorithm for controlling the orientation of the WT rotor has been developed based on data predicted by ANN and a method for controlling the power of WTs based on HCS. The control of active elements of the orientation system is carried out in real time with the prediction of the upcoming change in wind direction;

4. The results of testing the verified simulation model of the SWT-3.6-120 WT were obtained, demonstrating a decrease in the orientation error of the WT rotor to 1°, with an increase in the output power of the WT by 6.88%.

Theoretical and practical significance of the work:

1. A new simulation computer model of the WT has been developed, containing universal components that can be controlled using various external control systems, which reflects the functionality and flexibility of the new model. The verified computer model can be used by researchers, designers and users in the field of wind energy to simulate the operation of the orientation system of any WT.

2. A new combined algorithm for controlling WT power extraction with minimizing orientation error and increasing wind energy utilization coefficient based on the use of ANN and HCS data has been synthesized. This algorithmic approach can be used in practice for programming control systems of megawatt class WTs.

3. An increase in the efficiency of WT operation management based on the developed algorithms was noted in a wide range of variable components of wind speed and direction, which demonstrates the independence of algorithms from wind behavior.

The main provisions of the dissertation submitted for defense:

1. Results of research and analysis of experimental SCADA data of operating WTs and wind farms in the form of graphs of wind speed and direction, position of the rotor (nacelle), as well as output power;

2. A new computer simulation model of the SWT-3.6-120 WT manufactured by Siemens in the MATLAB/Simulink package, characterized by the completeness of the structure and control, designed to study the characteristics of WTs in accordance with the control algorithms used;

3. A new dynamic combined algorithm for determining WT performance with accurate, fast and efficient tracking of wind direction changes, with reduced yaw error;

4. The results of studies of the verified computer simulation model of the SWT-3.6-120 WT in terms of the influence of orientation error on the parameters of the output power in real time with the maintenance of the maximum value of the wind energy utilization factor, including with an increase in the service life of the WT.

Methodology and research methods. When solving the tasks, the research was carried out taking into account theoretical foundations of electrical engineering, wind power, neural networks, optimization and mathematical statistics. The simulation used technical characteristics of real WTs and SCADA data from wind farms. The MATLAB/Simulink is used to calculate and programmatically implement algorithms.

The reliability of the results, scientific statements, results of work and conclusions are justified by the correctness of the use of mathematical apparatus, the validity of modeling methods using well-known programs that have repeatedly confirmed their reliability, as well as detailed simulation methods that allow reproducing studies conducted by other scientists. In addition, the reliability is confirmed by the correspondence of the theoretical provisions to the simulation results.

Credibility and validity: The validity and degree of reliability of scientific provisions, conclusions and results is based on the use of known provisions of mechanics, aerodynamics, electro mechanics, electrodynamics, automatic control theory and computer simulation methods. The reliability of the results is determined by the correctness of the application of the mathematical apparatus, the validity of modeling methods using well-known programs that have repeatedly confirmed their reliability, as well as detailed simulation methods that allow reproducing the studies carried out by other scientists. In addition, the reliability is confirmed by the correspondence of the theoretical provisions to the simulation results.

Approbation of work: sections of the results in this dissertation were presented and discussed at the following conferences.

1. International Conference on Industrial Engineering, Applications and Manufacturing, (ICIEAM 2020), Sochi, Russia.

2. IEEE Russian Workshop on Power Engineering and Automation of Metallurgy Industry: Research & Practice, (PEAMI 2020), Magnitogorsk, Russian.

3. International Conference on Industrial Engineering, Applications and Manufacturing, (ICIEAM 2021), Sochi, Russia.

4. International Ural Conference on Electrical Power Engineering, (Ural Con 2021), Magnitogorsk, Russian.

5. International Conference on Industrial Engineering, Applications and Manufacturing, (ICIEAM 2023), Sochi, Russia.

Publications: 15 articles were published on the topic of the dissertation, including 5 articles in peer-reviewed scientific journals and publications recommended by the Higher Attestation Commission of the Russian Federation and the UrFU Attestation Council, of which 5 articles in publications indexed in the international database Scopus, 1 patent for a utility model and 1 certificate of official registration of a computer program.

Personal contribution of the author: The author determined the direction of the research, formulated the purpose and objectives of the research, analyzed achievements in the field of scientific research. Based on the analysis, methods and means of conducting research were selected, and computer mathematical models used in the study were developed. The development of the control system model and all the research were carried out directly by the author.

Compliance with the scientific specialty: The dissertation corresponds to the passport of the specialty 2.4.5. "Energy Systems and Complexes", and in particular, paragraphs 1, 2, 4, 6.

The structure and scope of the thesis: The dissertation consists of an introduction, 4 chapters, a conclusion, a list of references from 208 items and appendix. In total, the dissertation contains 156 pages of text with 72 figures, 6 tables and 2 appendices.

CHAPTER 1: CURRENT STATUS OF WIND ENERGY CONVERSION SYSTEMS, YAW SYSTEMS AND RESEARCH OBJECTIVES

Chapter 1 provides a historical overview and trends in wind energy and yaw control systems development. The key issues and challenges in the design and operation of wind energy conversion systems (WECS) and yaw system are studied, as well as development trends. Then, the technical research route and goals of the dissertation thesis are formulated through the analyzed results.

1.1 Background and significance of the subject

1.1.1 Background

Energy is the material basis for the survival and development of human society. With the continuous progress and development of society, human beings have a higher and higher demand for the development and utilization of energy. At present, most of the energy used by human beings originates from fossil energy. However, the storage of these resources on the earth is limited and is getting depleted, and the damage to the environment caused by the use of fossil energy has seriously affected human life. Conventional energy reserves, mainly coal, oil, and natural gas, are limited and depleting. The rapid consumption of fossil energy has brought a series of serious problems to mankind, such as environmental pollution and energy depletion. Therefore, the development and utilization of renewable energy have become a hot topic today, and the research for non-polluting renewable energy has become the main task of each country [3].

The renewable energy used in the world today mainly includes wind, solar, geothermal, biomass and tidal energy, etc. Among the many energy sources, wind energy is relatively simple to use, has huge reserves, and is non-polluting to the environment, so the development and utilization of wind energy are currently receiving great attention worldwide. As a clean and renewable energy source, wind energy has great advantages and prospects compared to other fossil energy sources. Since the 1980s, the wind power industry has been developing rapidly, and wind power technology has become the most promising renewable energy technology [4].

The world today is facing a serious energy crisis and climate crisis. First, fossil energy is still the mainstream energy that is widely used but increasingly scarce. Renewable energy technology has made great progress but still not enough to pick up the beam of the world economy. Second, the reserves of fossil energy are not unlimited, and after over 200 years of over-exploitation and use since the industrial revolution, the remaining reserves are very limited, and the restructuring of energy is imminent. Third, the environment which human beings depend on for survival is deteriorating, and the greenhouse effect is becoming prominent [5]. According to statistics, the global energy production industry emits about 26 billion tons of CO_2 per year, of which the share of emissions from electricity production alone reaches 41%; the International Energy Agency (IEA) expects that global CO_2 emissions will increase by 55% to over 40 billion tons by 2030, of which the share of emissions from electricity production will increase to 44%. This shows that the power industry is the main culprit of CO_2 emissions and even global climate change [6].

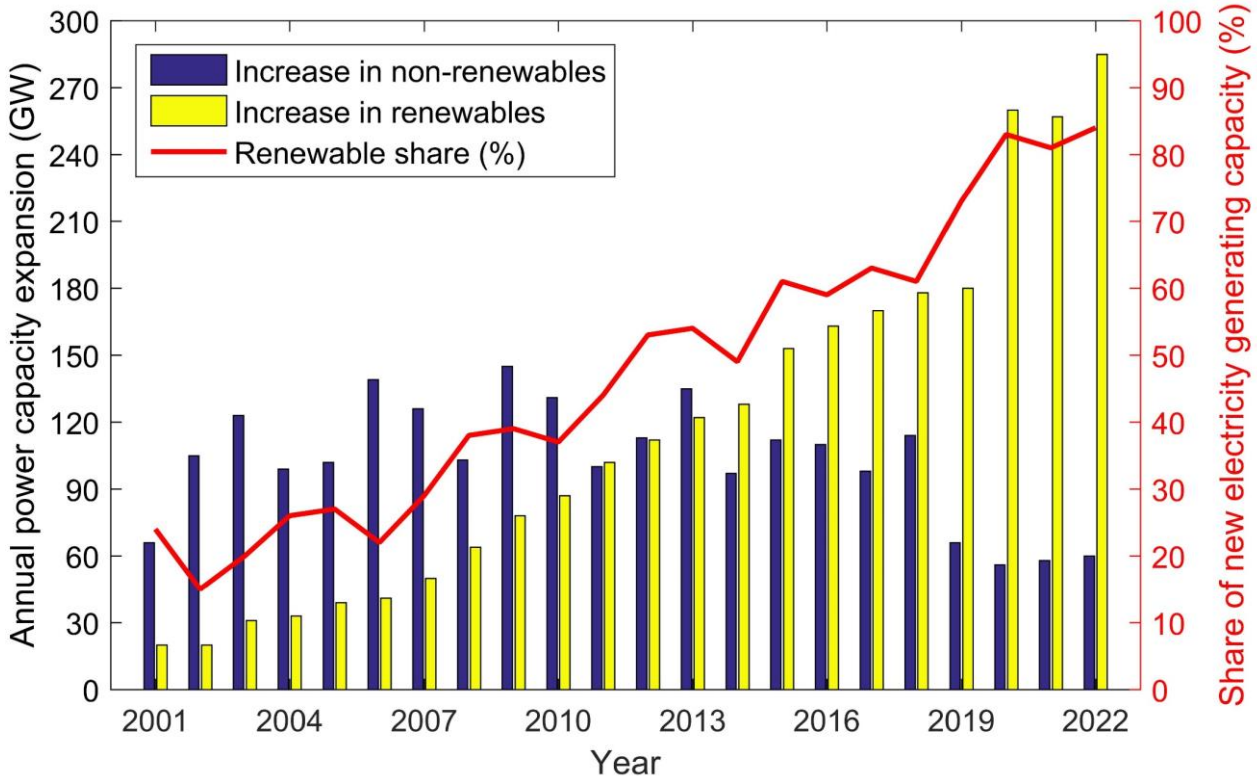

Figure 1.1. Renewable share of annual power capacity expansion

In the past two decades, with the continuous development of technology and human demand for electricity, it has added numerous power generation devices every

year. With the continuous development of renewable energy technologies, related power generation technologies have become more and more mature, and the cost of power generation has also been reduced, so it has added more and more renewable energy power plants around the world, the specific data is shown in **Figure 1.1**.

It can be seen from **Figure 1.1** that the growth rate of the installed capacity of traditional power plants is not high, and even in recent years, with the global emphasis on renewable energy power generation technology, the installed capacity of traditional power plants has even declined [7]. The installed capacity of renewable energy power plants is increasing year by year. Since 2014, the installed capacity of renewable energy has exceeded that of traditional energy sources, and the gap is increasing.

To cope with the global energy crisis and the increasingly serious environmental pollution problem, renewable energy utilization technologies (including hydropower, wind, solar, biomass, geothermal, marine, etc.) have received widespread attention from countries around the world, the installation data from 2011 to 2021 is shown in **Figure 1.2.**

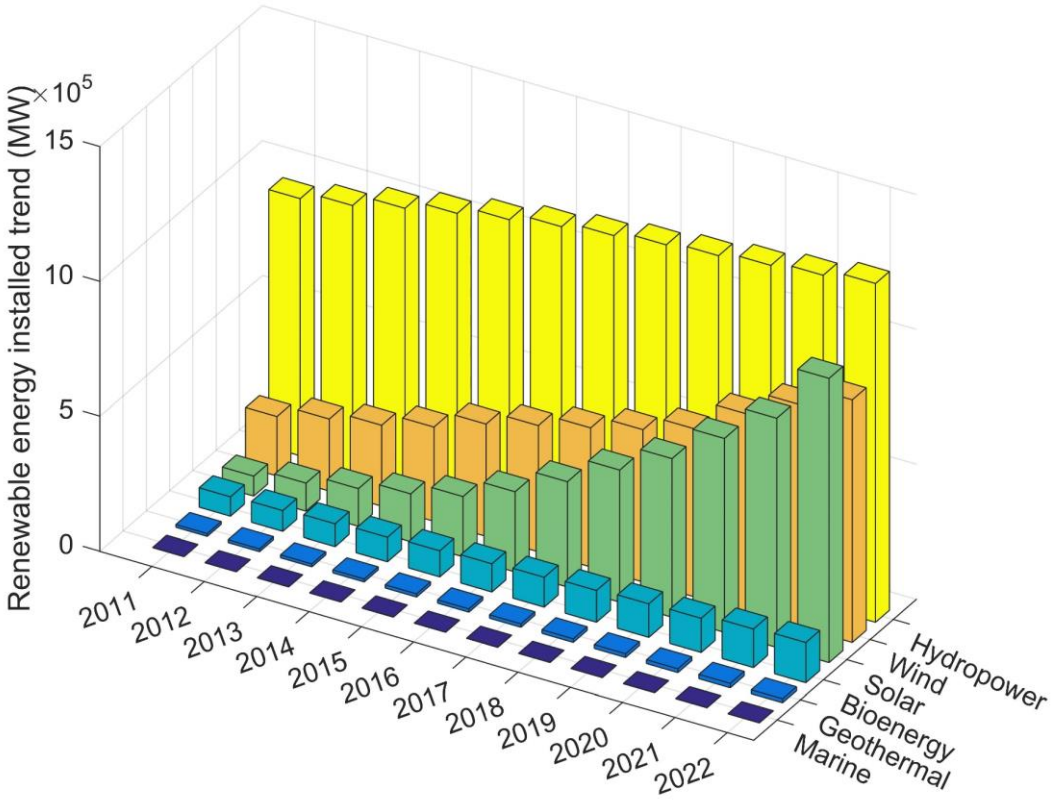

Figure 1.2. Renewable energy installed trend

From **Figure 1.2**, it can be seen that at present, the most widely used renewable energy technology is hydropower, but hydropower technology completely depends on water conservancy and is not applicable in some areas. The second-ranked renewable energy source is wind power, and in recent years, offshore wind power technology has gradually matured, and more and more wind turbines have provided services to the grid. Compared with other renewable energy technologies, wind power technology is a universally applicable and stable power generation technology, so its installed capacity is increasing year by year.

Data shows that the CO_2 emissions generated during the manufacture, installation, operation, and decommissioning of a wind turbine are "paid off" in roughly the first 3-9 months of the unit's operation. For the rest of its life, it will not produce any greenhouse gases [8]. Therefore, the active development of wind power generation can play a very important role in the increasing electricity supply, alleviating the pressure of environmental pollution, and promoting economic development.

Wind power is currently the most mature renewable technology, the most large-scale development conditions and commercial development prospects of wind energy utilization technology, especially the horizontal axis upwind three-blade wind turbine is currently the mainstream of the world wind power industry models [9]. In Denmark, Spain, Germany, and the United States, wind power accounted for 32%, 20%, 10%, 5% of the total electricity consumption of the country respectively, has become a veritable alternative energy and mainstream power [10].

According to the global wind power installation data released by the Global Wind Energy Council (GWEC) [11], the global wind power installed capacity reached 93.6 GW in 2021 (including onshore wind turbine installation 72.5 GW, offshore wind turbine installation 21.1 GW), with a cumulative annual growth rate of 7%, only 1.8% lower than the 2020 record; by the end of 2021, the cumulative installed capacity of global wind power had reached 837 GW (including onshore wind turbine installation 780 GW, offshore wind turbine installation 57 GW), with a cumulative annual growth rate of 12%. The wind energy historic development of new installations and total installations data are shown in **Figure 1.3**.

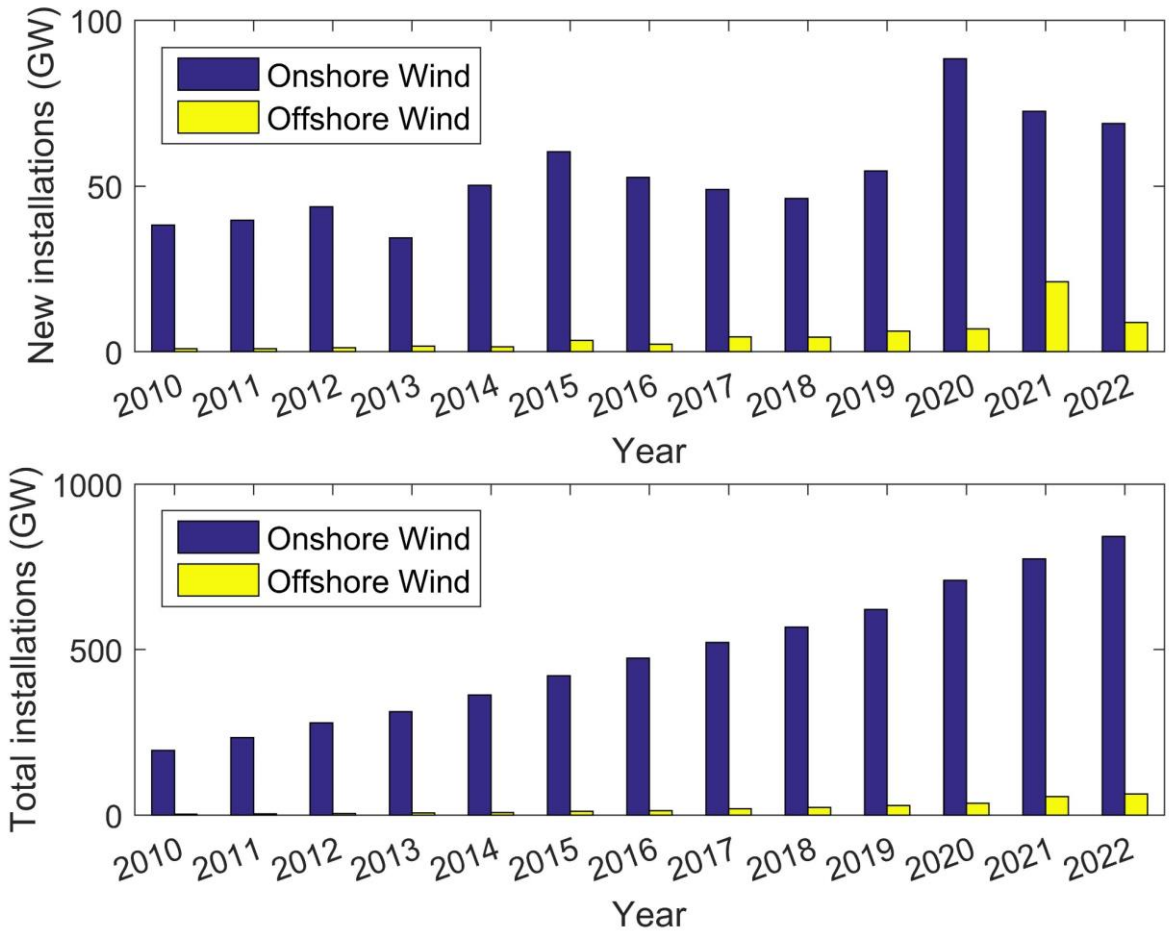

Figure 1.3. Historic development of wind energy

As shown in **Figure 1.3**, although new installations in the onshore wind market dropped to 72.5 GW in 2021, it was still the second highest year in history. The offshore wind market had a record year with more than 21 GW grid connected, three times more than the previous year, making 2021 the highest year ever. The application of offshore wind power technology provides a new solution to the energy crisis. In the past five years, the installed capacity of offshore wind power generation has continued to increase. Although there is still an enormous gap compared with onshore wind power generation, the overall development trend is good.

In the recent years, wind energy technology has received growing attention from scholars all over the world. The wind energy technology involves wind resource analysis, wind farm siting, wind turbine design, wind turbine control technology, and wind farm layout. Among them, the control technology of wind turbine directly affects the active power output and component fatigue loads and has become one of the research priorities.

According to the type of the control actuator, the control technologies of the horizontal axis wind turbine (HAWT) can be divided into pitch control, generator torque control, and yaw control. Among them, pitch and torque controls are the focus of research, and related papers account for more than 80% of wind turbine control literature. In contrast, the yaw control only receives limited attention, but it is indispensable for horizontal-axis wind turbines. And a failure survey revealed that the yaw system only contributes 1.4% of the whole turbine cost, but the yaw system downtime distribution probability was 13.3%, ranking third, and the average downtime per yaw system failure was 259.4 h, ranking second [12]. In addition, according to the wind farm survey in European countries such as Germany and Denmark, the yaw system failure rate accounted for 12.5% of the total failure rate of WTs [13]. Obviously, there has been an urgent need in improving the performance of the yaw control system.

In the existing research, there are three types of control objectives for yaw control systems [14][15], that is: (a) increasing the energy capture of a single wind turbine; (b) reducing the fatigue load of a single wind turbine; (c) maximizing the total power production and optimizing loads in wind farms.

(a) Increasing the energy capture of a single wind turbine: to improve the wind energy capture efficiency of a single wind turbine, it is necessary to consider how to obtain yaw error and reduce it, where the yaw error refers to the angle between nacelle and wind. There are three main ways to obtain yaw error: the method based on conventional wind direction sensor (weather vane), the method based on wind direction estimation, and the method without wind direction sensor. Some yaw control methods using the weather vane are on the assumption that the measured wind direction is the real value. These methods include logical control, traditional PID control, and hybrid control based on fuzzy control [16][17][18][19]. Meanwhile, some literature proposed to compensate yaw error to approximate the true value [20]. However, the contradiction between the fast change of wind direction and slow yaw execution might easily lead to frequent yaw action and large yaw error. In this context, the control method based on wind direction estimation was proposed. On the one hand, the future wind direction information was measured by advanced equipment [21] or predicted by models such

as time series models and neural network models [22][23]. On the other hand, the yaw system determined the optimal yaw position for the next period based on future wind direction information. By doing so, the extracted wind energy could be increased. In addition, considering the limitation of sensor accuracy and the inaccuracy of wind direction measurement caused by wind turbine wake, some scholars proposed yaw control methods without using wind direction sensors. Among them, the hill climbing search method was adopted [24], in which yaw error was calculated by comparing the maximum power currently available to the WT with the actual power output. On this basis, the hill climbing search method has been improved. In other literature, the wind speed information was used to calculate the difference between the optimal rotor speed and the actual rotor speed, and yaw error was determined by combining with MPPT [25][26].

(b) Reducing the fatigue load of a single wind turbine: a wind turbine experiences extreme and fatigue loads during its lifetime [27]. The WT is mainly subjected to fatigue loads (actuator load and aerodynamic load) during normal operations, and accordingly, extreme load is generally not considered in yaw control strategy design. The actuator load refers to repetitive motion of the actuator in the process of completing control requirements. Reducing the frequency and running time of yaw system is the easiest way to reduce the actuator load. As to the aerodynamic load, it was the periodic vibration generated by the inflow wind, including symmetrical and asymmetrical loads. In the existing studies, a large number of scholars have proposed to reduce the aerodynamic load of a single WT by controlling the pitch angle but seldom through the yaw controls. In recent years, aerodynamic load analysis of wind turbine with yaw misalignment has been made [28][29], and the results showed the potential of yaw control in reducing the aerodynamic load of a single WT.

(c) Maximizing the total power production and optimizing loads in wind farms: in wind farms, yaw control not only improves the total power production but also optimizes the overall fatigue load. Under the traditional yaw control, each wind turbine tried to capture the maximum wind energy, thus ignoring the wake effect [30]. Studies have shown that the average power of the entire wind farm can be reduced by the wake

effect by an average of 10% and up to 20% in severe cases [31]. Therefore, mitigating the wake effect is an urgent problem in wind farms. The yaw control could change the wake trajectory of the wind turbine, so as to reduce the influence of wake effect on the downstream wind turbines. Upstream wind turbines are yawed to the designated position after receiving the yaw instruction from the master controller, making the wake to deviate laterally from the downstream wind turbines. The research of yaw control in wind farms was mainly to increase the total wind energy capture by designing the optimal yaw angle, and it also included the fatigue load analysis of wind farm after the wake effect was mitigated [32][33][34].

1.1.2 Research purposes and significance

Wind energy has unique advantages: vast reserves, wide distribution, inexhaustible and clean, and is a green energy source of worldwide concern. However, as a product of nature, wind energy also has its natural disadvantages: uncontrollable randomness and intermittency of wind speed and direction changes. To maximize the utilization of wind energy, various control technologies are applied in wind turbines to cope with the random changes of natural wind: independent pitch control, generator torque control, yaw control, and other technologies to cope with wind speed fluctuations and frequent changes in wind direction, respectively [35].

Although modern wind turbine control technology has developed rapidly and many wind turbine control strategies or algorithms have been proposed, they mainly focus on pitch control technology, generator control technology and grid connection technology, etc. Yaw control technology has not achieved substantial and effective improvement and development, and there are still a lot of engineering problems in actual operation. Modern large wind turbines mostly adopt an active yaw system. Because of the characteristics of yaw action with low speed, heavy load, and set with system friction damping, the low-speed frictional self-excited vibration phenomenon of the yaw system occurs a lot, resulting in poor uniformity and low accuracy of yaw action, and it is easy to produce shock load and vibration noise during yaw. In addition, assembly errors, structural defects, lubrication, and other problems will also affect the smoothness of yaw torque transmission [36][37][38][39].

During the normal operation of the wind turbine, the yaw system often starts and stops frequently with the changing wind direction for windward control. With the change in wind speed and yaw angle, it will reflect the load, such as the fluctuation of yaw resistance torque and the change of output torque of the yaw drive during the unit yaw in the load fluctuation of the whole yaw system. The violent load fluctuation may lead to the unstable speed of the yaw system, which will have a significant impact on the vibration of the yaw system itself, wind turbine (blade), tower, nacelle, etc., and cause the over-excited vibration of the unit, resulting in downtime, and may even damage the yaw system components and other components of the unit, threatening the normal power generation and safe operation of the unit [12].

In actual operation, the wind turbine often has a series of engineering problems, such as frequent yaw, vibration overload, and downtime. The failure rate of the yaw system is not only high, but also once the failure occurs, the maintenance time is very long and the maintenance is very difficult so that the wind turbine in operation does not achieve the expected benefits or even losses. The failure rate among the components of the WECS is shown in **Figure 1.4**. From the failure rate and downtime, it can be seen that the failure rate of the yaw system is maintained at 6.7% ~12.5%, and the downtime caused by yaw failure accounts for 13.3% of the total downtime of the wind turbine [13][40][41].

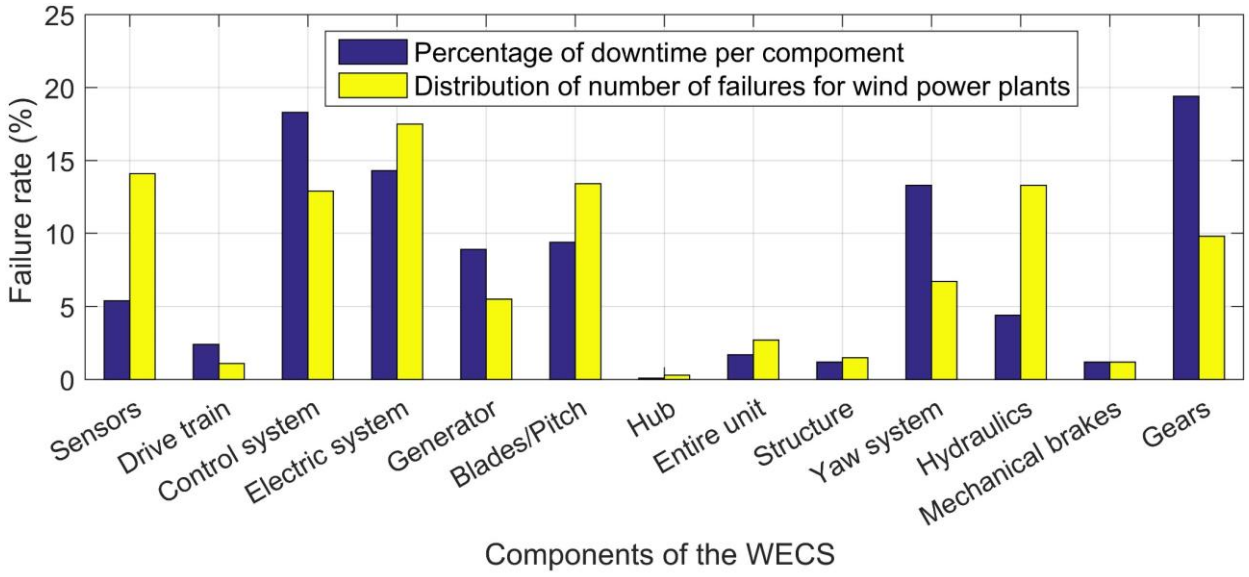

Figure 1.4. Failure rate among the components of the wind turbine (%)

The yaw system is an important part of the WT, the nacelle and WT self-weight load, the wind load from the nacelle including axial thrust, pitch moment, yaw moment, and other loads are carried by the yaw bearing and transmitted to the tower, yaw failure or error caused by the wind inaccuracy will further deteriorate the load condition of the WT, reducing power generation efficiency and even threaten the safety of the WT. Therefore, the yaw system becomes the key to control the wind turbine to face the wind correctly, and the problem of yaw failure has been plaguing the wind power industry for a long time, and they have found no reasonable solution.

1.2 Overall structure of wind turbine

1.2.1 Wind turbine composition

The basic working principle of the wind turbine is to push the wind turbine to rotate by natural wind, converting wind energy into rotating mechanical energy, mechanical energy is transferred to the generator through the main shaft or gearbox, which is converted into electrical energy, and the unstable electrical energy generated is transformed into stable electrical energy through inverter, chopper and frequency regulation through the converter, and finally output to the booster station to complete the transmission of electrical energy [42]. It is shown in **Figure 1.5**.

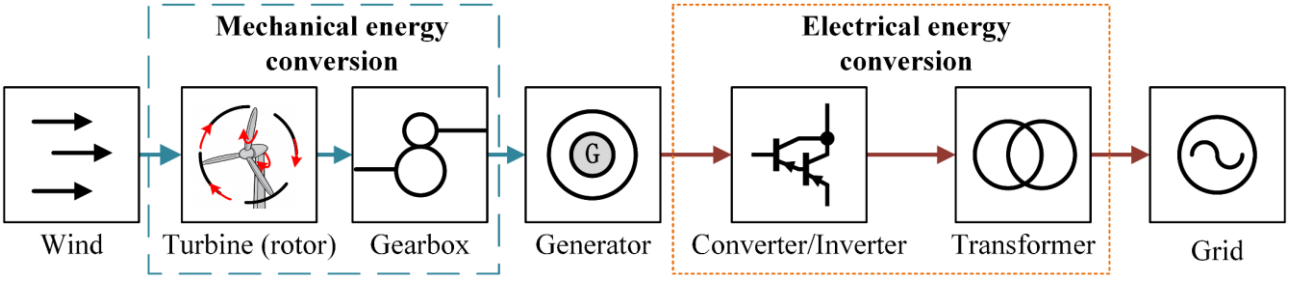

Figure 1.5. Energy conversion stage in a wind energy conversion system

1.2.2 Control systems for wind turbines

The control system of wind turbines is comprehensive. Especially for wind turbines running on the grid, the control system not only needs to monitor the grid, wind conditions, and unit operation data, control the units on and off the grid to ensure the safety and reliability of the operation process but also needs to optimize the control of the units according to the changes of wind speed and wind direction to improve the operation efficiency and power generation quality of the units.

The basic functions of the control system include basic operation control, output power control, operation status monitoring, fault detection/recording/processing, remote communication with the central control room, and safety protection control [43].

- Basic operation control of wind turbine: including standby, start-up, grid connection, off-grid, shutdown, yaw to wind, uncoupling, braking, heating/cooling, dehumidification, hydraulic pump start/stop, reset, lighting, etc.;
- Wind turbine output power control: including variable pitch and variable speed. Through variable speed to achieve maximum differential operation, the best blade tip speed ratio operation, constant speed operation; through variable pitch / variable speed to achieve constant power operation;
- Wind turbine operating status monitoring: including the status of each subsystem, power parameters, the temperature of key parts of the components, environmental/weather parameters, etc.;
- Wind turbine fault detection and recording/processing: including timely detection of faults, storage of a specified number of recent faults and alarm in a specified manner;
- Wind turbine safety protection control: including emergency safety chain protection, software safety protection, and lightning protection/grounding protection, etc.;
- The wind turbine should have a remote communication function with the upper computer in the central control room, so that the upper computer in the central control room can monitor the operation status of the turbine, display parameters, remote control, data storage, etc.

The wind turbine contains many subsystems with different time constants, such as pneumatic system, mechanical system, and electrical system. Usually, the dynamic response of the electrical system is much faster than that of the mechanical system. Due to the presence of power electronics in wind turbines, the time constants of each subsystem vary greatly, making the control system more complex compared to conventional power generation systems.

In the simulation modeling of wind power generation system, we often consider

the control system as the output power control system [44], i.e., pitch control, yaw control, generator control, maximum power point tracking control, and power electronic converter control, as shown in **Figure 1.6**.

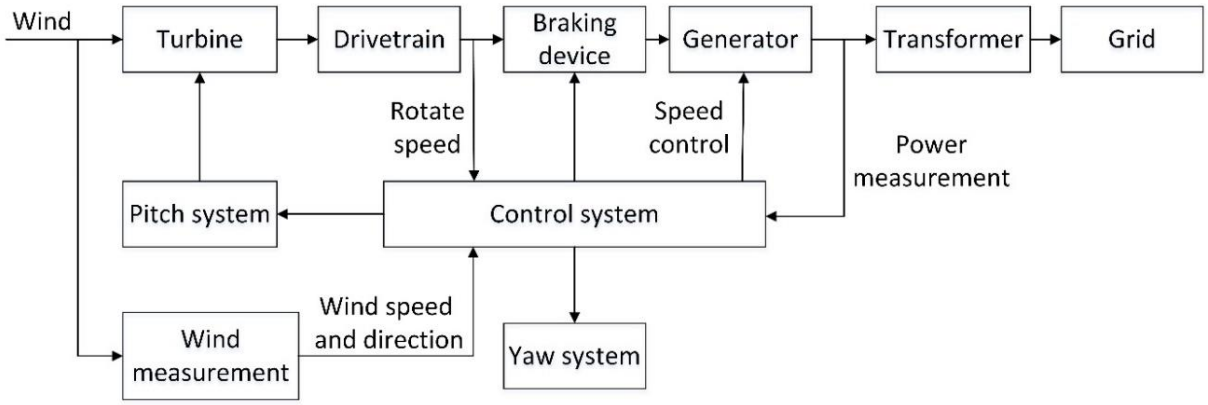

Figure 1.6. Schematic diagram of WECS

Pitch system is the process by which the blades mounted on the turbine's shaft rotate around their axis [45][46]. The pitch system is used to regulate the amount of energy captured by the wind turbine from the wind. This process changes the aerodynamic torque obtained by the wind turbine by adjusting the angle between the direction of the synthetic airflow on the blade airfoil and the geometric chord of the airfoil (angle of attack). The pitch system of the wind turbine mainly performs the following functions: 1) aerodynamic braking to ensure that the wind turbine can be safely shut down when the wind speed is too high or when it encounters a fault; 2) regulating the size of the wind energy captured by the wind turbine under various working conditions to ensure the safe and stable operation of the wind turbine; 3) suppressing the vibration of the wind turbine and the tower through the pitch control of the wind turbine to reduce the dynamic load of the wind turbine; 4) starting control of the wind turbine when the wind speed is higher than the starting wind speed The blade pitch angle is changed to a predetermined angle so that the blade speed rises gradually.

The rotation of the nacelle of the horizontal axis wind turbine around the tower is called yaw, and the yaw system of the wind turbine is generally divided into active yaw system and passive yaw system [47][48]. Passive yaw system refers to the yawing mode that relies on the wind to complete the unit's action against the wind through the

relevant mechanism, commonly there are three kinds of the tail rudder, rudder turbine, and downwind; active yaw refers to the yawing mode that uses electric or hydraulic drag to complete the unit's action against the wind, according to the feedback information from the anemometer, the control system automatically performs yawing, commonly there are two kinds of gear-driven and sliding ways. For large wind turbines, a gear-driven form of active yaw is usually used.

The generator controller must adapt to the speed of the wind turbine [49][50]. Therefore, the electrical torque of the generator must be able to be controlled. Depending on the type of generator used in the wind turbine, the controller is constructed differently. Depending on the purpose, the same generator can be used with different switching algorithms, such as DTC, vector control, etc.

When the wind turbine is operating below the rated wind speed, it cannot generate full power [51]. The main control system should be able to coordinate and control the pitch system, converter, and other related components according to the control strategy of the unit so that the wind turbine speed always tracks the best blade tip speed ratio operation.

The main control system should be able to coordinate and control the pitch system, converter, and other related components according to the control strategy of the wind turbine so that the wind turbine speed always follows the optimal blade tip speed ratio and the wind speed-power curve is consistent with the optimal power curve to capture the maximum wind energy.

In variable-speed wind turbines, power electronic converters play the role of power regulation [52]. The grid-side converter regulates the active and reactive power flowing into the grid. In WECS, changes in wind speed and the resulting changes in generator power output cause large fluctuations in the DC bus voltage. Therefore, the control of the grid-side converter must ensure that the DC bus voltage remains stable during large fluctuations in generator voltage or power. At the same time, the grid-side converter must also be able to control the load voltage on the grid side by regulating the reactive power exchanged between the wind turbine and the grid.

1.3 Function and principle of yaw system

For HAWTs, the efficient utilization of wind energy depends not only on the aerodynamic design of the blades and the selection of the wing shape, but also to the efficient tracking of wind direction changes by the turbine. The yaw system is the actual actuator to achieve accurate and effective wind alignment of the wind turbine, to ensure that the turbine reaches the maximum windward side, and to improve the utilization of wind energy, which is an indispensable key component of horizontal axis wind turbine, as shown in **Figure 1.7** [53]. The random and intermittent changes of natural wind and the negative effects of inherent characteristics, such as anti-peak regulation and tower shadow effect, all place high demands on the yaw system.

Figure 1.7. Wind turbine yaw system

The yaw control system plays an important role in improving the wind energy utilization of the unit, but the yaw system is affected by the complex operating conditions of random perturbations and uncertainties as well as its multivariate nonlinearity, which makes it difficult to build an accurate mathematical model of yaw. This requires the yawing system to have better operational stability and robustness.

1.3.1 Wind turbine yaw system control part and drive part

The yaw system of wind turbines consists of two major parts: the yaw control part and the yaw drive part, as shown in **Figure 1.8**. The control part includes: weather vane (wind direction sensor), yaw controller, uncoupling sensor. The drive part includes: yaw bearing, yaw drive unit, yaw brake [54][55].

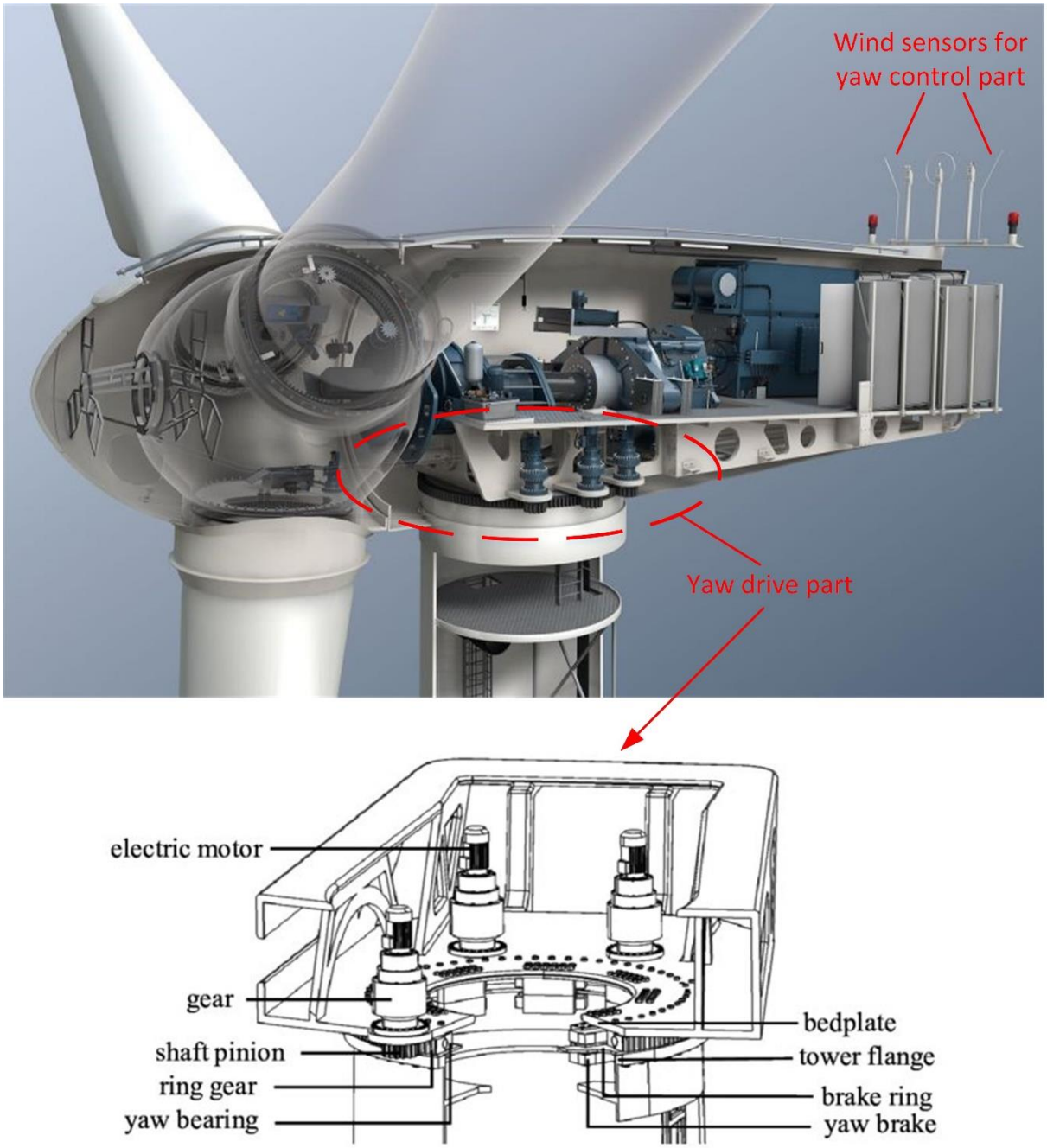

Figure 1.8. Example of a yaw system

Yaw control part: The control part is a servo system unique to wind turbines that are used to control the wind turbine to steadily track changing wind directions and can automatically unwind the cable when it becomes tangled.

It should be noted that there are some differences between the weather vane and anemometer installed on wind turbines and the wind measurement equipment used for meteorological and climate analysis. Two specific aspects are as follows: (1) Because it is only used to control the work of the yaw system, it is not used for the precise measurement of wind direction and wind speed, so the accuracy is usually low; (2) The weather vane is installed on the top of the nacelle to rotate with the nacelle, so it can only measure the approximate angle between the nacelle and the direction of the incoming wind to determine from which direction to yaw against the wind, and cannot detect the actual direction of the wind.

The weather vane is mounted on a fixed bracket on the fiberglass nacelle cover of the wind turbine and can rotate synchronously with the wind turbine. The yaw controller is responsible for receiving and processing signals and sending control commands according to the control requirements.

Since wind turbines always choose the shortest distance and shortest time to track the wind, sometimes due to the changing pattern of wind direction, it is possible for wind turbines to track the wind in one direction for a long time, which will cause the winding of the cable, and if the winding circle is too much and exceeds the specified value, it will cause damage to the cable. To prevent this phenomenon, an unwind sensor is usually installed. The unwind sensor is installed at the bottom of the cabin and engages with the yaw ring through a nylon gear so that during the yaw, the nylon gear also rotates together. A multi-stage reduction by worm wheel, worm screw, and gear transmission drives a set of cams, each cam drives a micro switch, which sends a different signal command. The microprocessor uses the signals from each micro switch to determine whether the cable needs to be unhooked. The microprocessor uses the signals from the micro switches to determine whether to unhook, which direction to unhook and when to stop unhooking.

Yaw drive part: there are two types of yaw bearings commonly used: sliding bearings and slewing bearings. Sliding bearings are commonly used with engineering plastics as shingles, which can work properly even in the absence of lubrication. Shaft tile is divided into shaft up thrust tile, radial thrust tile, and shaft down thrust tile three

types, respectively, used to bear the nacelle and blade weight generated by the axial force parallel to the direction of the tower, the blade transfers to the nacelle perpendicular to the tower direction of the radial force and the nacelle overturning moment. Thus, the various forces and moments on the nacelle are transmitted to the tower through these three types of shingles (Nordtank and Vestas units both use this type of yaw bearing). The slewing bearing is a large bearing of special construction, which can withstand radial and axial forces in addition to overturning moments. This kind of bearing has become a standard part of mass production. Slewing bearings are usually available in construction types with internal or external gears for yaw drives. Most wind turbines currently in use of this type of yaw bearing.

The yaw drive consists of a yaw motor and a yaw reduction gear mechanism. The yaw drive usually uses an open gear drive. The large gear is fixed at rest on the top of the tower, mostly in an internal gear configuration, and the small gear is driven by a nacelle-mounted drive. To obtain a symmetrical drive torque, two or more drives are usually used to drive the yaw system for large wind turbines. The yaw drives are mostly motor-driven, and the appropriate output speed and torque are obtained through gear reducers. Mechanism). A combination of a one-stage turbine reducer and a one-stage planetary reducer is also used (VESTAS units use this mechanism).

To ensure that when the wind turbine stops yawing will not be due to the wind load on the blade and passive deviation from the wind direction, the wind turbine most of them are equipped with yaw brakes. For the yaw system with slewing bearing, because the slewing bearing is rolling friction, the friction resistance is small, so the yaw brake must be used to prevent the nacelle from passively deviating from the wind direction when stopping yaw. To ensure the stability of the yaw, the yaw brake also has a brake motor, and an additional friction damping ring is added to the rotary bearing.

1.3.2 Yaw system function

The yaw system is a unique servo system of the WT, which is an essential part of the wind turbine electrical control system. It has two functions: one is to control the wind turbine to track the wind direction; the other is to automatically unwind the cables leading from the nacelle when the wind turbine becomes tangled due to yaw.

The principle of wind turbine yaw is to detect wind direction and wind speed by wind sensor and send the detected wind signal to the microprocessor. The microprocessor calculates the angle between the wind direction signal and the nacelle position, to determine whether the nacelle direction needs to be adjusted and in which direction it should be adjusted.

The yaw system has the following main functions [56]:

(1) automatic yaw controlled by the weather vane;

(2) manual yaw;

(3) weather vane controlled 90° side wind;

(4) automatic uncoupling.

The error value of the wind vane is relatively large, and there is no linear relationship between the data measured by the wind vane and the actual wind angle. Due to the influence of wind vane measurement accuracy, the wind vane cannot function in the range of ±15°, sacrificing this part of the wind. So the wind vane cannot guarantee the control accuracy in a small range, which not only reduces the wind energy capture, but also makes the symmetrical wind turbine paddle run with uneven force, leading to the vibration of the unit and the fatigue of the blade, and the load of the tower increases.

A typical working principle diagram of the yaw system is shown in **Figure 1.9**. The weather vane transmits the measured wind direction signal to the yaw control system, and after the signal comparison and judgment, the control system sends a clockwise or counterclockwise action signal to the yaw motor, and the yaw motor executes the yaw command to complete the yaw action [57].

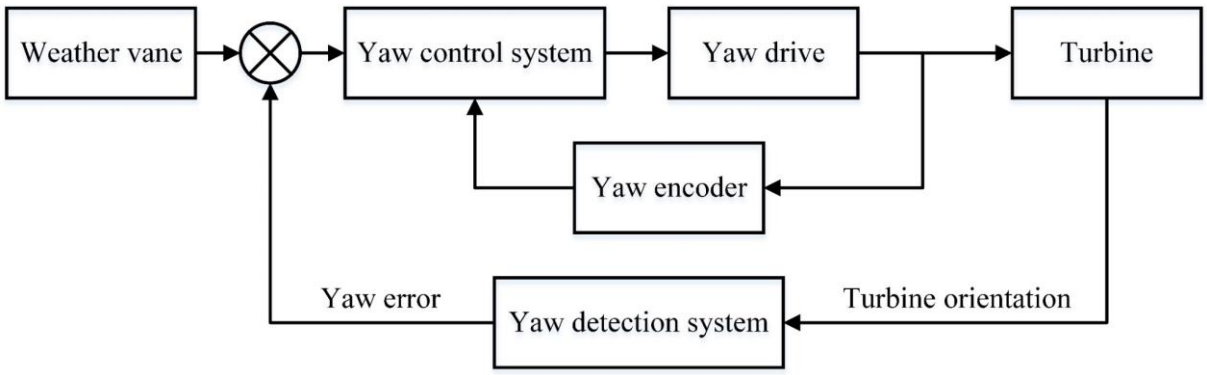

Figure 1.9. The yaw system fundamental diagram

According to the function of the yaw system and the specific yaw action, the yaw control process can be divided into automatic yaw, manual yaw, 90° side wind and automatic uncoupling [58], as shown in **Figure 1.10**. Among them, the optimization of yaw angle during normal operation of the unit is the focus of this paper, so only the optimization method of yaw angle during yaw is emphasized here, and other yaw control processes are slightly considered and not focused on.

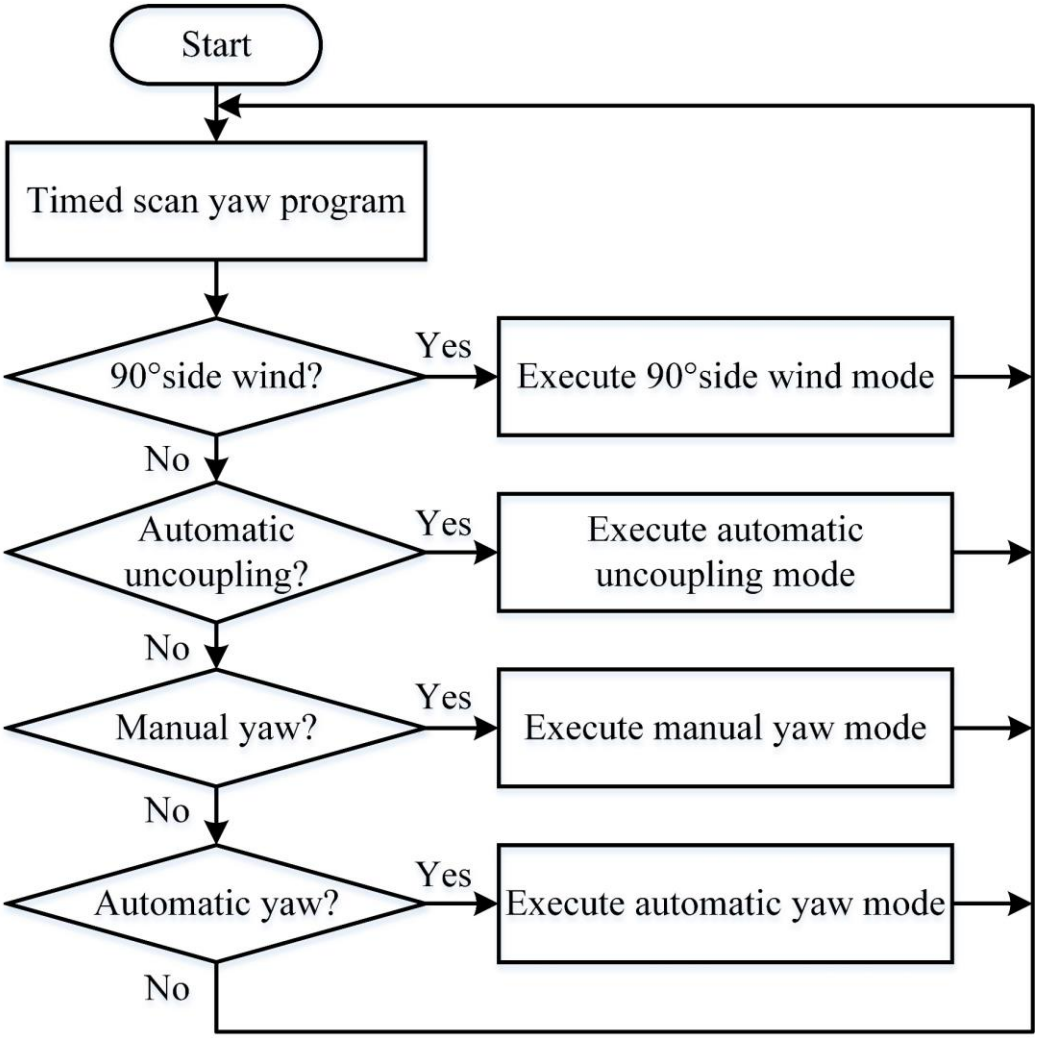

Figure 1.10. The yaw control flowchart

(1) Automatic yaw

This process yaw controller determines the yaw situation by the wind direction signal measured by the wind vane, and then carries out yaw control. The wind direction is always changing, it is random and uncertain, in order to improve the power generation and reduce the load of the wind turbine wind turbine must be accurate to the wind, so that the axial direction of the impeller and the wind direction is basically

consistent. When the wind direction changes within the allowable range, i.e., within the tolerance angle, the system does not yaw; and when the wind direction changes beyond the allowable error range, the system issues a yaw command, and the wind vane and yaw motor constitute the wind system to perform corrective actions to make the wind turbine accurate to the wind. The wind direction changes frequently, but the magnitude is not large, so a certain allowable error, i.e. tolerance angle, is usually set, such as 15°.

When the wind direction changes by more than 15°, the WT collects the wind direction signal through the weather vane and compares the angle between the wind direction and the nacelle axis with the allowable error angle. When the yaw system operates until the angle between the wind direction and the nacelle axis is within the set error threshold, the yaw system will stop aligning the wind and complete the yaw.

When the wind angle variation range is less than 15°, the accuracy of weather vane is not enough at this time, and it is necessary to execute yaw to wind by the pre-set yaw control strategy. Therefore, most of the operating wind turbines are yawing at an acute angle, but for a wind turbine that has just been shut down, there may be a situation of yawing at an obtuse angle.

Let the yaw error angle measured by the weather vane be θ and the nacelle yaw angle sum be α. The allowable error of yaw is $\pm\beta$ (generally around 15°), which is positive when the nacelle is turned clockwise and negative when it is turned counterclockwise.

1) When the angle $\theta \leq \pm\beta$ is measured by the weather vane, no yaw operation is performed.

2) When $\beta < \theta \leq 90°$, the nacelle is positively tuned to θ.

3) When $90° < \theta \leq 180°$, it indicates that the obtuse angle yaw is carried out, and to effectively prevent the cable from winding up, the cumulative angle sum α is read in the yaw direction, and the conditional uncoupling limit of yaw is set to $\pm\gamma$. When $\alpha + \theta < \gamma$, the nacelle is positively tuned to θ. When $\alpha + \theta$ is greater than the conditional uncoupling limit, the reverse is adjusted to $360° - \theta$.

4) When $-90° < \theta < -\beta$, the nacelle is negatively adjusted to θ.

5) When *-180°< θ ≤ -90°*, read the sum of the yaw direction angle *α*, when *α + θ > -γ*, the nacelle is negatively adjusted to *θ*; when *α + θ* is less than the condition uncoupling limit, the nacelle is positively adjusted to *360°+ θ*.

The whole process is shown in **Figure 1.11**.

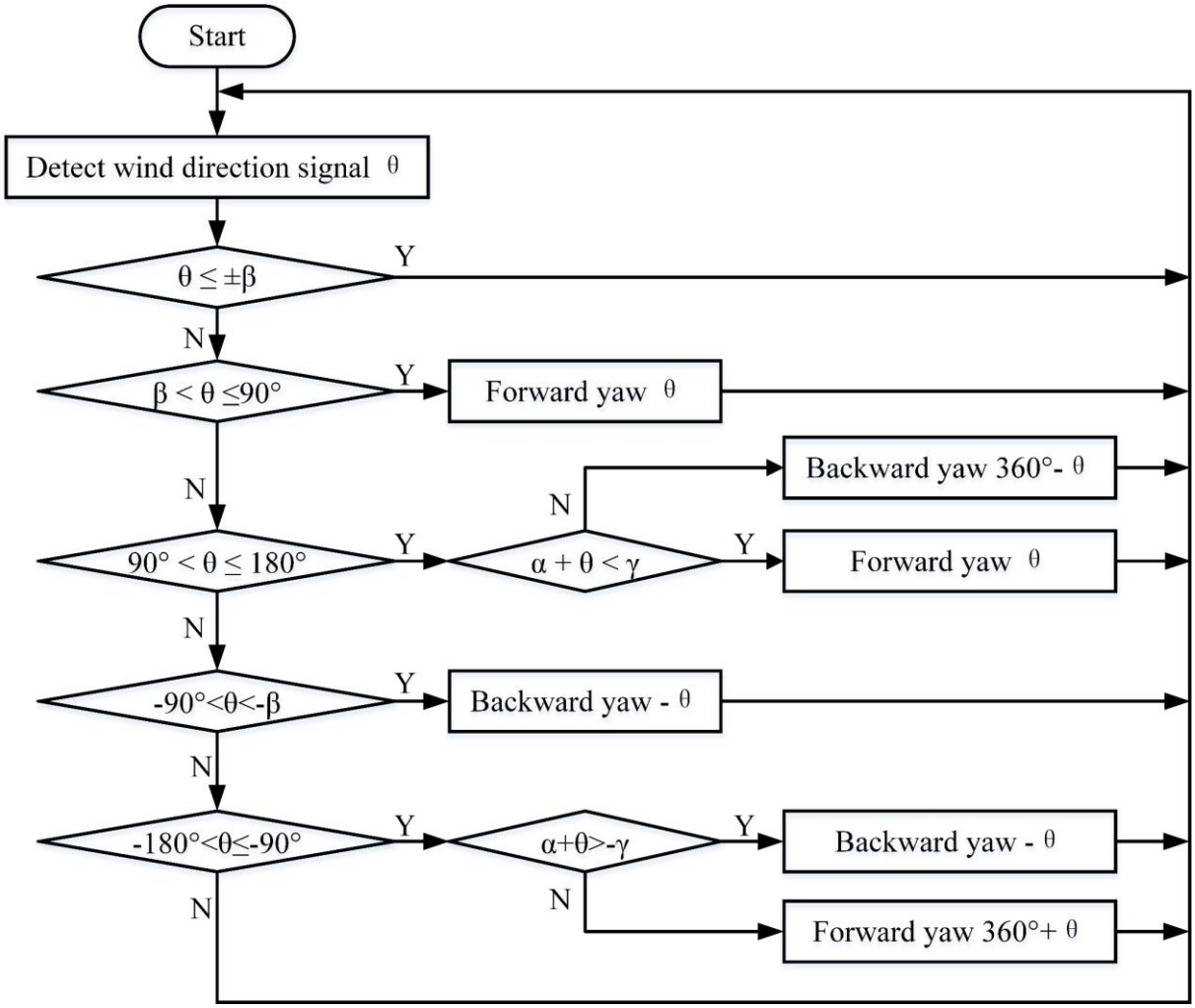

Figure 1.11. The flow chart of automotive yaw system

(2) Manual yaw

Manual yaw is a backup yaw solution when the automatic yaw fails. When the wind turbine fails and needs to be repaired, and when manual uncoupling is required, the manual command is used to realize the yaw operation of the wind turbine. The process is shown in **Figure 1.12**.

The manual yaw control process is as follows: after receiving a manual yaw command, the control system is first determined to be in automatic yaw. If there is no yaw operation at this time, the automatic yaw is locked; if the system is detected to be in yaw, then the yaw is locked.

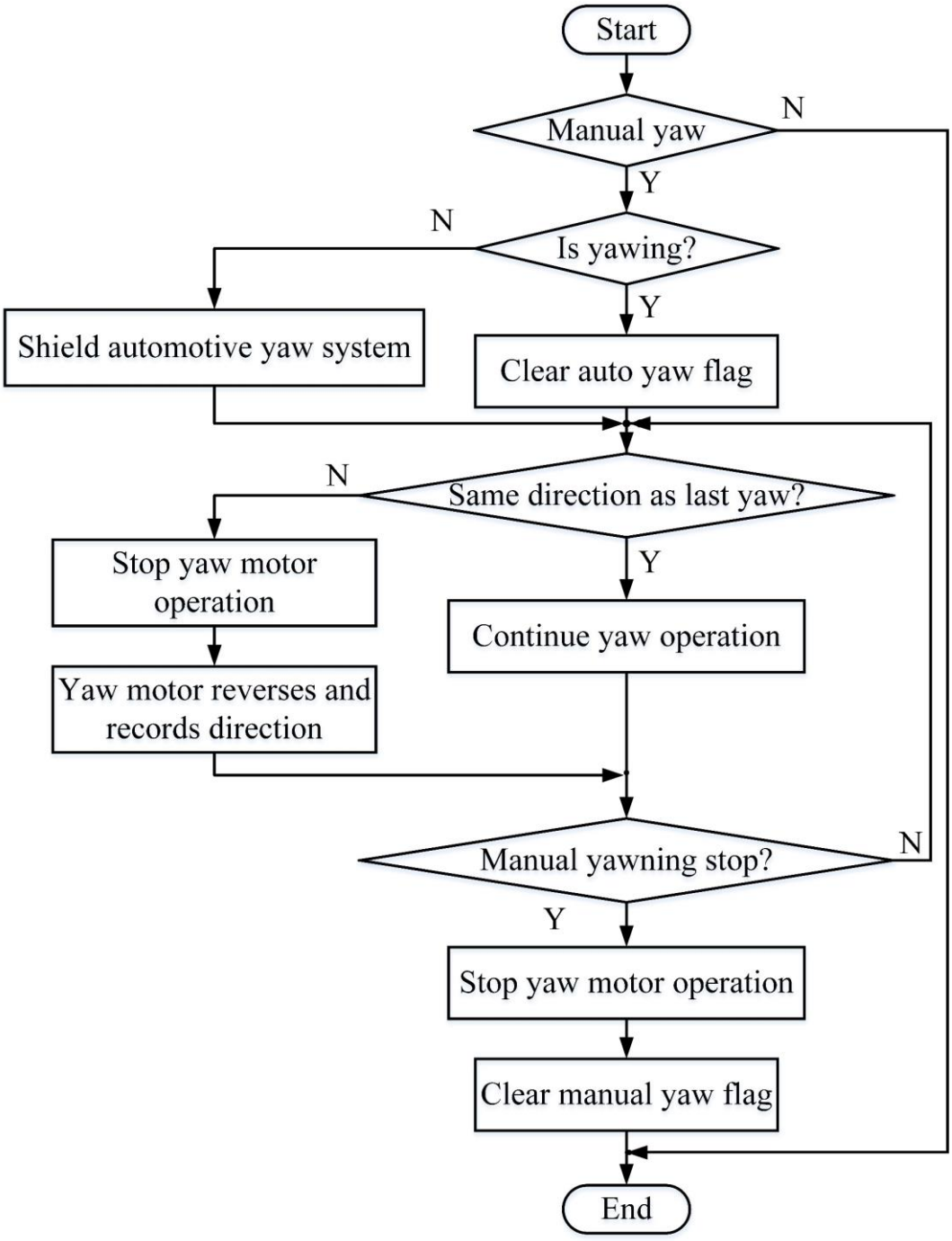

Figure 1.12. The flow chart of manual yaw system

If the system is in the yaw state, the automatic yaw flag is cleared; after that, the manual yaw direction signal is compared with the last one to see if it is the same. If the two manual yaw directions are the same, the manual yaw is executed. If the two manual yaw directions are not the same, stop the yaw motor, release the yaw gate, run in the opposite direction and record the yaw direction; when the yaw reaches a suitable position against the wind, the system detects the stop signal and stops the yaw, and then the system zeroes the manual yaw mark, which completes the manual yaw process.

(3) 90° side wind

The 90° side wind is a kind of protective measure for wind turbines. When there are very strong winds, storms exceeding the cut-out wind speed, or wind turbine speed exceeding the specified speed, we use the 90° side wind to protect the wind turbine.

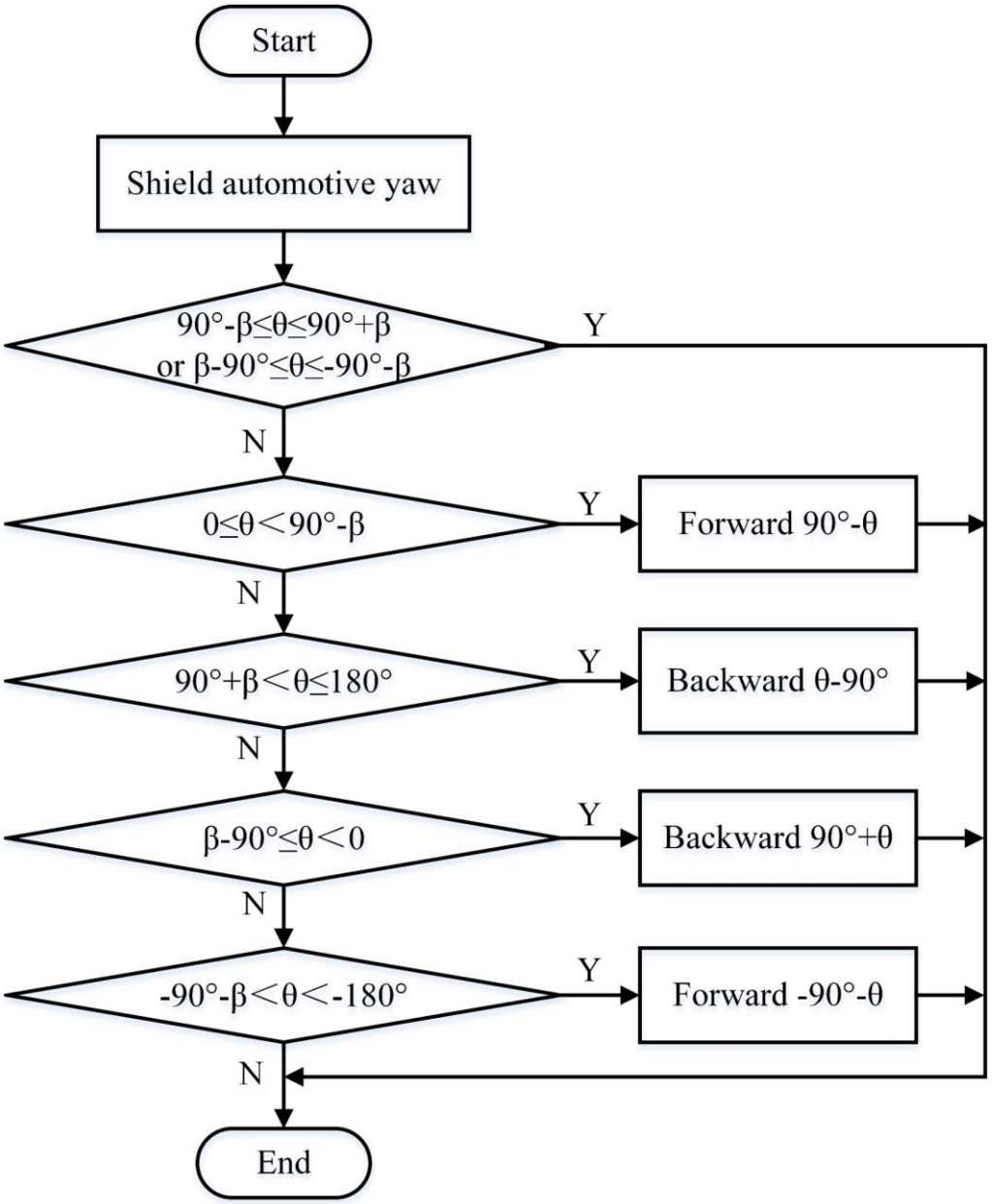

Figure 1.13. The flow chart of 90°wind direction

When there is a 90-degree wind measurement, the nacelle needs to take the shortest path, and at the same time when the 90-degree side wind is over, the nacelle needs to take the shortest path, and at the same time the system blocks the automatic yaw command; when the 90-degree side wind is over, the nacelle needs to hold the airlock tight, considering that the wind speed is, the system can continue to track the

change of wind direction so that the wind turbine can keep the side wind position in the extreme environment and reduce the possibility of a loss of wind turbines to the minimum. The process is shown in **Figure 1.13**.

For the $90°$ side wind, the allowable error is still taken as $\pm\beta$. The operation process of $90°$ side wind is to adjust $90° - \theta$ positively when the angle measured by weather vane is $0 \leq 90° < -\beta$; not to operate when $90° - \beta \leq \theta \leq 90° + \beta$; adjust $\theta - 90°$ negatively when $90° + \beta < \theta < 180°$. When the angle measured by the weather vane $\beta - 90° \leq \theta < 0°$, adjust $90° + \theta$ negatively; when $\beta - 90° \leq \theta \leq -90° - \beta$, do not operate. When $-90° - \beta < \theta < 180°$, the positive adjustment is $90° - \beta$.

(4) Automatic uncoupling

The uncoupling device is an indispensable and important device of the yaw system. If the yaw system rotates in the same direction many times, the cable may be twisted and strangled. When the automatic uncoupling of the system fails, the number of wind turbine pole turns is set in the system, and when the number of pole turns is reached, the number of turns is reached, the cable switch will work automatically and the system will stop and wait for manual uncoupling.

When the limit switch is triggered, the system determines whether to uncouple clockwise or counterclockwise according to the information sent by the trigger switch.

When the system detects that the output signal of the limit switch is 1, the system will drive the nacelle to rotate negatively to uncouple.

When the system detects the output signal of the limit switch is -1, the system will drive the nacelle to rotate positively to uncouple.

During the uncoupling process, the signal of the proximity switch is detected at the same time, until the yaw angle of the nacelle is recorded by the proximity switch is within a certain range (generally 30°), then the uncoupling is finished; at this time, the yaw motor is stopped and the system is in standby mode, and the automatic unhooking completion signal is sent to the central controller.

The signal from the limit switch is LS and the angle value recorded by the proximity switch is RS. The flow is shown in **Figure 1.14**.

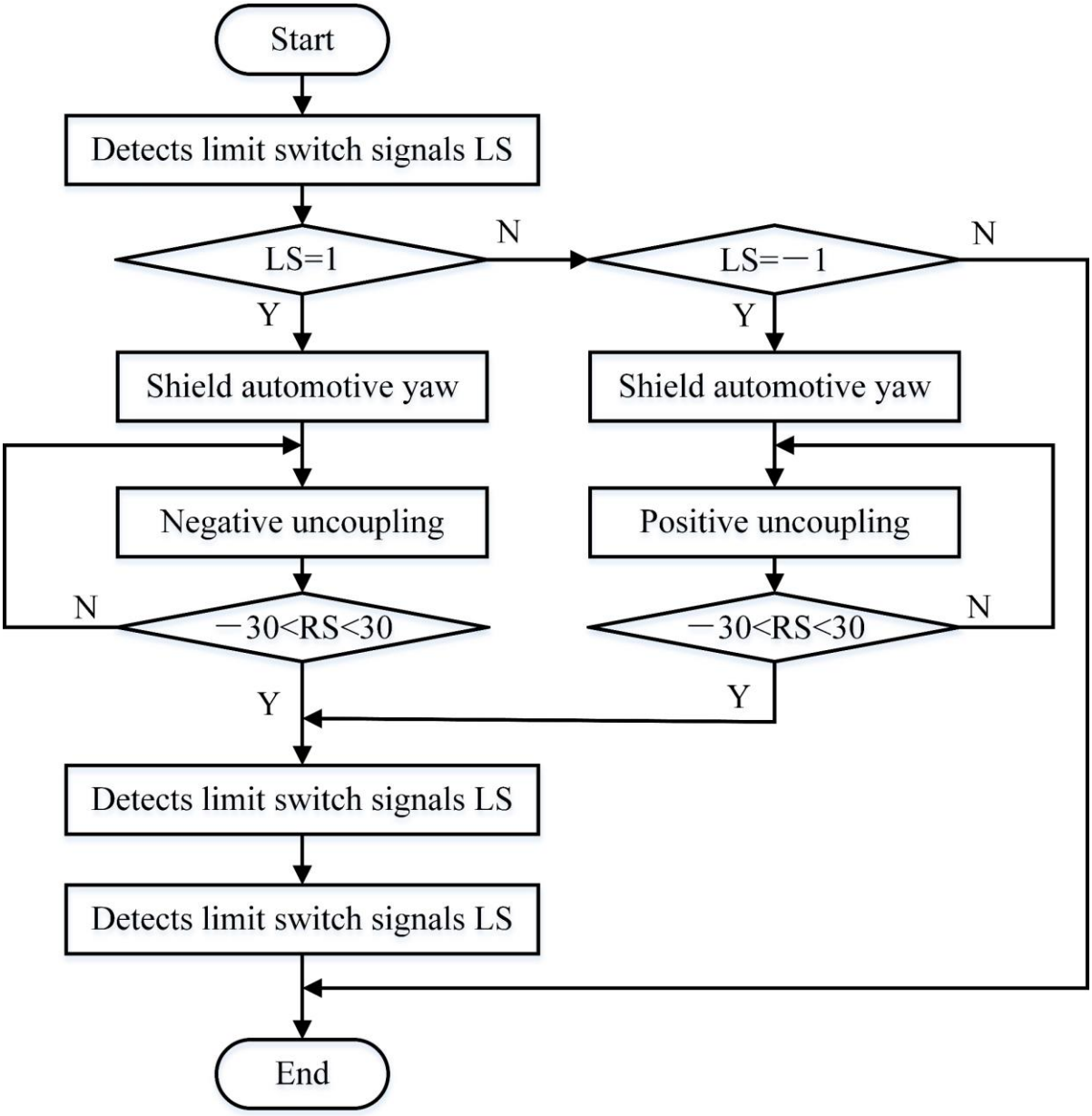

Figure 1.14. The flow chart of automotive cast loose

1.3.3 Typical yaw control strategies

At present, the mainstream WTs in the world adopt horizontal axis wind power generation, and the yaw system is indispensable as its unique mechanism. The stability of the operation of the yaw system determines the benefit of the WT and also the service life of the WT. To ensure that the yaw system can operate as stably as possible and improve the power generation and economic benefits of WTs, a lot of research and analysis has been done in recent years on the active yaw control algorithms mainly applied to large WTs, and various effective strategies and algorithms for completing the yaw system against the wind have been proposed, among which the representative research results are shown in **Figure 1.15**.

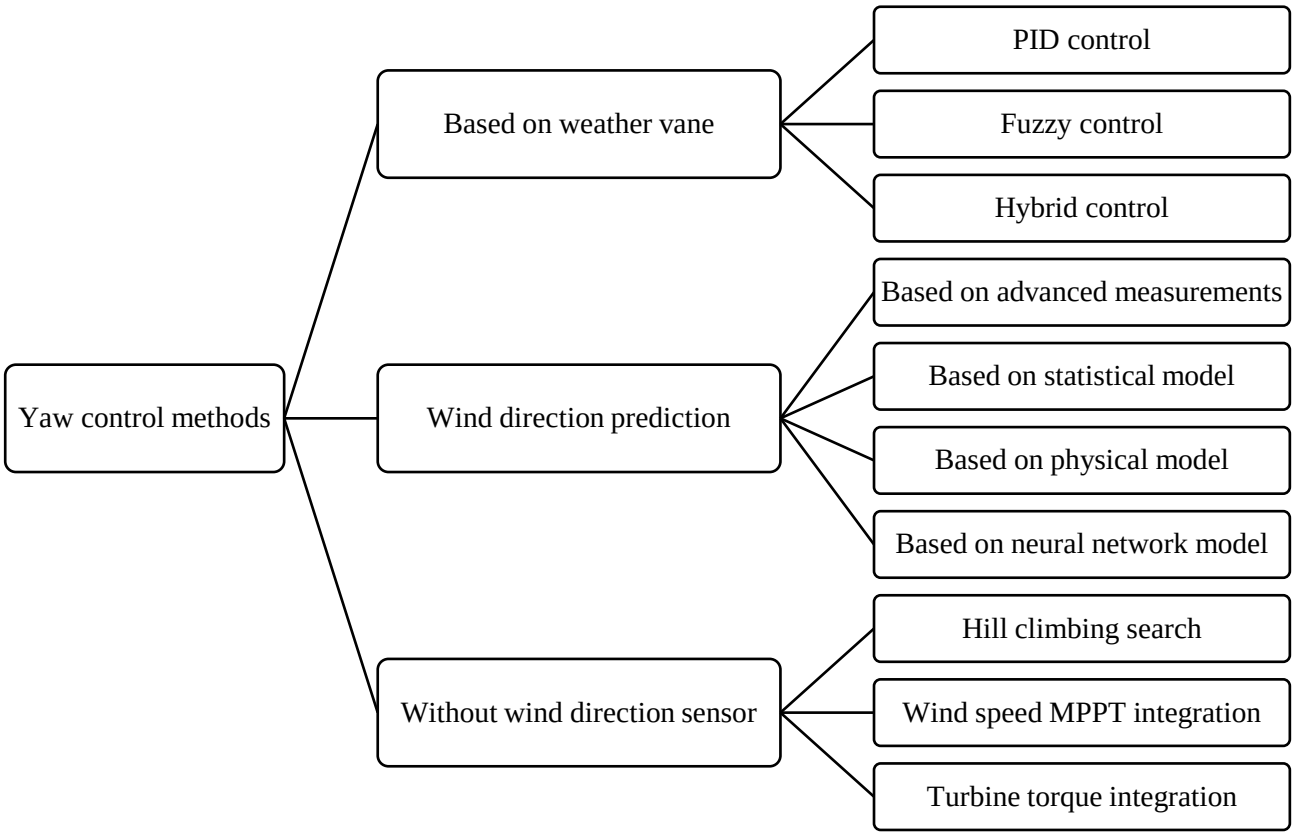

Figure 1.15. Control strategies for wind turbine yaw system

Generally speaking, yaw control methods can be divided into three categories: (1) based on weather vane; (2) wind direction prediction; (3) without wind direction sensor.

Among them, the yaw control method based on the weather vane is mainly based on a single control model, such as PID control [19], fuzzy control [59], Kalman control [60] and so on. These are all based on the wind direction information provided by the weather vane to control the WT, which has obvious shortcomings such as large error, low accuracy and yaw delay, so it is impossible to track the wind direction change in real time.

As for the wind direction prediction yaw control method, some advanced measurement equipment such as LiDAR [21], although the accuracy is high, but limited by expensive cost and immature technology, it cannot be widely used; as for the use of physical models [61], statistical analysis [62] and neural networks [63], the accuracy of wind direction prediction is relatively high, but the error of the prediction result is large in many cases.

For the yaw control method that does not require a wind direction sensor, the hill climbing search algorithm is more commonly used [64]. In theory, this algorithm can reduce the yaw error angle to the greatest extent, but in practical application, it is easily affected by the wind speed, and the size of the step size also directly affects the time and accuracy of the yaw; in addition, there is a method of combining the wind speed MPPT controller with the yaw, and the method of indirectly calculating the yaw angle according to the torque of the wind turbine. Because the yaw system is indirectly controlled, the accuracy is not high, there is also a yaw delay.

With the development of technology, hybrid control technologies have emerged, and many hybrid control technologies have appeared in yaw control methods, such as Vane-Hill Climbing (V-HC) [65], Kalman-Hill Climbing (K-HC) [66], Fuzzy-PID [67], etc. These hybrid control technologies can combine their advantages and avoid their disadvantages to the greatest extent. The existing hybrid control methods are shown in **Table 1.1**.

After analyzing the results of these hybrid yaw control methods, the following conclusions can be drawn. The hybrid control of LiDAR and SCADA systems has good accuracy (<5°) [68], but the high investment is not generally applicable at present. The hybrid yaw control method based on weather vane to provide wind direction information, such as V-HC, K-HC, Fuzzy-PID, Chaotic Particle Swarm Optimization - PID (CPSO-PID) [69], these hybrid control methods generally have strong robustness, it is easy to control. Although these hybrid control methods can compensate for the weather vane error to a certain extent, the overall yaw error is still in the range of 2° to 6°, if the parameters of the control system are not set properly, the error will be larger. Hybrid control methods based on wind direction prediction, such as Autoregressive integrated moving average - Kalman (ARIMA-Kalman) [70], Least-squares support-vector machines - Long short-term memory neural network (LSSVM-LSTM) [71], usually have higher prediction accuracy (<4°, the absolute error is about 2°), but in the case of large changes in wind speed, temperature and air pressure, the prediction result will have a large error (10°~20°). As for the hybrid yaw control method that does not require wind direction sensor, the advantages of MPPT-Active yaw method are that it

is easy to implement, low cost, and the accuracy is acceptable (5°) [26]. But the yaw error is indirectly calculated by wind speed and rotor speed, so it is influenced by wind speed sensor accuracy. In general, the hybrid control method is the trend of the future yaw system, which can avoid the shortcomings brought by the single control method to the greatest extent.

Table 1.1 Performance of hybrid yaw contorl system

<table>
<tr><th colspan="2">Hybrid methods</th><th>Advantages</th><th>Disadvantages</th><th>Error</th></tr>
<tr><td rowspan="5">Based on weather vane</td><td>LiDAR-SCADA</td><td>Measure wind direction information at a long distance</td><td>Have an expensive cost; related technologies are immature</td><td>< 5°</td></tr>
<tr><td>V-HC</td><td rowspan="2">Strong robustness, fast control speed</td><td rowspan="3">Rely on weather vane, cannot track the wind direction in real-time</td><td rowspan="3">2° ~ 6°</td></tr>
<tr><td>K-HC</td></tr>
<tr><td>Fuzzy-PID</td><td rowspan="2">Adaptivity (parameters adjust automatically), robustness</td></tr>
<tr><td>CPSO-PID</td></tr>
<tr><td rowspan="2">Wind direction prediction</td><td>ARIMA-Kalman</td><td rowspan="2">Predict future wind direction</td><td rowspan="2">Rely on historical data; wind uncertainty is not considered</td><td rowspan="2">< 4°</td></tr>
<tr><td>LSSVM-LSTM</td></tr>
<tr><td>Without wind direction sensor</td><td>MPPT-Active yaw</td><td>Easy to implement, low cost; without negative effect of wind direction sensor</td><td>Disturbed by wind speed</td><td>< 5°</td></tr>
</table>

By comparing these yaw control methods, it is not difficult to see that the performance of wind direction prediction (neural network prediction) and hill climbing

search method is generally more applicable, and the accuracy is high. Whether it is the design of new wind turbines or the retrofitting of old wind turbines, these two methods are the easiest to implement and cost-effective.

1.4 Conclusion of chapter 1

Chapter 1 classifies and summarizes the current problems in the operation of wind power generation according to the development trend of wind turbines and the evolution of wind power generation technology, and determines the direction and focus of the research to optimize the yaw error angle of the yaw system.

The yaw system can not only effectively improve the utilization rate of wind energy, but also reduce the unbalanced aerodynamic load on the blades and prolong the working life of the WT to a certain extent. However, most of the existing yaw control methods have problems such as large yaw error and yaw delay. Through analysis, the most effective methods to solve these problems are the hill climbing search method and the neural network predicting wind direction method. However, these two methods cannot perfectly solve the problems of the previous yaw system when they operate alone. Therefore, it is considered to combine the two methods to design a hybrid yaw control method to optimize the existing yaw system.

In order to solve the problem of yaw delay, the designed hybrid yaw control method first uses neural network to predict the wind direction in a single control cycle, and drives the nacelle to the position in advance according to the predicted future wind direction, so as to avoid the power loss caused by slow and untimely yaw speed. In order to solve the problem of large yaw error and wind direction fluctuation, the designed hybrid yaw control method uses the hill climbing search method to find the accurate wind direction position in the remaining time of the control period after the nacelle reaches the predicted position. It can also track changes in wind direction in real time with high precision.

The hybrid yaw control method designed in this dissertation has the advantages of small yaw error, easy implementation and cost-effectiveness. Whether upgrading the yaw system of the old wind turbine or designing the yaw system of the new wind turbine, this hybrid yaw control method is the best choice.

CHAPTER 2: WIND ENERGY CONVERSION SYSTEM ANALYSIS AND MODELING

In this chapter, the operating principle of the wind energy conversion system and yaw system is introduced. The aerodynamic changes of the wind turbine during the yaw process are also analyzed in detail, as well as the resulting problems, such as yaw aerodynamic load and power loss. At the same time, according to the aerodynamic model of the wind turbine and the mathematical model of the power equipment in the WECS, a simulation model is built in MATLAB/Simulink to simulate the target wind turbine and test various control algorithms.

2.1 Basic theory of wind turbine aerodynamics

2.1.1 Momentum theorem in yaw process

Direct application of the momentum theorem to the blade disk in yaw is problematic (assuming a rotating blade as a disk). For the whole blade, the momentum theorem can only be used to determine the average induced velocity. In the absence of yaw, some variation in the induced velocity of the blade is allowed in the radial direction; however, in yaw process, the induced velocity cannot be treated in this way because the annular volume of the blades varies with orientation. If the force acting on the blade disk is perpendicular to the blade disk, then the average induced velocity caused by the change in fluid momentum is also perpendicular to the blade disk. Due to the influence of the component of the induced velocity perpendicular to the wind direction, the wake yaws to one side. When there is no yaw movement, the average induced velocity y of the blade disk is half of that with wake [72].

If the wind direction is kept fixed, the angle between the blade axial direction and the wind direction, i.e. the yaw angle, is made Y, as shown in **Figure 2.1**. It is assumed that the change of momentum in the blade axial direction is equal to the rate of change of the mass flow through the blade disk during this time and the rate of change of the velocity perpendicular to the blade disk [73][74].

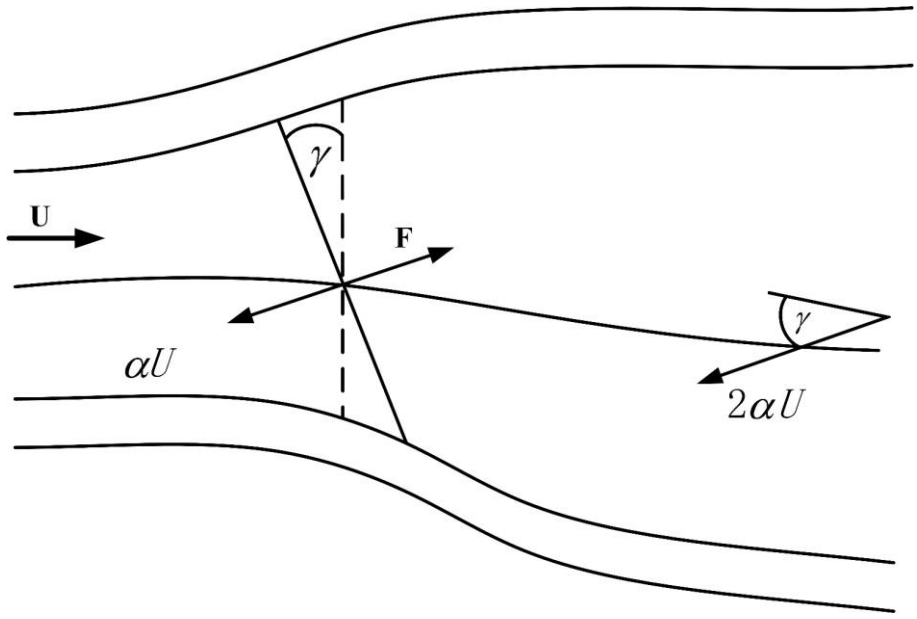

Figure 2.1. Offset wake and induced velocity during wind turbine yaw process

The force of the air acting on the blade disk is

$$\mathrm{F} = \rho \mathrm{A_d} U_\infty (cos\gamma - \alpha) 2\alpha U_\infty \tag{2.1}$$

Where ρ is the air density through the blade disk, $\mathrm{A_d}$ is the cross-sectional area of the blade disk, $\mathrm{U_\infty}$ is the air flow velocity at infinity, γ is the yaw angle, and α is the axial induction factor.

Therefore, the thrust coefficient of the blade is

$$\mathrm{C_T} = \frac{F}{\frac{1}{2}\rho A_d U_\infty^2} = 4\alpha(cos\gamma - \alpha) \tag{2.2}$$

Then the generated power is

$$\mathrm{P} = \mathrm{F U_\infty}(cos\gamma - \alpha) = \frac{1}{2}\rho A_d U_\infty^3 4\alpha(cos\lambda - \alpha)^2 \tag{2.3}$$

The wind energy utilization coefficient of the turbine is

$$\mathrm{C_P} = \frac{P}{\frac{1}{2}\rho A_d U_\infty^2} = 4\alpha(cos\gamma - \alpha)^2 \tag{2.4}$$

In order to find the maximum value of $\mathrm{C_P}$, the axial induced factor α in **Eq. (2.4)** is derived and made to be zero, then we have

$$\alpha = \frac{\cos\lambda}{3} \tag{2.5}$$

$$\mathrm{C_{Pmax}} = \frac{17}{26}\cos^3\gamma \tag{2.6}$$

Figure 2.2 shows the variation of power decreasing with increasing yaw angle. When the yaw error is 0°, that is, the wind turbine is exactly facing the wind and there is no yaw error, $\alpha = 1/3$, C_P=16/27≈0.593. C_P≈0.593 is the maximum value that the wind energy utilization coefficient can reach is called the Betz limit, which is also the theoretical maximum value that the wind energy utilization coefficient of a wind turbine can reach, but this value cannot be reached in actual operation. When the yaw error is not equal to 0°, that is, when the wind turbine is in the yaw state, the above momentum theorem can be used to determine the average axial flow induced velocity for the entire wind turbine, but the axial flow induction factor is affected by the yaw error. In this case, it is not suitable to apply the momentum theorem to each blade element at different positions.

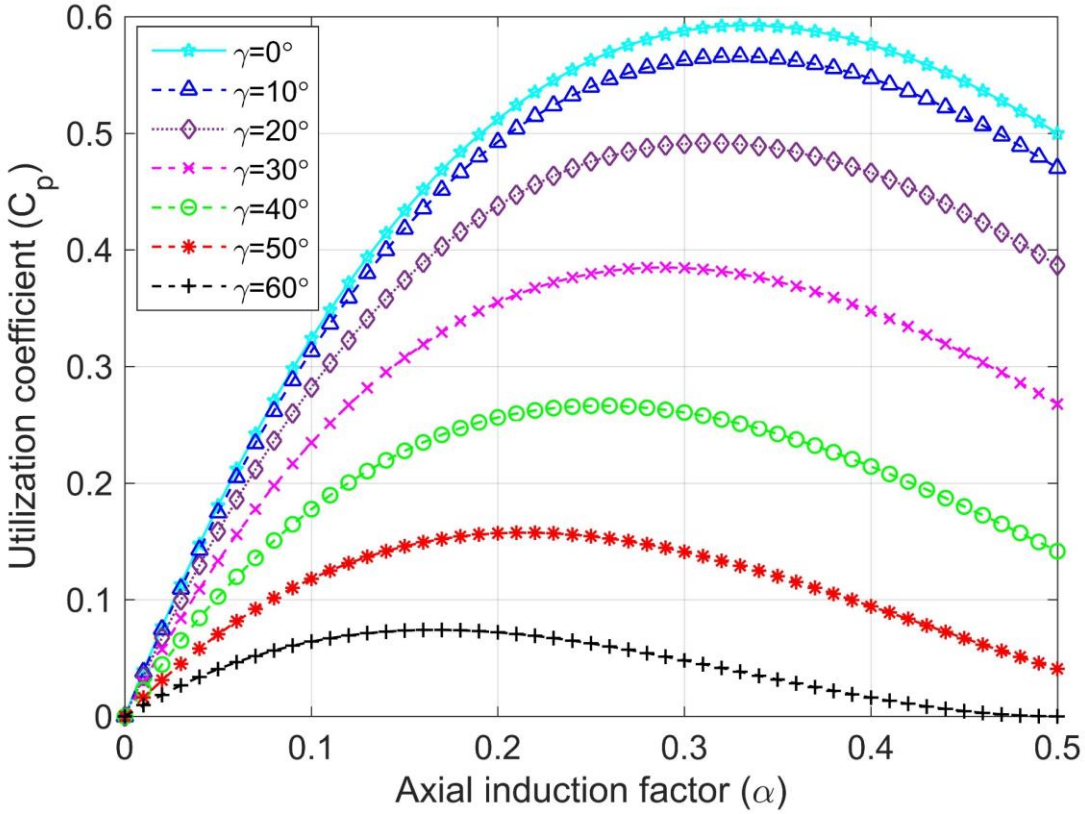

Figure 2.2. Curves of wind energy utilization coefficient with yaw angle and axial induction factor

The $\cos^3\gamma$ law is generally applicable to the power assessment of wind turbines when they are yawed. The above analysis can be used to determine the average axially induced velocity on the blade, but it is not appropriate to apply momentum theory to each blade element compared to the case without yaw [75].

2.1.2 Blade element theory in yaw process

To analyze the blade element theory in yaw process, we must first start from the blade element theory without yaw. The blade element is the blade divided into many micro-segments along the axial direction, and each micro-segment is a blade element. A single blade element is thought to be a two-dimensional airfoil, along the blade axial to the blade element on the force and moment of integration, so that the airflow on the blade force and moment can be calculated [76].

For a wind turbine with the number of blades being N, the radius of the blade tip being R, the chord length of the blade element being c, the pitch angle (the angle between the blade disk and the zero lift line of the airfoil) being β, and both the chord length and the pitch angle varying along the blade axis [77], as shown in **Figure 2.3**.

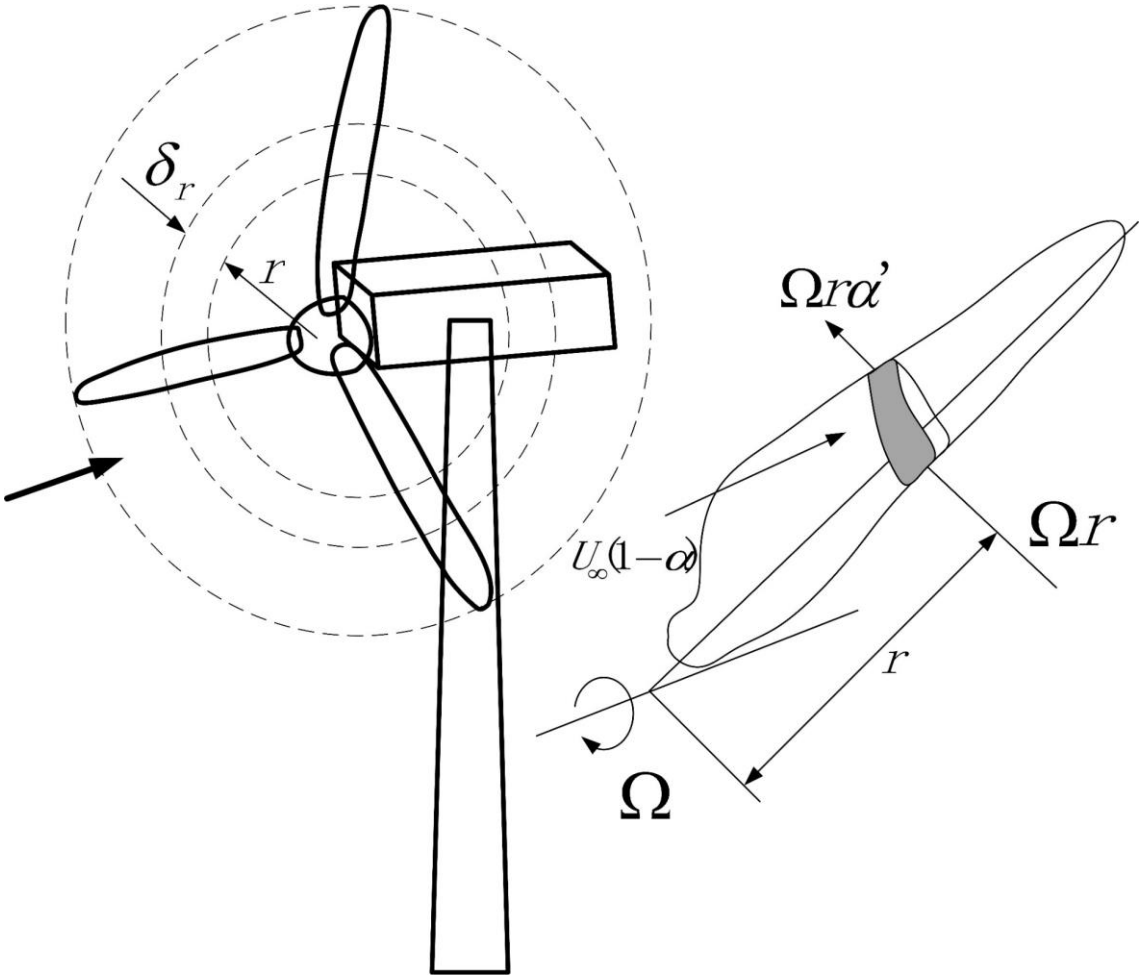

Figure 2.3. Sweep circle of blade element

At the same time, considering the rotation of the wake, the airflow downstream of the blade rotates at a tangential speed of $2\alpha'\Omega_r$ at a radial distance r from the rotation axis. **Figure 2.4** illustrate all the velocities and forces on the blade element at

radius *r* with respect to the chord length. Let the rotational angular velocity of the blade be Ω and the incoming wind speed be U_∞; the sum of the tangential velocity Ω_r of the blade element and the tangential velocity $\alpha'\Omega_r$ of the wake is the net tangential flow velocity $\Omega_r(1+\alpha')$ of the blade [74].

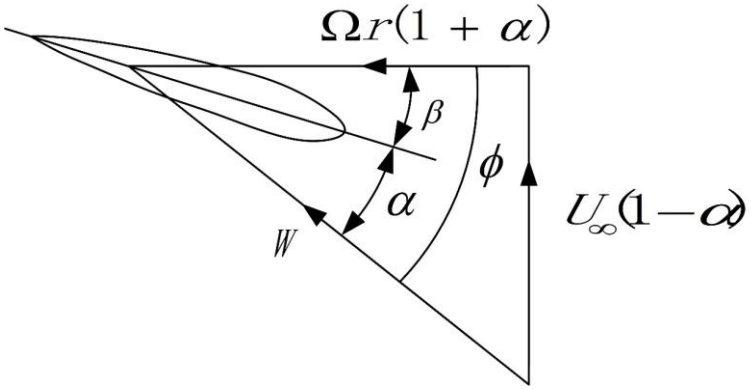

Figure 2.4. Blade element velocities

From **Figure 2.4**, we can obtain the ensemble velocity on the blade element as

$$W = \sqrt{U_\infty^2(1-\alpha)^2 + \Omega^2 r^2(1+\alpha')^2} \tag{2.7}$$

The angle between the combined velocity and the rotating blade disk is ϕ, then

$$\sin\phi = \frac{U_\infty(1-\alpha)}{W} \tag{2.8}$$

$$\cos\phi = \frac{\Omega r(1+\alpha')}{W} \tag{2.9}$$

The angle of attack here is

$$\alpha = \phi - \beta \tag{2.10}$$

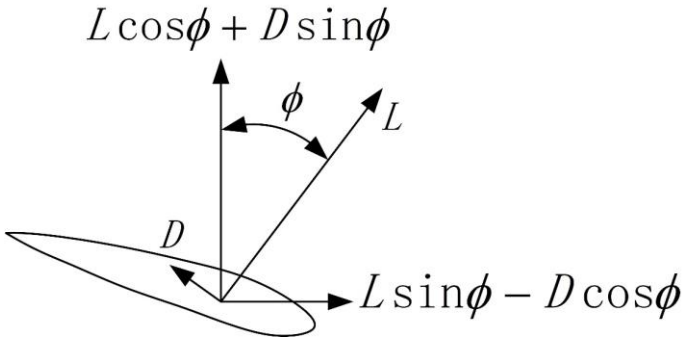

Figure 2.5. Blade element forces

According to the α, the lift-drag coefficients C_l and C_d of the blade element airfoil can be obtained by looking up the difference table, the local blade element coordinate system is shown in **Figure 2.5** [78][79].

The lift force perpendicular to the direction of the combined velocity W at the wingspan length δr on the blade is

$$\delta \mathrm{L} = \frac{1}{2}\rho W^2 c C_l \delta_r \tag{2.11}$$

The resistance parallel to the direction of the combined velocity W is

$$\delta \mathrm{D} = \frac{1}{2}\rho W^2 c C_d \delta_r \tag{2.12}$$

Let $\mathrm{C_x}$ be the normal coefficient, and $\mathrm{C_x} = C_l cos\phi + C_d sin\phi$

Let $\mathrm{C_y}$ be the tangential coefficient, and $\mathrm{C_y} = C_l sin\phi - C_d cos\phi$

The axial force acting on the ring of the blade disk at δ_r from the axis is

$$\mathrm{dF} = \frac{1}{2} N\rho c W^2 C_x \delta_r \tag{2.13}$$

The torque acting on this ring is

$$\mathrm{dM} = \frac{1}{2} N\rho c W^2 C_y r \delta_r \tag{2.14}$$

It is problematic to apply the blade element theory directly to a wind turbine in yaw conditions. Because the airflow on the local blade element is unstable in yaw process, and the blade element theory can only represent part of the equation of the vortex, it is incomplete to replace the momentum theory in this respect. However, it is not clear how large or important the non-constant force is. If the non-constant force is large, then the blade element theory is not applicable, and the results obtained by applying the theory will be irrelevant to the measurement results; if the non-constant force is small, then the results should have some correspondence with the actual values. The airflow velocity at any point on the blade disk during yaw will not vary with time, and if an infinite number of blades is assumed, then there is no additional mass term to consider. The variation of the angle of attack at any point on the blade with time means that the two-dimensional lift should be corrected by a lift deficit function.

Neglecting the effect of shedding wake, the net velocity on the blade element is shown in **Figure 2.6**. The velocity component in the radial direction is not represented in the figure because it has no effect on the angle of attack and lift [80].

The air flow angle ϕ is determined by the velocity component of the diagram:

$$\tan\phi = \frac{\begin{bmatrix} U_\infty\left(cos\gamma - \alpha(1 + jF(\mu)K(\chi)sin\psi)\right)\ldots \\ +\Omega r a' cos\psi sin\chi(1 + sin\psi sin\chi) \end{bmatrix}}{\left(\Omega r\left(1 + \alpha' cos\chi(1 + sin\psi sin\chi)\right)\right)\ldots} \tag{2.15}$$
$$+U_\infty cos\psi\left[\alpha tan\frac{\chi}{2}(1 + F(\mu)K(\chi)sin\psi) - sin\gamma\right]$$

where r is the radius of the circle, $\mu = \frac{r}{R}$,, F(μ) is the airflow expansion coefficient, K(χ) is the wake tilt angle function, and ψ is the blade azimuth angle measured in the direction of rotation.

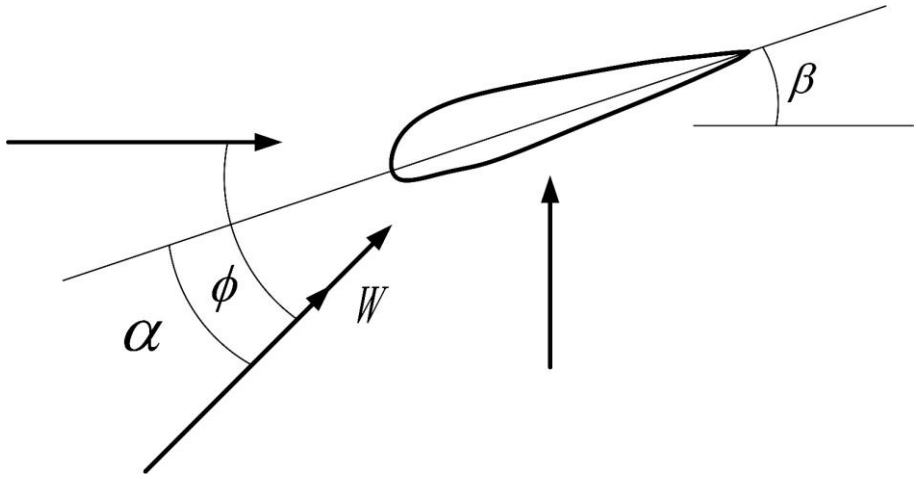

Figure 2.6. Velocity components on leaf elements

The angle of attack α is

$$\alpha = \phi - \beta \tag{2.16}$$

The angle of attack of the blade element can still be calculated from **Eq. (2.10)**. The lift and drag coefficients of the airfoil are the same as in the case of no yaw error, and also depend on the calculation of the angle of attack of each blade element. According to the above corrected blade element theory at yaw, the wind load acting on the blade element sweep ring can be calculated.

2.1.3 Blade element-momentum (BEM) theory in yaw process

According to the assumptions of BEM theory, the forces acting on a blade element are balanced with the momentum change produced by the airflow through the blade element [76] [81]. Since the directions of the axial momentum change and the angular momentum change of the airflow passing through the micro-ring are perpendicular and parallel to the rotor rotation plane, respectively, it is necessary to decompose the aerodynamic components in the local blade element coordinate system

to these two directions [36][74]. For a radius of r and a radial thickness of δ_r the thrust force on the entire ring can be calculated by the following equation:

$$\delta L\cos\phi + \delta D\sin\phi = \frac{1}{2}\rho W^2 Nc(C_l cos\phi + C_d sin\phi)\delta_r \tag{2.17}$$

The angle corresponding to the unit area swept out on the ring when the blade rotates is $\delta\psi$. The unit force applied at this time is

$$\delta F_b = \frac{1}{2}\rho W^2 Nc(C_l cos\phi + C_d sin\phi)\delta_r \frac{\delta\psi}{2\pi} \tag{2.18}$$

Where $C_x = C_l cos\phi + C_d sin\phi$, and the real degree of chord length $\sigma_r = \frac{Nc}{2\pi r}$, then

$$\delta F_b = \frac{1}{2}\rho W^2 \sigma_r C_x r\delta_r\delta\psi \tag{2.19}$$

Considering the blade tip loss, the induced factor α of the airflow should be replaced by αf, using the vortex theory then

$$\delta F_m = \frac{1}{2}\rho U_\infty^2 4\alpha f\left(\cos\gamma + \tan\frac{\chi}{2} sin\gamma - \alpha f sec^2\frac{\chi}{2}\right) r\delta\psi\delta_r \tag{2.20}$$

The pressure drop due to rotating wake is not included in Eq. (2.20), but if the pressure drop is included, it is necessary to calculate the rotating wake velocity using vortex theory. Even if fluctuations in the amount of vortex ring attached to the blade are ignored, the operation to calculate the rotating wake velocity is still complex. Since the pressure drop due to the rotating wake is small in the absence of yaw process, it can be assumed that the pressure drop due to the rotating wake is negligible in the case of yaw process [82][83][84].

The moment of the force applied to the axial blade element in the wake is

$$\delta M_b = \frac{1}{2}\rho W^2 Nc\left(cos\psi sin\chi C_x + cos\chi C_y\right) r\delta_r \frac{\delta\psi}{2\pi} \tag{2.21}$$

Where $\sigma_r = \frac{Nc}{2\pi r}$, then

$$\delta M_b = \frac{1}{2}\rho W^2 \sigma_r\left(cos\psi sin\chi C_x + cos\chi C_y\right) r^2\delta_r\delta\psi \tag{2.22}$$

By applying the momentum theorem to the entire blade element sweeping annular surface element, the distribution of the axial flow induction factor α with the

radius r can be obtained, which reflects the radical change of the annular volume. Therefore, it is necessary to integrate along the ring to solve the momentum change rate on the entire blade element swept surface. For the axial momentum, we have

$$\int_0^{2\pi} \frac{1}{2}\rho U_\infty^2 4\alpha f\left(cos\gamma + \tan\frac{\chi}{2} sin\gamma - \alpha f sec^2\frac{\varphi}{2}\right) r\delta_r d\psi = \int_0^{2\pi} \frac{1}{2}\rho W^2 \sigma_r C_x r\delta_r d\psi$$

After simplification, we get

$$8\pi\alpha f\left(\cos\gamma + \tan\frac{\chi}{2} sin\gamma - \alpha f sec^2\frac{\chi}{2}\right) = \sigma_r \int_0^{2\pi} \frac{W^2}{U_\infty^2} C_x d\psi \tag{2.23}$$

The rate of change of angular momentum is the product of the mass flow per unit area through the blade disk and the tangential velocity and radius

$$\delta M_m = \frac{1}{2}\rho U_\infty^2 \lambda\mu 4\alpha' f(cos\gamma - \alpha f)(\cos^2\psi + \cos^2\chi \sin^2\psi) r^2\delta_r\delta\psi \tag{2.24}$$

Integrating along the ring, we have

$$\int_0^{2\pi} \frac{1}{2}\rho U_\infty^2 \lambda\mu 4\alpha' f(cos\gamma - \alpha f)(\cos^2\psi + \cos^2\chi \sin^2\psi) r^2\delta_r d\psi$$

$$= \int_0^{2\pi} \frac{1}{2}\rho W^2 \sigma_r (cos\psi sin\chi C_x + cos\chi C_y) r^2\delta_r d\psi$$

After simplification, we get

$$4\alpha' f(\cos\gamma - \alpha f)\lambda\mu\pi(1 + \cos^2\chi) = \sigma_r \int_0^{2\pi} \frac{W^2}{U_\infty^2}(cos\psi sin\chi C_x + cos\chi C_y) d\psi \tag{2.25}$$

The integral values in equations **Eq. (2.23)** and **Eq. (2.25)** can be determined, and their solutions can be solved by multiple iterations. The initial values of α and α' are both zero. In the yaw state, for each blade element position μ and azimuth angle ψ on a given blade, the inflow angle ϕ can be calculated from **Eq. (2.15)**. If the pitch angle β of the blade element is also known, the angle of attack α can be obtained according to **Eq. (2.10)**. Lift coefficient C_l and drag coefficient C_d can be found in the airfoil data. After obtaining the position value (constant μ) of the sweep ring, it can be calculated by integrating. The new value of the axial induction factor α can be solved by **Eq. (2.23)**, and the tangential induction factor α' can be solved by **Eq. (2.25)**. Repeated iterations are performed for the same sweep ring until a satisfactory convergence effect is achieved before moving to the next sweep ring position (constant

μ). As long as the tangential induction factor α' is calculated, the basic form of the blade element theory (**Eq. (2.19)**) and the momentum formula (**Eq. (2.20)**) can be used to find the value of the axial induction factor α that varies with the azimuth angle. The above is the blade element-momentum theory for stable yaw.

2.2 Load and yaw error during yaw process

Wind turbine axes and wind direction are usually not parallel, and wind turbines operate in a yaw condition in most cases. The efficiency of a WT in yaw condition is lower than the efficiency of a WT in precise wind alignment, and the efficiency assessment is a crucial indicator when evaluating the energy output of a wind farm.

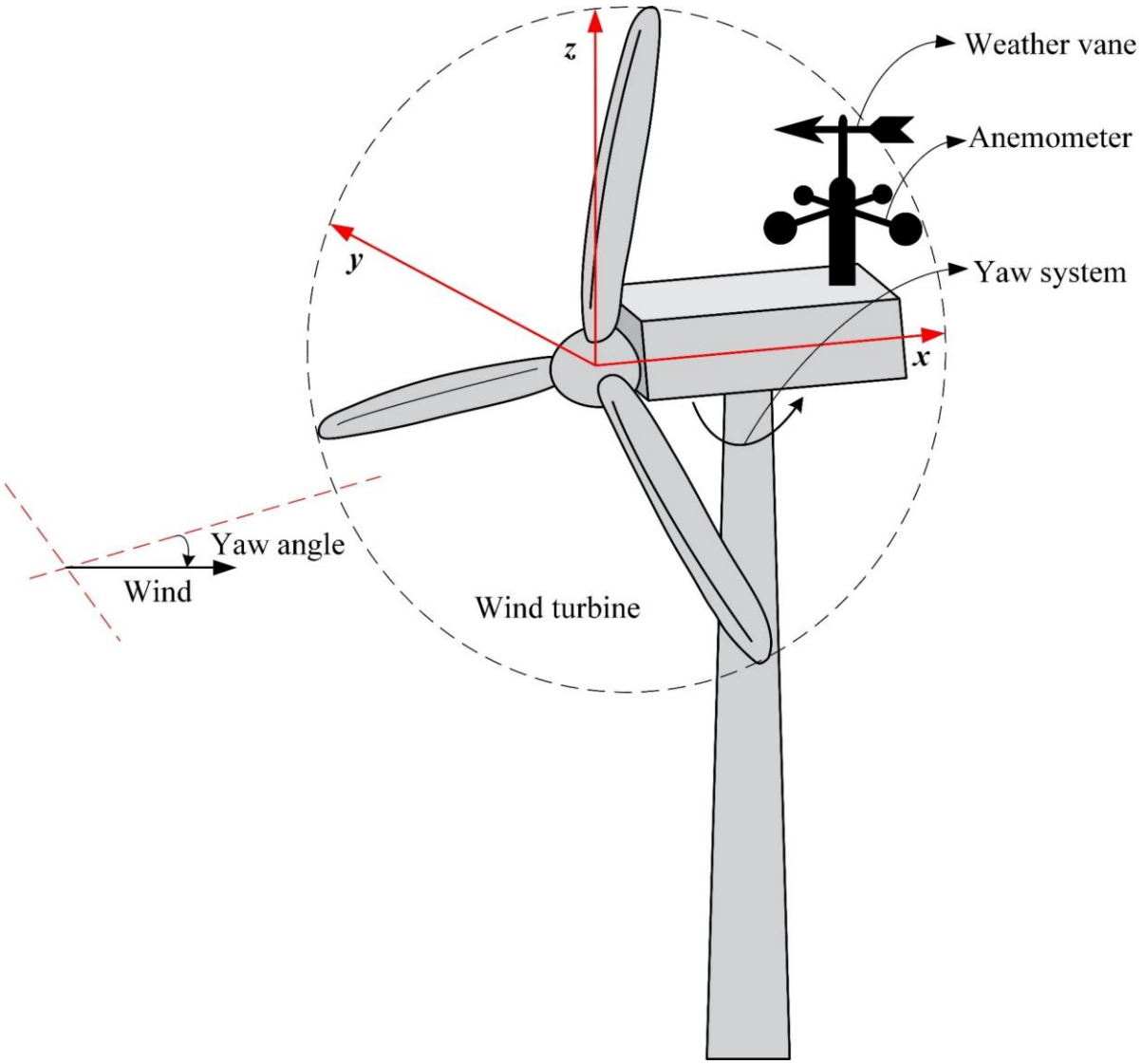

Figure 2.7. Wind turbine coordinate system and yaw error angle

When the wind speed is stable, if the yaw error is 0°, the wind turbine is precisely aligned with the wind, the induced speed on the whole blade disk is the same, and the

load on the wind turbine is balanced; if the yaw error is not 0°, the wind turbine deviates from the wind direction by an angle [85], as shown in **Figure 2.7**.

Due to the rotation of the wind turbine, the induced speed will change at different azimuth and radial positions, and the angle of attack of each blade will also change continuously. At this time, the force acting on the blades will not only produce driving torque and axial thrust, but also pitch torque and yaw torque. The load on the wind turbine is fluctuating, and the fluctuation of the load is related to the size of the yaw error, which makes the estimation of wind turbine characteristics complicated [86][87].

The wind direction is constantly changing during the actual operation of wind turbines in wind farms, and there is a certain lag in the tracking of the wind direction by the blade, so the axial direction of the blade of the wind turbine is not always parallel to the wind direction. In order to improve the wind energy capture rate of the blade, the wind turbine needs to yaw against the wind frequently. Due to the aerodynamic characteristics of the yaw process, this will cause the unit to generate yaw load, including yaw angle and wind speed changes resulting in resistance moment and gyroscopic force. The yaw load will cause the yaw speed fluctuation of the yaw system, and the yaw speed fluctuation will cause the unit to generate additional load, which in turn will pose a threat to the stability and safety of the unit operation [88].

2.2.1 Blade force and moment during wind turbine yaw process

(1) Blade force

Once the airflow induced factor is derived (**Eq. (2.5)**), the blade force can be calculated [78][89]. The blade normal force perpendicular to the rotating surface of the blade on the unit wingspan is

$$\frac{\mathrm{d}}{\mathrm{dr}}F_x = \frac{1}{2}\rho W^2 c C_x \tag{2.26}$$

Its variation is synchronized with the variation of the blade azimuth. The combined force perpendicular to the blade rotation plane can be obtained by integrating the different azimuth angles along the length of each blade by and then summing them.

Similarly, the blade tangential force per unit wingspan is:

$$\frac{\mathrm{d}}{\mathrm{dr}}F_y = \frac{1}{2}\rho W^2 c C_y \tag{2.27}$$

The torque on the blade about the blade rotation axis is:

$$\frac{\mathrm{d}}{\mathrm{dr}}Q = \frac{1}{2}\rho W^2 crC_y \tag{2.28}$$

As with the normal force, the total torque is obtained by integrating along the axial direction of each blade and summing over all blades. The blade torque will also vary with the azimuth position, so in order to find the average torque value, the azimuth angle needs to be integrated again [90][91][92].

(2) Yaw moment and tilt moment of wind turbine yaw

As the airflow is expandable, the airflow flowing through the blade during yaw process is not uniform, and the angle of attack of the blade in the upper wind region is larger than that in the lower wind region [73][74][93], as shown in **Figure 2.8**. Therefore, the lift in the upper wind region of the blade is greater than that in the lower wind region, and the differential of the force perpendicular to the blade disk is distributed in this manner. This results in a net moment based on the yaw axis to align the axial direction of the blade with the wind direction [35], i.e., the yaw moment.

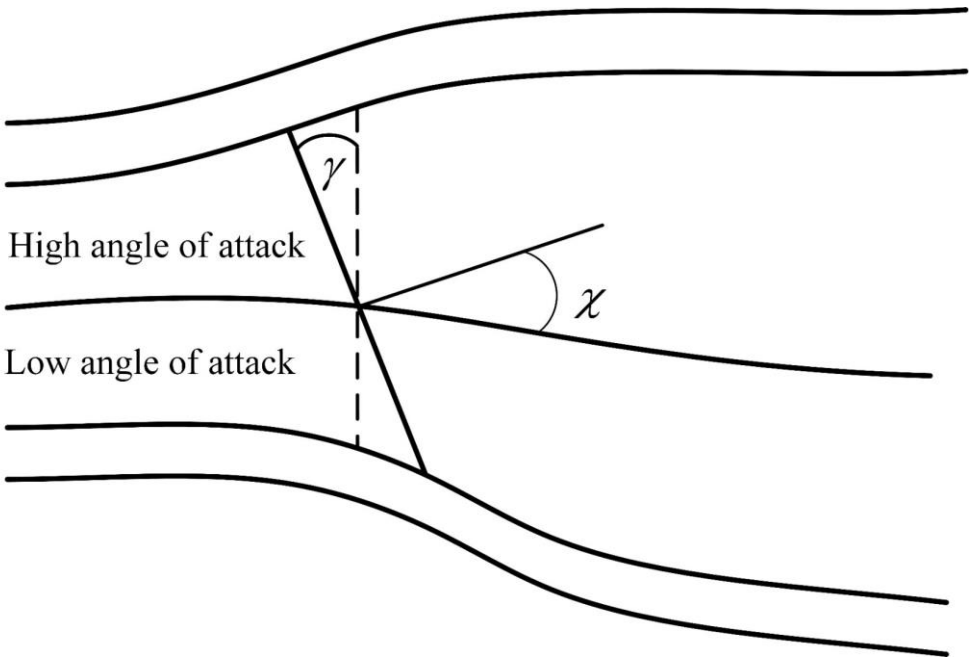

Figure 2.8. Different angles of attack due to airflow expansion

The yaw moment can be obtained from the **Eq. (2.26)** for the force perpendicular to the blade disk [73][94].

$$\frac{\mathrm{d}}{\mathrm{dr}}M_x = \frac{1}{2}\rho W^2 crsin^h \psi C_x \tag{2.29}$$

It also varies with the azimuth of the blades. The total yaw moment of a single blade at each azimuthal position can be obtained by integrating along the blade axis. The yaw moment on the blade during the wind turbine yaw process is obtained by summing the moments of all blades in the corresponding phase.

The tilting moment at yaw can be obtained by a similar calculation, which is a moment about the horizontal diameter axis of the blade [74].

$$\frac{\mathrm{d}}{\mathrm{dr}}M_z = \frac{1}{2}\rho W^2 crcos^h \psi C_x \tag{2.30}$$

and consequently, the yaw moment and tilting moment are reduced (typical values h = 1.0–3.0) [35]. For different operating conditions and wind turbine types, the value of h is different. Normally, the value of h is 1, but in some special cases, the value of h may be 2 or 3.

2.2.2 Calculation of the compensation angle for the correction of the weather vane error

1) Wind error

The yaw control process of the WT is to transmit the wind direction signal measured by the weather vane to the yaw controller for yawing action. The weather vane itself has an inherent accuracy when it is designed, and because the weather vane is usually installed at the end of the nacelle on the WT, which leads to the weather vane in the WT with the measured wind direction accuracy is not high, there is a certain error. Usually use the following two parameters to measure the weather vane error: the wind error value and the wind error variance value. The wind error is the angular displacement of the wind direction relative to the axial direction of the blade [95].

At present, all WTs that use weather vane to measure wind direction have wind measurement errors. This error is due to the inherent accuracy of the weather vane is very small, usually around 1°. Mainly because the weather vane is installed at the end of the nacelle, when the wind blows through the blade before the weather vane measurement, and the rotating blade will produce a rotating vortex, thus affecting the wind direction of the wind flowing through the blade, which leads to the wind direction measured by the weather vane and the actual wind direction blowing to the blade there

is a large error. The wind blowing to the blade will produce tangential induced velocity and axial induced velocity, usually the influence of the blade rotating vortex on the wind is commonly used to determine the axial and tangential induced factors, so we can correct the wind error by finding the induced factor and calculating the compensation angle that should be increased [20]. The calculation of the compensation angle is based on the derived axial and tangential induced factors by means of the trigonometric equation.

In **Section 2.1**, we introduced the blade momentum theory, and here we can calculate the axial and tangential induced factors by the blade momentum theory. It is assumed that the wind speed is 12m/s, the blade speed is 10 rad/s, the blade is divided into 30 parts, the initial value of the axial induction factor is 0.3, and the tangential induction factor is 0.

$$8\pi\alpha f\left(\cos\gamma + \tan\frac{\chi}{2} sin\gamma - \alpha f sec\frac{\chi}{2}\right) = \sigma_r \int_0^{2\pi} \frac{W^2}{U_\infty^2} C_x d\psi \tag{2.31}$$

$$4\alpha' f(\cos\gamma - \alpha f)\lambda\mu\pi(1 + \cos^2\chi) = \sigma_r \int_0^{2\pi} \frac{W^2}{U_\infty^2} (cos\psi sin\chi C_x + cos\chi C_y) d\psi \tag{2.32}$$

Using **Eq. (2.31)** and **Eq. (2.32)** iteratively to know the convergence, the two induced factors can be found as: α=0.4233, α'=0.0686. Therefore, the compensation angle θ' can be calculated for the wind direction angle measurement error caused by the blade rotation, as shown in **Eq. (2.33)**.

$$\theta' = \arctan\left(\frac{\alpha'}{\alpha}\right) \tag{2.33}$$

In this condition, $\theta' = \arctan\frac{0.0686}{0.4233} \approx 9$. The relationship between the compensation angle and the tangential induced factors in the same direction is shown in **Figure 2.9** [96].

By adding the compensation angle to the wind direction data measured by the weather vane, the error between the corrected wind direction data and the actual wind direction is obviously reduced. So in order to reduce the measurement error of the weather vane of the wind turbine, the wind direction data should be the compensation angle add the measured wind direction data.

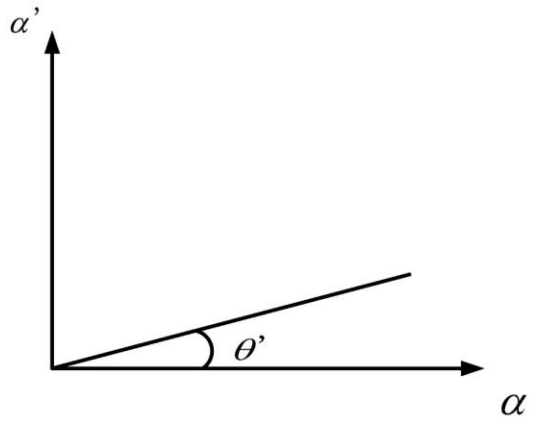

Figure 2.9. Relationship between correction compensation angle and induction coefficient

The actual operation of the error still exists is due to two reasons: on the one hand is due to the measurement data itself there is error, other hand is due to the blade airfoil type of the difference surface caused [97].

2) Yaw system tolerance angle with correction of compensation angle

After the error between the wind direction measured by the weather vane and the actual wind direction is solved by the correction of the compensation angle, the corrected wind direction data can be predicted directly by applying the neural network. The core of the four processes of WT yaw control is the automatic yaw function, which is also the yaw control process requiring the highest wind direction accuracy.

In the current common automatic yaw control, there is a tolerance angle. The existence of the tolerance angle is due to the fact that on the one hand, the wind direction changes randomly and uncertainly, with frequent transient changes, but the magnitude is not large, and there is a certain error in the wind direction measured by the weather vane; on the other hand, if the yaw system yaws frequently to the wind with the direction change, and the unit yaws during operation will inevitably produce the load fluctuation of the yaw system, and the load fluctuation will cause the rotational speed fluctuation of the yaw system. Yaw speed fluctuation will have a great impact on blade and tower vibration, which will pose a great threat to the safety and stability of wind turbines. Therefore, in order to reduce the load fluctuation caused by the frequent yawing of wind turbines, we can reduce the number of yaws by setting a tolerance angle, and then improve the stability of yaw system.

The tolerance angle of the current wind turbine is about 15°, which includes both the weather vane error and the tolerance angle to improve the yaw stability. The optimal yaw tolerance angle of wind turbine based on LIDAR wind measurement is 5°~7° [68][98], because the LIDAR wind measurement error is negligible, and the tolerance angle is only set to reduce the yaw action, reduce the load fluctuation and improve the stability of the turbine. The yaw tolerance angle of wind turbine with weather vane measurement can be set to 9° when the correction compensation angle is added. The yaw tolerance angle is reduced from 15° to 9°, which can largely reduce the asymmetric moment on the blade caused by the yaw to wind deviation, but the reduced yaw tolerance angle will inevitably lead to frequent yaw movements, which in turn will cause yaw load fluctuations and thus reduce the overall stability of the WT [99].

2.2.3 Yaw error and wind direction calculation

When the wind direction changes or the unit is not allowed to yaw against the wind, the wind direction will deviate from the wind turbine axis by a certain angle, which is called the yaw error angle, referred to as yaw error.

Studies have found that most of the time, modern wind turbines are in yaw operation, the causes of this phenomenon are many, boiled down to three main aspects: (1) the wind in nature is affected by many factors with great randomness, wind speed and wind direction are changing all the time. (2) the wind turbulence generated by the wind turbine in the upward direction after absorbing wind energy and making the local wind direction discrete, thus creating a large disturbance to the weather vane in the downwind direction of the wind turbine, which will keep swinging and reduce the accuracy of wind measurement and cannot accurately measure the actual wind direction, resulting in the yaw control system not getting the ideal control signal, which in turn leads to the low accuracy of the unit yaw to wind. (3) to avoid frequent yaw damage to the unit, the yaw control strategy of modern wind turbines requires the system to have certain inertia to ensure the stability of the overall operation of the unit, i.e. to maintain the current yaw attitude within a certain angle range and for a certain period when the average wind direction changes. All these factors make it impossible to align the turbine to the wind direction in real-time.

For horizontal axis wind turbine, to improve the utilization rate of wind energy and power generation efficiency, the WT should rotate the nacelle against the wind according to the shortest path during yaw process to eliminate the yaw error. Firstly, needs to solve the starting and steering problems of the yaw motor, then it is the correspondence between the wind angle θ_w, the angle of the wind turbine axis direction θ_r and the yaw angle θ_y. The angle between the wind direction and the wind turbine axis direction is as follows (all the angles mentioned are relative values) [48].

1) When the angle between the wind direction and the direction of the wind turbine axis is less than 180°, and the yaw angle in this case is:

$$\theta_y = \theta_w - \theta_r \tag{2.34}$$

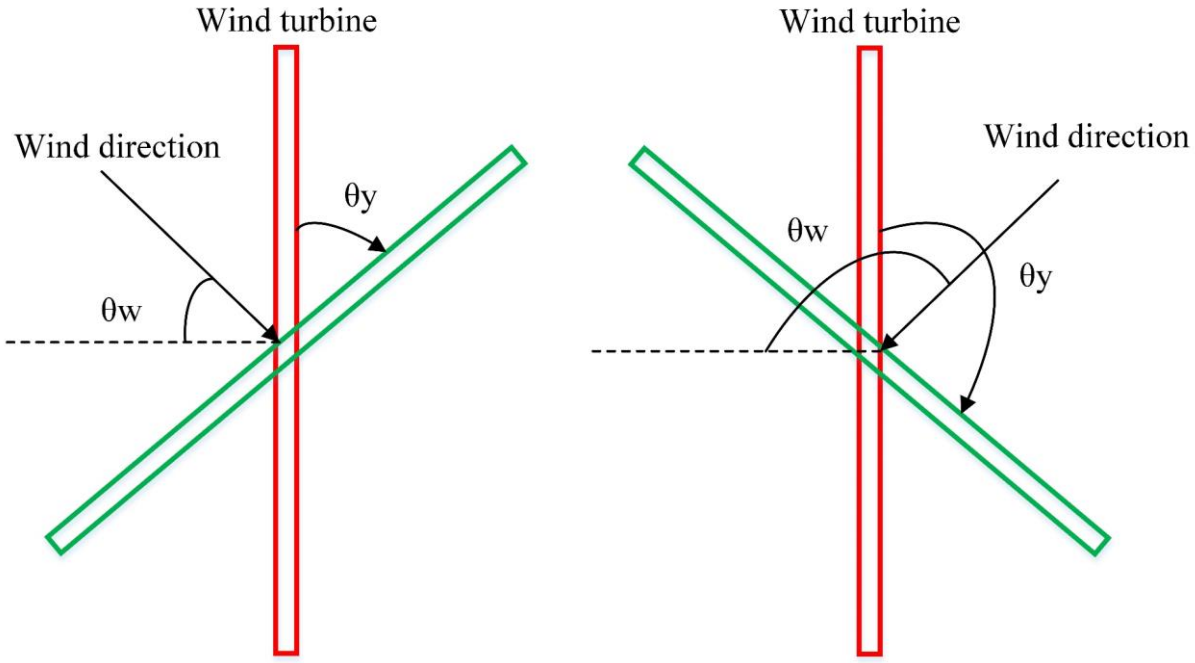

Figure 2.10. Yaw angle when the wind direction angle less than 180°

Normally, the wind direction angle is relative to the direction of the wind turbine axis, i.e., taking θ_r = 0°, then we can get

$$\theta_y = \theta_w \tag{2.35}$$

As shown in **Figure 2.10**, the red line represents the initial position of the wind turbine, and the green line represents the position of the wind turbine after yawing into the wind. At this time, the yaw drive motor is turning, and the nacelle is adjusted clockwise to θ_y.

2) The angle between the wind direction and the axis of the wind turbine is greater than 180°, and the yaw error angle at this time is

$$\theta_y = 360° - |\theta_w - \theta_r| \tag{2.36}$$

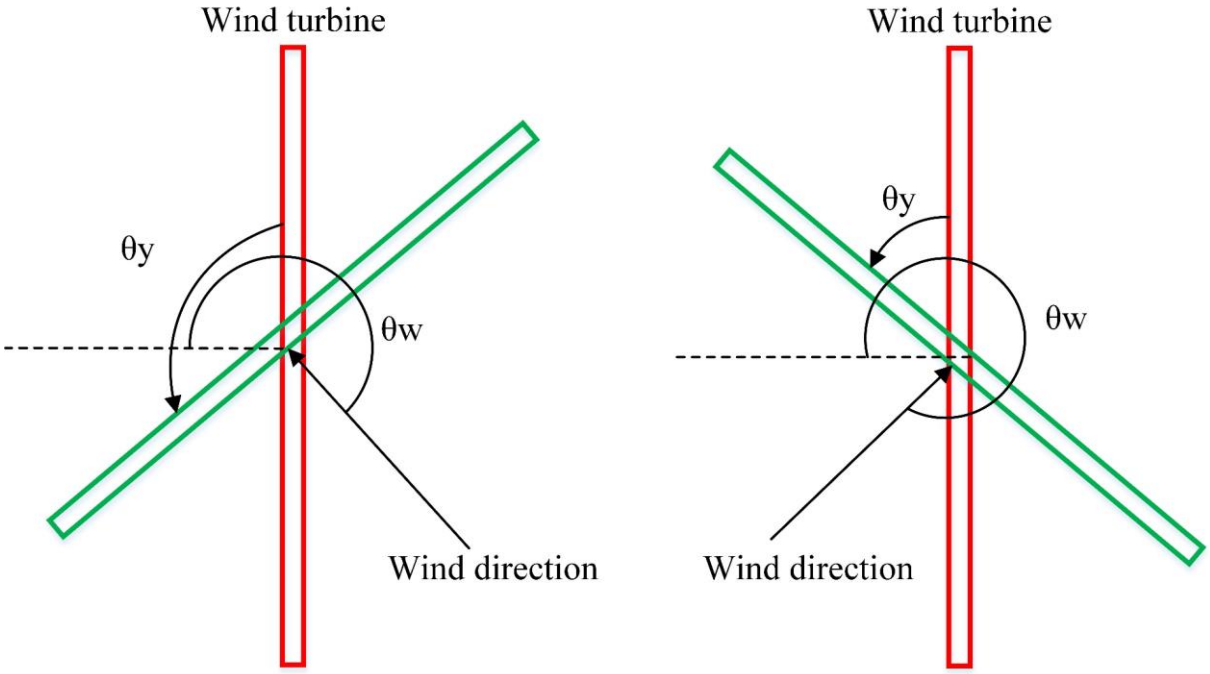

Figure 2.11. Yaw angle when the wind direction angles greater than 180°

As shown in **Figure 2.11**, the red line represents the initial position of the wind turbine, and the green line represents the position of the wind turbine after yawing against the wind. At this time, the yaw drive motor is reversed and the nacelle is adjusted counterclockwise to θ_y.

2.3 Wind energy conversion system modeling

2.3.1 Wind source modeling

Wind speed: The wind is a natural phenomenon on earth, caused by the heat radiated from the sun. The sun shines on the earth's surface, and the temperature difference between different parts of the earth's surface due to uneven heating causes atmospheric convection movement to form the wind. The natural wind has a size and direction and is usually described by wind speed or wind force to describe the size of the wind, and wind direction to describe the direction of the wind.

The operation status and power generation of wind turbines directly depends on the wind speed, so the focus is on the size of the wind speed and various factors affecting the wind speed such as turbulence, wind shear, and tower shadow effect. In

wind power technology, wind speed is often used: instantaneous wind speed, average wind speed, and hub wind speed.

The instantaneous wind speed refers to the instantaneous value of wind speed, which has a great influence on the short-time operation status and real-time power of the unit [100]. It is the main influencing factor of load fluctuation and power fluctuation [101][102].

The average wind speed refers to the average wind speed observed several times in a certain period, expressed by V_0. The average wind speed is an important parameter reflecting the wind resource condition.

The hub wind speed refers to the average wind speed at the center of the wind turbine, which is expressed as V_H. The hub wind speed is used for many design parameters such as cut-in wind speed, cut-out wind speed, rated wind speed, etc.

Real-time wind speed modeling methods that satisfy the statistical wind energy characteristics consist of many: one is to reproduce the time-series samples of wind speed from the perspective of wind speed power spectral density with known frequency domain information; one is based on time series theory, and wind speed modeling is realized by AR, ARMA and other models; and one describes wind speed by statistical data in the form of probability distributions (commonly used are Weibull and Rayligh probability distribution). However, these modeling methods require a large amount of actual wind field information, and the method of estimating parameters is troublesome and not suitable for dynamic wind speed simulation. In this chapter, a combined wind speed model (a combination of four types of winds: basic wind, gradient wind, gust wind, and random wind) is used, which can reflect the characteristics of wind conditions in nature and is also suitable for engineering simulations.

In order to more accurately describe the random and intermittent characteristics of wind energy, the spatiotemporal model of wind speed change usually divides the combined wind into four parts: basic wind, gust, gradient wind and random wind.

$$\mathrm{v(t)} = \bar{v} + v_g(t) + v_\tau(t) + v_n(t) \tag{2.37}$$

Where $\bar{v}$ is basic wind speed (m/s); v_g is gusts wind (m/s); v_τ is gradient wind speed (m/s); v_n is random wind speed (m/s).

(1) Basic wind speed

It always exists during the normal operation of the wind turbine and basically reflects the change of the average wind speed of the wind field. The magnitude of the rated power delivered by the wind generator to the system is also mainly determined by the basic wind. The Weibull distribution parameters obtained from the wind measurement of the wind farm can be approximately determined.

$$\bar{v} = c\Gamma\left(1 + \frac{1}{k}\right) \tag{2.38}$$

In the calculation, it is generally considered that the basic wind speed does not change with time, so a constant value can be taken.

(2) Gust wind

In order to describe the characteristics of sudden changes in wind speed, gusts are usually used for simulation. During this period, wind speed has a cosine characteristic. The dynamic stability analysis of power systems, especially when analyzing the impact of wind power systems on grid voltage fluctuations, examine the dynamic characteristics under large wind speed changes.

$$v_g = \begin{cases} 0 & t < t_{g1} \\ \frac{V_{gmax}}{2}\left[1 - cos2\pi\left(\frac{t - t_{g1}}{T_g}\right)\right] & t_{g1} \le t \le t_{g1} + T_g \\ 0 & t > t_{g1} + T_g \end{cases} \tag{2.39}$$

Where T_g is gust cycle; t_{g1} is gust start time; V_{gmax} is gust amplitude.

(3) Gradient wind

The gradual change of wind speed is simulated by gradient wind, that is,

$$v_\tau = \begin{cases} 0 & t < t_{r1} \\ V_{rmax}\dfrac{t - t_{r1}}{t_{r2} - t_{r1}} & t_{r1} \le t \le t_{r2} \\ 0 & t > t_{r2} \end{cases} \tag{2.40}$$

Where V_{rmax} is gradient wind amplitude; $t_{r1}$is gust start time (the time when the gradient wind starts to change); t_{r2} is the time when the gradient wind ends.

(4) Random wind

Usually, a random component v_n, is superimposed on the average wind speed to reflect the random fluctuation of the wind speed. Its simulation formula is:

$$v_n = V_{n\_max} R_{am}(-1,1)\cos(\omega_v t + \varphi_v) \quad (2.41)$$

Where V_{n_max} is magnitude of random component; R_{am} is random numbers evenly distributed between -1 and 1; ω_v is the average distance of the wind speed fluctuation, usually 5; φ_v is random variables uniformly distributed between 0 ~ 2.

Table 2.1 shows the combined wind speed model parameters. Based on the **Eq. (2.37) ~ Eq. (2.41)**, the combined wind speed with a basic wind speed of 8 m/s and a time series of gusts, gradient winds and random wind speeds can be obtained, the results is shown in **Figure 2.12**.

Table 2.1 Parameters of combined wind speed model

Items	Parameter
Basic wind speed (m/s)	8
Peak gust (m/s)	3
Gust start time(s)	5
Gust cycle (s)	10
Maximum gradient wind speed (m/s)	2
Gradient wind start time (s)	5
Gradient wind stop time (s)	35

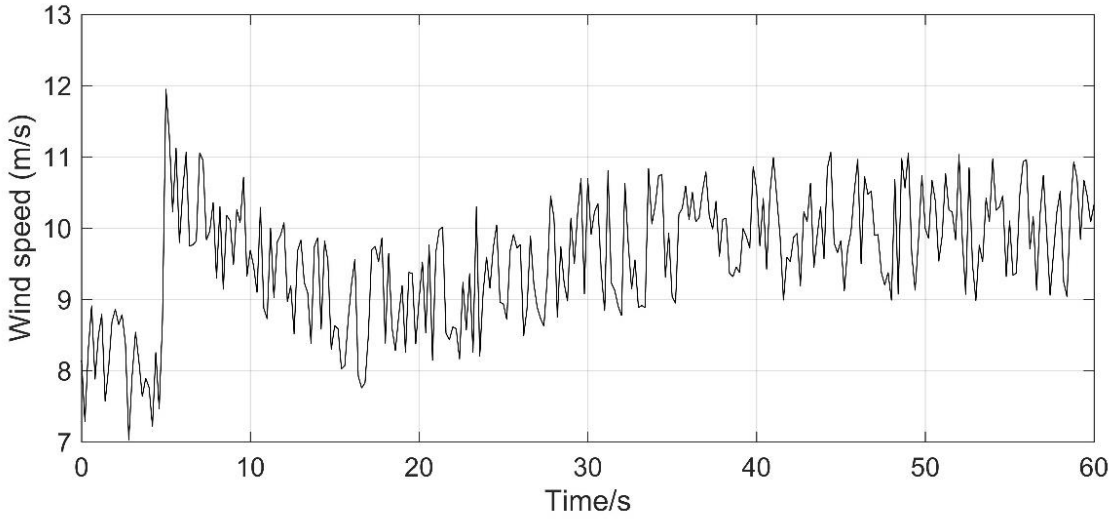

Figure 2.12. Combined wind speed distribution model

Wind direction: Wind is a vector quantity, not only the size (wind speed) in time shows a periodic distribution, in the direction (wind direction) also has a certain periodic distribution pattern. The instantaneous wind direction is changing all the time

and cannot be predicted. However, by continuously recording the average wind direction at a certain location for a long time, a cumulative distribution map of various wind directions can be obtained.

In wind energy utilization, the parameter that describes the statistical characteristics of wind direction is wind frequency. In a certain period (month, season, year or years), the cumulative number of wind directions in a certain direction, the percentage of the total number of all wind directions (including static wind) accumulated in the period is called wind frequency, that is:

$$\text{Frequency of wind direction} = \frac{\text{number of occurrences}}{\text{total number of observations}} \times 100\% \quad (2.42)$$

There are various methods to describe the wind direction, normally we use the angle to indicate the wind direction as 360°, the north wind corresponds to 0° (or 360°), the east wind corresponds to 90°, the south wind corresponds to 180°, the west wind corresponds to 270°, and other subdivision of the wind direction can be calculated from this, as shown in **Table 2.*2***.

Table 2.2 The 16 azimuth of the wind direction

Cardinal Point	Azimuth Degrees	Cardinal Point	Azimuth Degrees
North (N)	0.00°	South (S)	180.00°
North-Northeast (NNE)	22.50°	South-Southwest (SSW)	202.50°
Northeast (NE)	45.00°	Southwest (SW)	225.00°
East-Northeast (ENE)	67.50°	West-Southwest (WSW)	247.50°
East (E)	90.00°	West (W)	270.00°
East-Southeast (ESE)	112.50°	West-Northwest (WNW)	292.50°
Southeast (SE)	135.00°	Northwest (NW)	315.00°
South-Southeast (SSE)	157.50°	North-Northwest (NNW)	337.50°

Wind frequency is usually expressed by a wind frequency rose figure (named because the graph resembles a rose flower), referred to as wind rose. It is based on the cumulative percentage value of wind in each direction for a certain period of time (month, season, year or years) in a certain area, and is drawn on a polar figure in a certain proportion, usually with 16 compass bearings. The most common wind rose figure is a circle with 16 rays drawn uniformly from the center of the circle at equal angles, they represent 16 different directions, and the length of each ray is proportional to the frequency of the wind in this direction. The frequency of the still wind is at the point of the circle. The distance of the point on the ray of the wind rose diagram from the center of the circle indicates the magnitude of the frequency of the wind blowing in the direction of the center of the circle from this point. For example, **Figure 2.13** is the rose diagrams of the wind direction at a certain place.

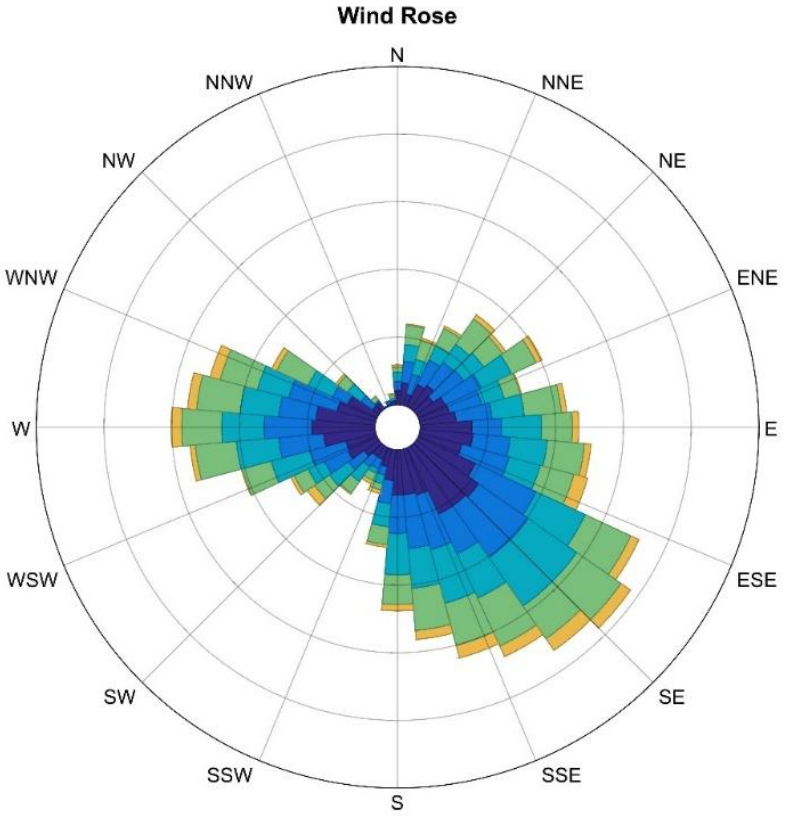

Figure 2.13. The 16 azimuth of the wind direction

The following information can be obtained from the wind rose diagram:

(1) Prevailing winds: It means the direction with higher wind frequency in the annual wind rose chart drawn based on local multi-year observation data. If the wind rose is drawn on a quarterly basis, it can have four seasons of prevailing winds.

(2) Wind rotation direction: refers to the wind direction rotates with the season. In the monsoon area, the wind direction gradually transitions from northerly to southerly and then from southerly to northerly during the year. In some areas, the wind direction does not gradually transition but directly alternate, which is the wind rotation does not exist.

(3) Minimum wind frequency: refers to the two prevailing wind direction corresponding to the axis roughly perpendicular to the wind direction on both sides of the smallest wind direction. While the prevailing wind direction has seasonal wind rotation nature, the minimum wind frequency should be on the other side of the rotation direction.

When analyzing the impact of obstacles near the wind farm on the wind turbine layout, if the obstacle is in a location with a low wind frequency, the impact of the obstacle on the wind turbine can be ignored. These are the descriptions of wind speed and wind direction in meteorology. In the field of wind power technology, the focus on wind speed and direction The focus on wind speed and direction is very different.

For wind direction, wind turbines are not concerned with the natural azimuth of the wind, as long as the yaw system can drive the wind turbine to track the wind direction, it can operate normally and generate electricity. Because of the wind direction, the wind turbine is affected by the accuracy of the yaw system and the delay of the system, which will cause the turbine to operate under the yaw error for a long time, reducing the utilization rate of wind energy, and at the same time, generates unbalanced load on the wind turbine, which adversely affects the unit.

Figure 2.14 describes the effect of changes in wind speed and direction (yaw angle) on the output power of the wind turbine [103]. The wind speed directly determines the upper limit of the output power of the wind turbine, and the yaw angle affects the actual wind energy utilization of the wind turbine. Therefore, under the premise that the wind speed cannot be changed, the yaw angle needs to be reduced as much as possible, so as to improve the wind energy utilization rate of the wind turbine. When the yaw angle is 10°, the power loss of the wind turbine will reach about 5%; when the yaw angle is 15°, the power loss of the wind turbine will reach about 10%;

when the yaw angle is 20°, the power loss of the wind turbine will reach about 17%. In the actual operation of the wind turbine, the yaw angle of the conventional yaw system is generally between 5° and 20°, and the average yaw angle is about 9°. With the influence of other factors, the average power loss will be about 10%. Therefore, a yaw optimization control algorithm that can minimize the yaw angle is one of the key factors to improve the wind energy utilization rate of wind turbines.

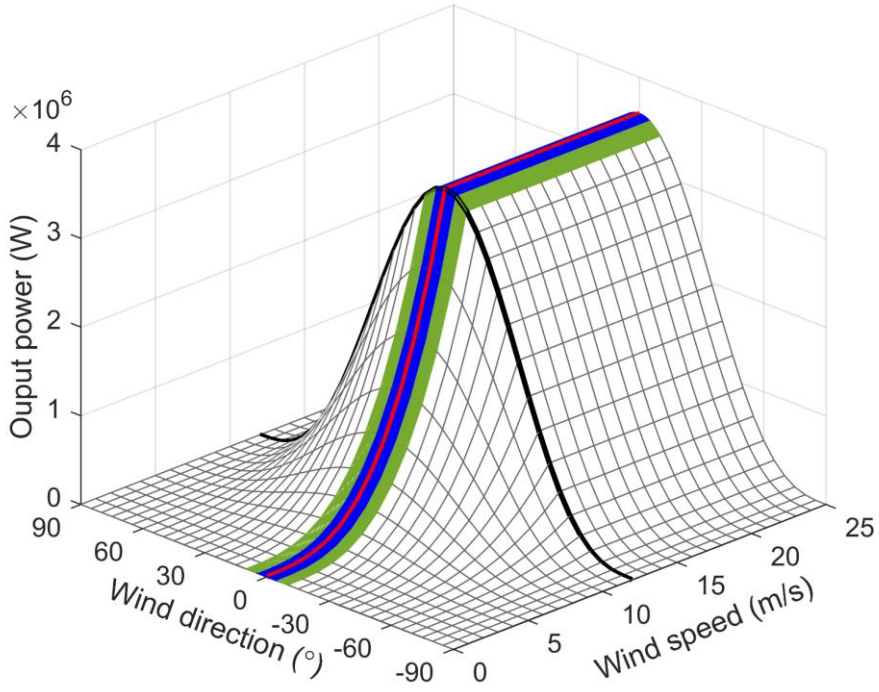

Figure 2.14. Influence of wind speed and direction on the wind turbine output power

2.3.2 Wind turbine modeling

According to **Section 2.1**, the output power of wind turbine is determined by wind speed and wind direction, the output power of wind turbine can be written by [104][105][106]:

$$\mathrm{P_{wt}} = \frac{1}{2}\rho S C_p(\lambda,\beta,\gamma)v^3 = \frac{1}{2}\rho\pi R^2 C_p(\lambda,\beta,\gamma)v^3 \tag{2.43}$$

The relation between wind turbine output power and torque is:

$$\mathrm{T_{wt}} = \frac{P_{wt}}{\Omega_{wt}} \tag{2.44}$$

The power coefficient $C_p(\lambda,\beta,\gamma)$ is determined by empirical equation:

$$\begin{cases} P = \mathrm{P_W} * C_p = \dfrac{1}{2}\rho\pi R^2 v^3 C_p(\lambda,\ \beta) \\ C_p = \left(0.5176 * \left(\dfrac{116}{\lambda_i} - 0.4\beta - 5\right) e^{-\frac{121}{\lambda_i}} + 0.0068\lambda\right) \\ \dfrac{1}{\lambda_i} = \dfrac{1}{\lambda + 0.08\beta} - \dfrac{0.035}{1+\beta^3} \\ \lambda = \dfrac{\omega_t R}{v} \end{cases} \tag{2.45}$$

Which

$$\lambda = \frac{2\pi \mathrm{R_{wt}} n_{wt}}{v} = \frac{\Omega_{wt} R_{wt}}{v} \tag{2.46}$$

Therefore, using **Eq. (2.44) ~ Eq. (2.46)**, a simulation model of the wind turbine can be established based on the MATLAB/SIMULINK environment, and the completed wind turbine model is shown in the **Figure 2.15**.

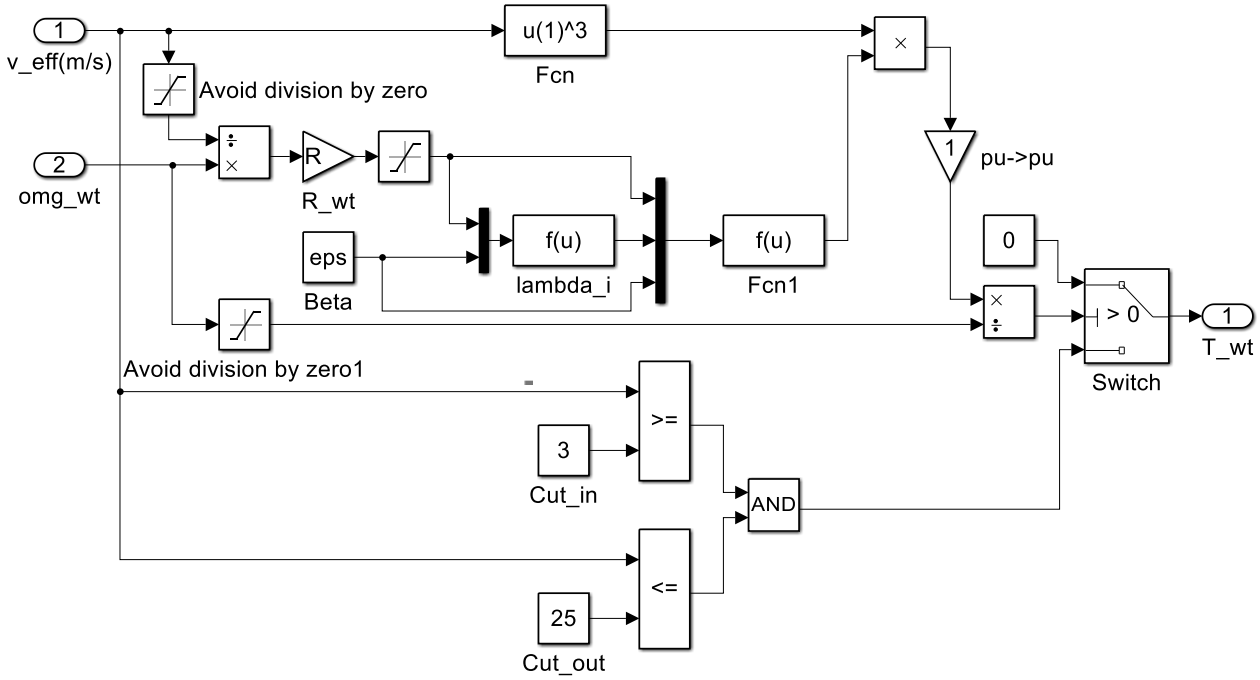

Figure 2.15. Modeling of wind turbine

In the model, the input variables "v", "omg_wt", "beta", and "gamma" are effective wind speed, rotor angular velocity, blade pitch angle, and yaw angle, respectively. These four input variables can determine the operating state and output power of the WT. Using the tip speed ratio, blade pitch angle and yaw angle, the power coefficient can be determined through the $C_p(\lambda,\beta,\gamma)$ equation. After knowing the power coefficient and the current wind speed, the mechanical power output by the rotor

can be calculated, and then the mechanical torque output can be calculated. It should be noted that "cut_in" and "cut_out" are cut-in wind speed and cut-out wind speed respectively. When the wind speed is in this range, the WT model outputs the calculated value, otherwise the output is zero.

2.3.3 Drivetrain modeling

According to the analysis in **Section 1.2**, the mechanical transmission chain of the wind power generation system is mainly composed of 5 parts: wind turbine rotor, low-speed transmission shaft, gear box, high-speed transmission shaft and generator rotor. There are many research methods for shafting models, and the equivalent concentrated mass method is often used when stress distribution and mechanical strength design are not required [107][108][109].

When ignoring the shaft stiffness and damping coefficient, the model of the wind turbine transmission chain is further simplified, as shown in **Figure 2.16**, which is called single-mass model, represented by the following formula [110][111][112].

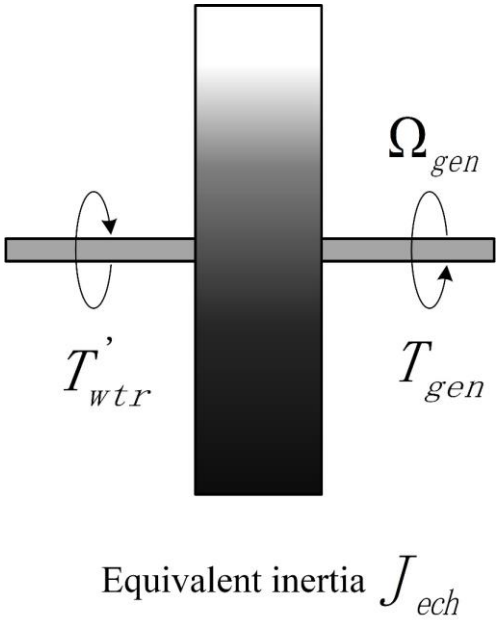

Figure 2.16. Single mass model of WECS

$$\mathrm{T_{gen}} - T'_{wtr} = J_{ech}\frac{d\Omega_{gen}}{dt} \tag{2.47}$$

Among them, the equivalent moment of inertia is

$$\mathrm{J_{ech}} = J_{gen} + \frac{J_{wtr}}{K_{gear}^2} \tag{2.48}$$

The equivalent wind turbine output torque is

$$T'_{wtr} = \frac{T_{wtr}}{K_{gear}} \tag{2.49}$$

The simulation model of the single-mass drive chain established in the MATLAB/SIMULINK environment is shown in the **Figure 2.17**.

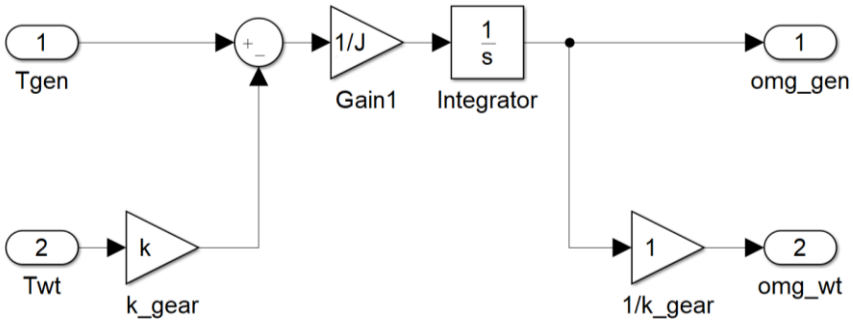

Figure 2.17. Modeling of drivetrain

Among them, the input "T_gen" and "T_wt" are the generator and wind turbine torque respectively; the output "omg_gen" and "omg_wt" are the mechanical angular velocity of the generator and wind turbine respectively.

2.3.4 Generator modeling

Induction generators (IG) have different dynamic mathematical models in different coordinate systems, so the mathematical models of induction generators in different coordinate systems can be established in the MATLAB/SIMULINK environment as needed [113][114][115]. For the purpose of simulation, MATLAB/SIMULINK software is used to construct a mathematical simulation model of the induction generator in the synchronously rotating *x-y* coordinate system [116][117][118]. It is an effective way to construct a simulation model using the induction generator state equation. The state equation of the induction generator in the synchronously rotating *x-y* coordinate system is

$$\frac{d\boldsymbol{i}_{\mathrm{xy}}}{dt} = \boldsymbol{A}\boldsymbol{i}_{xy} + \boldsymbol{B}\boldsymbol{u}_{xy} \tag{2.50}$$

In the formula, $\boldsymbol{i}_{\mathrm{xy}}$ represents the induction generator current matrix, which is

$$\boldsymbol{i}_{\mathrm{xy}} = \left[i_{sx}\ i_{sy}\ i_{rx}\ i_{ry}\right]^T \tag{2.51}$$

$\boldsymbol{u}_{xy}$ represents the induction generator voltage matrix, which is

$$\boldsymbol{u}_{xy} = \left[u_{sx}\ u_{sy}\ u_{rx}\ u_{ry}\right]^T \tag{2.52}$$

A and **B** are the coefficient matrix, respectively

$$\mathbf{A} = \begin{bmatrix} -\frac{R_s}{\sigma L_s} & \omega_1 + \frac{\omega_r L_m^2}{\sigma L_s L_r} & \frac{R_r L_m}{\sigma L_s L_r} & \frac{\omega_r L_m}{\sigma L_s} \\ -\omega_1 - \frac{\omega_r L_m^2}{\sigma L_s L_r} & -\frac{R_s}{\sigma L_s} & -\frac{\omega_r L_m}{\sigma L_s} & \frac{R_r L_m}{\sigma L_s L_r} \\ \frac{R_s L_m}{\sigma L_s L_r} & -\frac{\omega_r L_m}{\sigma L_r} & -\frac{R_r}{\sigma L_r} & \omega_1 - \frac{\omega_r}{\sigma} \\ \frac{\omega_r L_m}{\sigma L_r} & \frac{R_s L_m}{\sigma L_s L_r} & -\omega_1 - \frac{\omega_r}{\sigma} & -\frac{R_r}{\sigma L_r} \end{bmatrix} \tag{2.53}$$

$$\mathbf{B} = \frac{1}{\sigma \mathrm{L_s} L_r} \begin{bmatrix} L_r & 0 & -L_m & 0 \\ 0 & L_r & 0 & -L_m \\ -L_m & 0 & L_s & 0 \\ 0 & -L_m & 0 & L_s \end{bmatrix} \tag{2.54}$$

σ is leakage coefficient of generator

$$\sigma = 1 - \frac{\mathrm{L_m^2}}{L_s \cdot L_r} \tag{2.55}$$

Considering that the electromagnetic torque equation is

$$\mathrm{T_e} = \frac{3}{2} n_p L_m \left(i_{sy} i_{rx} - i_{sx} i_{ry}\right) \tag{2.56}$$

Therefore, based on **Eq. (2.50) ~ Eq. (2.56)**, the dynamic model of the IG built using MATLAB/SIMULINK simulation software is shown in the **Figure 2.18**.

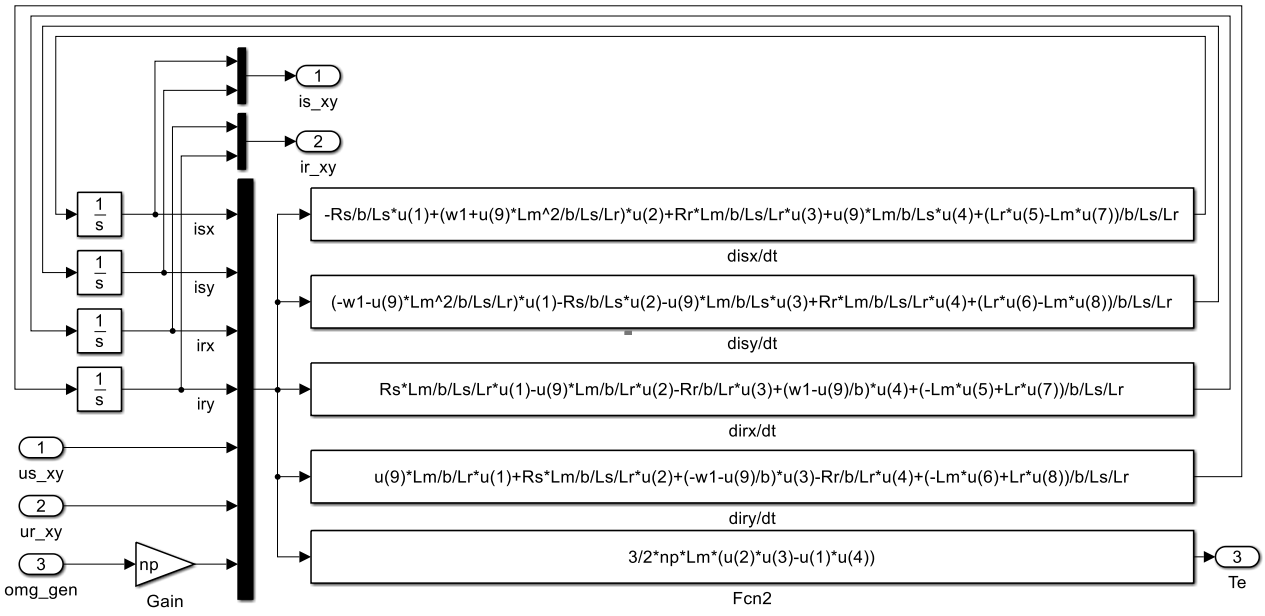

Figure 2.18. Dynamic model of the induction generator

Among them, the input "us_xy" is the x and y axis voltage components of the stator in the two-phase synchronous rotating x-y coordinate system; the input "ur_dq" is the x and y axis voltage components of the rotor in the two-phase synchronous rotating x-y coordinate system; "omg_gen" is the mechanical angular velocity of the generator. The output "is_xy" is the current components of the stator windings in the x and y axis under the synchronously rotating x-y coordinate system; the output "ir_xy" is the x and y axis current components of the rotor in the synchronously selected x-y coordinate system; the output "Te" is the electromagnetic torque.

The induction generator stator flux linkage oriented control strategy is to orient the x-axis in the synchronously rotating *x-y* coordinate system in the stator flux linkage direction [118][119][120]. Compared with other vector oriented control strategies, its control system is quite simple. There are two different ways to realize this control strategy, namely the optimal speed given method and the optimal power given control method.

The optimal speed given method, the control goal is to keep the tip speed ratio at the optimal value, so as to ensure that the wind turbine runs at the optimal power factor at medium and low wind speeds [121][122][123][124]. The optimal power given method is to take the maximum active power theoretically output by the induction generator as the reference power to realize the maximum wind energy capture of the wind turbine [125][126][127].

The optimal power given control method is dual-channel and double-closed-loop control: reactive power control and active power control.

The reactive power control channel is given reactive power, which is compared with the output reactive power of the induction generator wind power generation system, and the two-phase rotor is obtained through the PI controller. The x-axis reference current in the synchronous rotation x-y coordinate system is compared with the rotor current of the induction generator to obtain the x-axis component of the rotor control voltage in the two-phase synchronous rotation x-y coordinate system. The mathematical equations of the reactive power control are shown in **Eq. (2.57)**:

$$\begin{cases} u_{rx} = \left(K_p + \dfrac{K_i}{s}\right)\left(i_{rxref} - i_{rx}\right) - \Delta u_{rx} \\ u_{ry} = \left(K_p + \dfrac{K_i}{s}\right)\left(i_{ryref} - i_{ry}\right) - \Delta u_{ry} \\ \Delta u_{rx} = \omega_2 \sigma L_r i_{ry} \\ \Delta u_{ry} = -\omega_2 \sigma L_r i_{rx} - \omega_2 \dfrac{L_m^2}{L_s} i_{ms} \end{cases} \tag{2.57}$$

Where: u_{rx}, u_{ry} are rotor voltages; K_p is the proportional gain adjustment of rotor current controller; K_i is the integral gain adjustment of rotor current controller; i_{rxref}, i_{ryref} are reference values of rotor current x and y axis components.

The active power control channel is given by the optimal active power, compared with the output active power of the induction generator wind power generation system, the y-axis reference current in the x-y coordinate system of the rotor two-phase synchronous rotation is obtained through the PI controller, and then the y-axis current in the x-y coordinate system of the two-phase synchronous rotor rotation of the induction generator is obtained. The components are compared to obtain the x-axis component of the rotor control voltage in the two-phase synchronous rotation x-y coordinate system, so as to achieve the maximum power output of the wind turbine. The mathematical equations of the active power control are shown in **Eq. (2.58)**:

$$\begin{cases} i_{rxref} = \dfrac{L_s}{L_m} i_{sx} - i_{ms} \\ i_{ryref} = \dfrac{L_s}{L_m} i_{sy} \\ i_{sx} = (K_p + \dfrac{K_i}{s})(Q_{sref} - Q_s) \\ i_{sy} = (K_p + \dfrac{K_i}{s})(P_{sref} - P_s) \end{cases} \tag{2.58}$$

Where: K_p is the proportional gain adjustment of the power controller; K_i is the integral gain adjustment of the power controller; P_{sref} is active power reference value; Q_{sref} is reactive power reference value.

Through theoretical analysis, a simulation model under the environment of MATLAB/SIMULINK simulation software for optimal power given control can be built. The detailed structure is shown in the **Figure 2.19**.

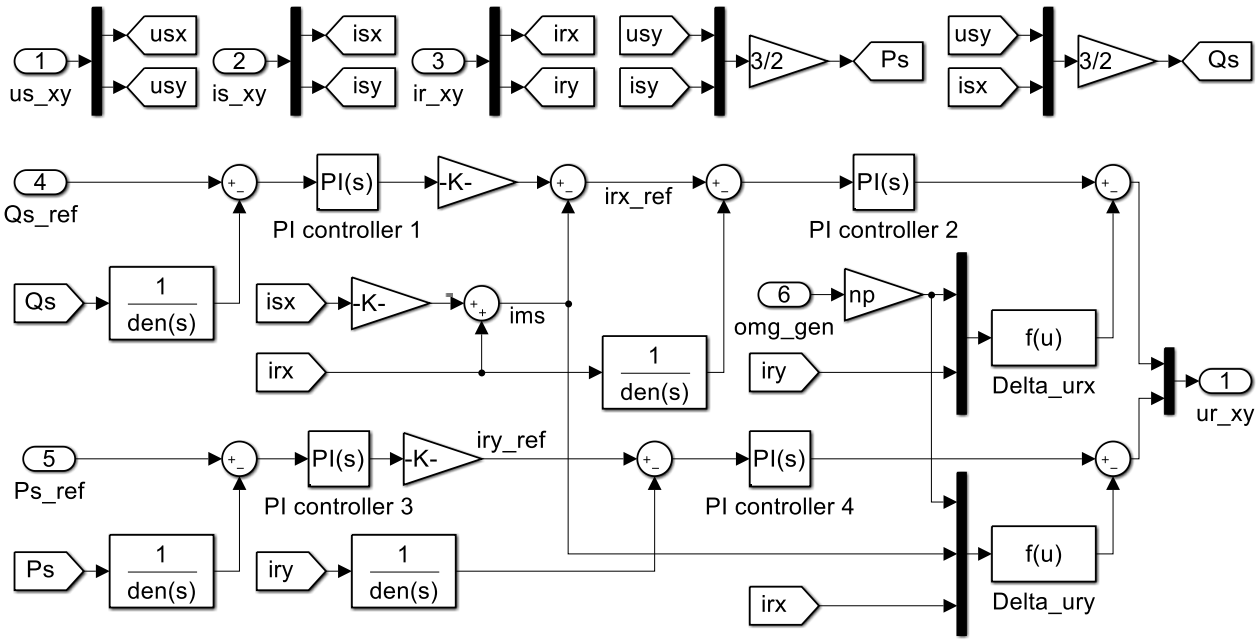

Figure 2.19. Modeling of optimal power given control

Among them, the input "is_xy" is the stator x and y-axis current components in the two-phase synchronous rotation x-y coordinate system; the input "us_xy" is the stator x and y-axis voltage components in the two-phase synchronous rotation x-y coordinate system; the input "ir_xy" is the rotor x and y axis current components in the two-phase synchronous rotation x-y coordinate system; the input "Qs_ref" and "Ps_ref" are the reference values of the stator reactive power and active power of the induction generator; and the output "ur_xy" is the rotor x and y axis voltage components in the two-phase synchronous rotation x-y coordinate system.

2.3.5 Overall Model

Based on the above-mentioned simulation model of each component of the wind power generation system, a simulation model of the entire system can be built, as shown in the **Figure 2.20**.

The subsystem "Wind" is the wind speed model, which provides effective wind speed data for the WECS. The subsystem "Wind turbine" is a WT model. It calculates the output mechanical torque "T_wt" of the WT through the input wind speed data "v_eff" and the rotational speed data "omg_wt" of the WT, and provides a torque signal for the drivetrain model, and the power factor signal "Cp" is provided. The subsystem "Drive train" is a drive train model, which uses the WT mechanical torque "T_wt" and the electromagnetic torque signal "T_gen" to calculate the generator speed "omg_gen"

and the WT speed "omg_wt". The subsystem "Power controller" is the control model of the optimal power given method. The active power reference value "Ps_ref" is calculated by the power reference value calculation subsystem "Power reference value" using the input generator speed data "omg_gen". The reactive power "Qs_ref" is set according to the required reactive power, and the stator voltage "us_xy", stator current "is_xy" and rotor current "ir_xy" are provided by the induction generator subsystem "IG". The stator voltage "us_xy" of the induction generator model "Generator" is provided by the power subsystem "Electrical source", and the rotor control voltage "ur_xy" is provided by the subsystem "Power controller".

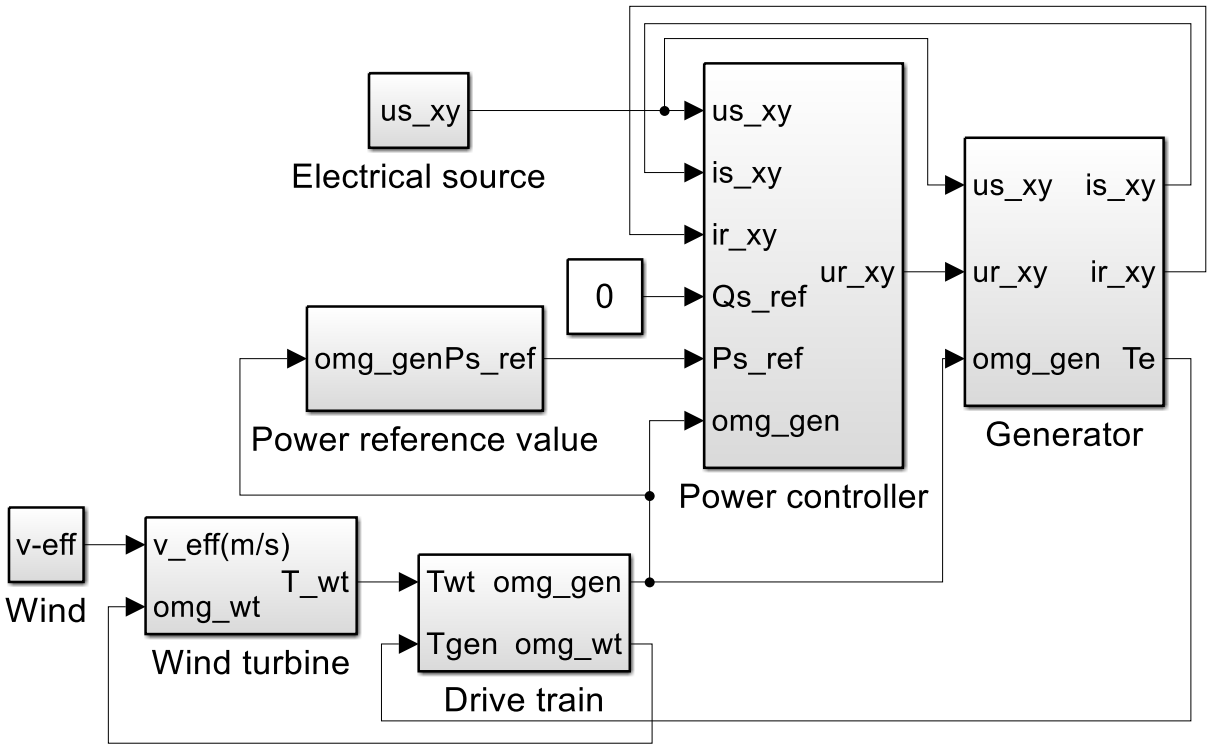

Figure 2.20. Modeling of WECS

Theoretical output power simulation experiment of the WECS: in order to verify that the wind power generation simulation system can simulate the theoretical output power curve of the wind turbine, first, set the real wind turbine on the continuous natural working condition interface of the wind power experiment simulation software according to parameters in **Table 2.3**. Then, input the value from the cut-in wind speed of 3 m/s to the cut-out wind speed of 25 m/s, and use the electrical control module to control the speed of the wind turbine to follow the change of the wind speed to maintain the optimum tip speed ratio or rated speed, so that the wind turbine can achieve

maximum power capture and does not exceed rated output power. Finally, the theoretical output power value of the wind turbine is recorded, and the theoretical output power simulation curve of the wind power generation simulation system is obtained as shown in **Figure 2.21**.

Table 2.3 Theoretical output power simulation experiment parameter setting

Variable	Value
Blade number	3
Turbine radius	60m
Cut-in wind speed	3 m/s
Rated wind speed	12.5 m/s
Cut-out wind speed	25 m/s
Maximum power coefficient (C_p)	0.44
Rated power	3.6 Mw
Gearbox ratio	1:119
Air density	1.225 kg/m^3

Comparing the simulation result **Figure 2.21** with the theoretical output power curve **Figure 2.22** of the real WT, the theoretical output power curve of the wind power simulation system is basically consistent with the theoretical output power curve of the real WT. When the wind speed reaches the cut-in wind speed of 3 m/s, the wind power generation system starts to generate electricity, and this stage is the start-up stage. As the wind speed gradually increases, the wind energy utilization coefficient also increases gradually. When the wind speed value is from 5 m/s to 10 m/s, the wind energy utilization coefficient basically remains unchanged. At this stage, the wind energy utilization coefficient is constant, and the maximum wind energy utilization coefficient is in progress. When the wind speed reaches the rated wind speed of 12.5 m/s, the WT starts to maintain the rated power of 3600 kW to generate electricity. The operating areas of the two are consistent with the operating areas of the wind power generation system under different wind speeds, which verifies that the simulation system can correctly simulate the theoretical output power curve of the WT.

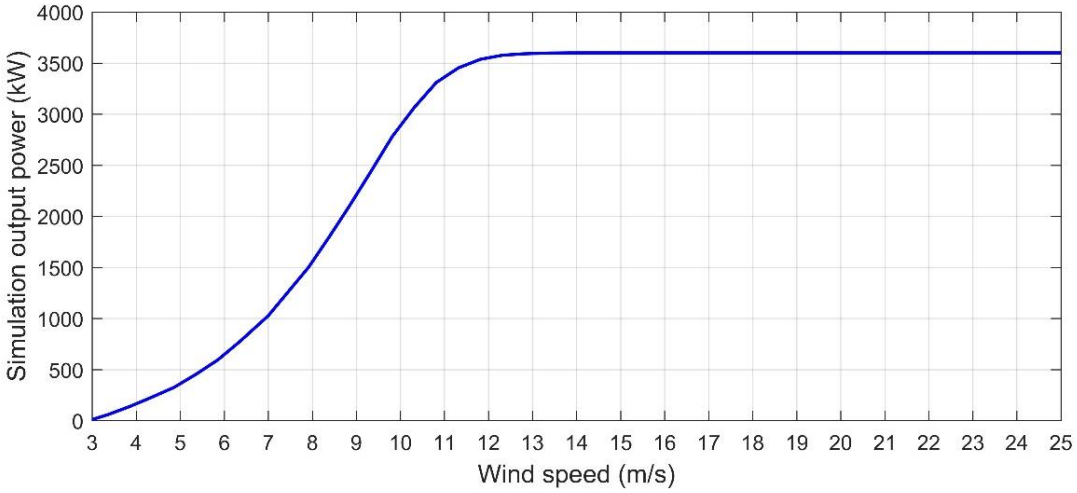

Figure 2.21. Theoretical output power curve of the simulated system

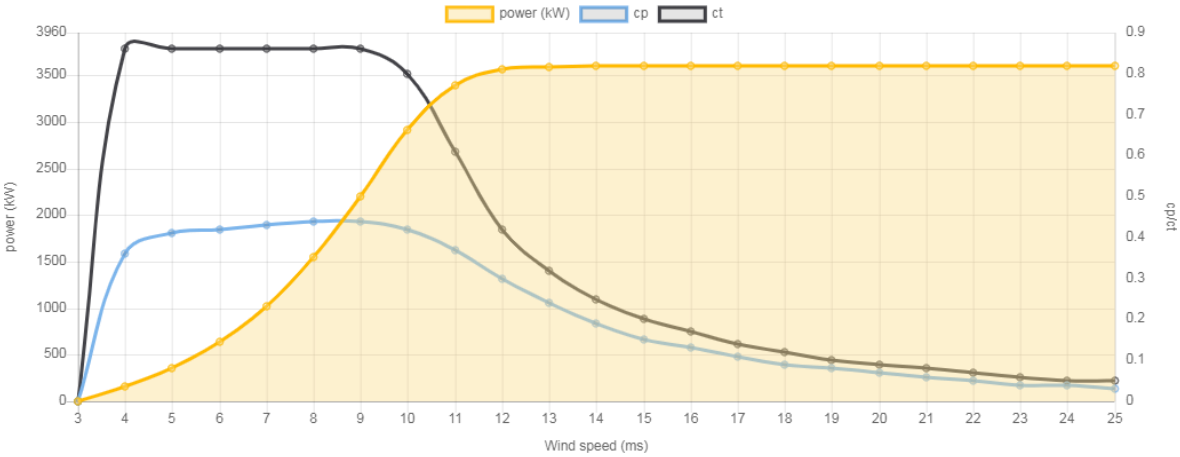

Figure 2.22. Theoretical output power curve of a real wind turbine

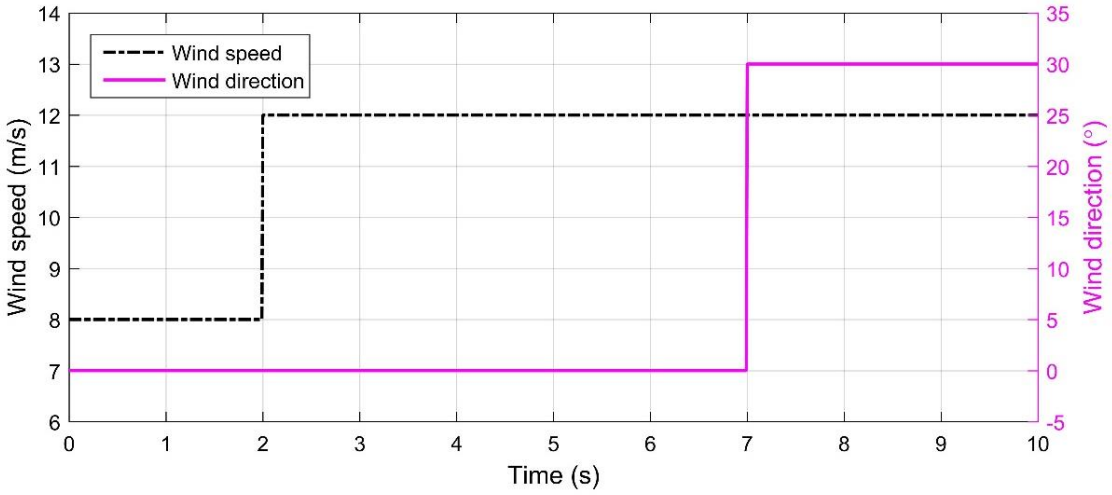

Figure 2.23. Input wind source of WECS simulation model

To test the system response of the WECS simulation model to fluctuations in wind speed and direction, the following simulations were performed. In terms of system input, step signals are used for both wind speed and wind direction, as shown

in **Figure 2.23**. The initial value of the wind direction is 8 m/s, and it changes to 12 m/s at 2s, which basically reaches the rated wind speed; the initial value of the wind direction is 0°, and it becomes 30° at 7s, which means that the yaw error is 30° at 7s.

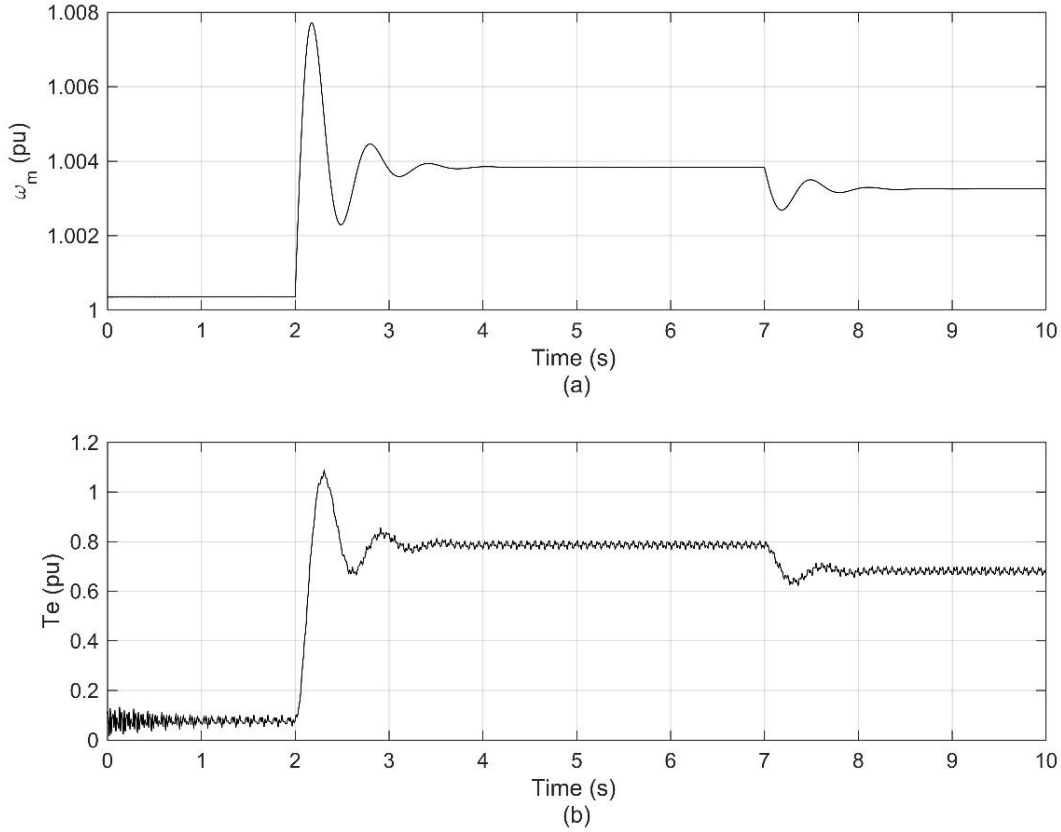

Figure 2.24. (a) Rotor speed of generator (b) Electromagnetic torque of generator

For the rotor speed and electromagnetic torque of the generator, because the WECS simulation model has control systems to adjust the stability during operation, after the wind speed and wind direction change, the stability can be quickly restored to ensure the stable operation of the system, as shown in **Figure 2.24**.

During operation, the electrical parameters of the generator output are shown in **Figure 2.25**. Because in this WECS simulation model, the control method of current regulation is used, so it can be seen that when the wind speed and wind direction fluctuate, the three-phase current in (a) also changes, but it will reach a steady state after the system is stabilized. The three-phase voltage remains unchanged throughout the process, as shown in (b), and the effective value of the three-phase voltage is 690V. (c) shows the change of the active power of the system during operation. The simulation data is consistent with the actual operation data, which verifies the accuracy of the simulation model.

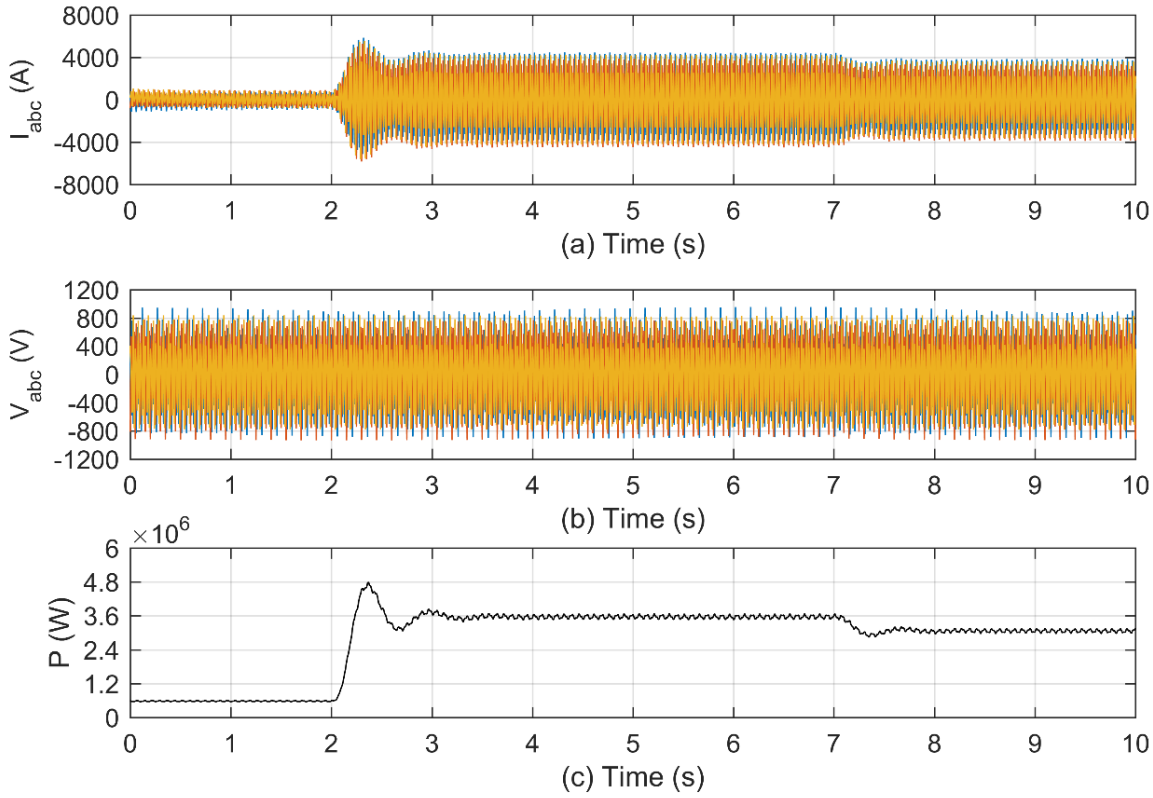

Figure 2.25. (a) 3-phase current of WECS (b) 3-phase voltage of WECS (c) Output power of WECS

2.4 Conclusion of chapter 2

This chapter presents the basic theory of wind energy conversion system. According to the research content of the full text, the aerodynamic state, force and load of the wind turbine conversion system during yaw process are analyzed, and the error generated by the yaw system is optimized. Finally, according to the analysis results, the wind energy conversion system is modeled in MATLAB/SIMULNK, and a general wind energy conversion system model with typical control systems is established. The model can be used for the subsequent optimization of the yaw control strategy to verify the proposed yaw control strategy under ideal conditions.

CHAPTER 3: BASIC THEORY AND CONTROL STRATEGY OF WIND TURBINE YAW SYSTEM

In this chapter, based on the existing yaw control algorithms, the neural network prediction algorithm and hill climbing search algorithm for the yaw system of the WECS are designed, and a simulation model is built in MATLAB to verify the developed yaw control algorithm.

3.1 Yaw control algorithm based on predicted wind direction

3.1.1 The basic principle of prediction algorithm

For decades, both domestic and foreign countries have been devoted to the research of wind power prediction methods, striving to improve the accuracy of wind power prediction [128]. In recent years, research on wind power prediction technology has developed rapidly, and many new methods and ideas have emerged. According to the different modeling methods, they can be mainly divided into physical modeling method, statistical modeling method, intelligent learning method and combined modeling method that incorporates multiple methods.

1) Physical modeling method

The physical method, mainly with the help of numerical weather forecasts (NWP), determines the meteorological information of the future time period, and after conducting topography, wake and spatial correlation analysis in the area around the wind turbine, obtains micro-scale meteorological information such as wind speed and wind direction at the hub height of the wind turbine, and finally solves the output power of the wind turbine by following the equations of mass, momentum and energy conservation through the mapping relationship of the original power curve [129].

This method does not require training through historical data, and with the support of high-precision meteorological forecast data, the prediction results are relatively accurate and more suitable for short-term forecasting [130]–[134]. However, this method relies on a large amount of topographic and meteorological data, requires the cooperation of experts in multiple fields, constructs a model with many empirical parameters [135][136], and the model is very complex leading to poor portability,

which makes the method inapplicable in many cases.

2) Statistical modeling method

Unlike physical models, statistical models analyze the mathematical distribution patterns from historical data, i.e., they make predictions by summarizing spatial and temporal information in the data [137]. Conventional statistical modeling method usually takes wind power time series and wind speed time series as the basis, and establishes the mapping relationship between historical data and predicted power values according to the process of model identification, parameter estimation and model validation [138].

The statistical method is simple to model and only requires historical data to establish the mapping between the input features and the output power series to be predicted, and then the predicted values are obtained by substituting this mapping into the measured data. The method is based on historical wind farm data for wind power impact factors for feature engineering, based on a large number of historical meteorological data and power data for statistical regression fitting, commonly used methods are regression analysis [139], time series method [140], Kalman filter method [141], random time series method [137], support vector machine (SVM) method [142] and so on.

Statistical methods are usually easier to implement than other methods, model economy and save computing power, however, wind energy has typical nonlinear and non-stationary characteristics, only through the establishment of functional form, can achieve certain results for wind power prediction, for example, in a relatively short time range (48 hours) using these methods, can predict a more satisfactory result [143][144]. To further improve the accuracy of wind power prediction, further optimization of the wind power model is required, and statistical methods become very unstable over longer time ranges.

Overall, the statistical methods are simple to model and have achieved some results for wind power prediction by establishing functional relationships to obtain time- and space-dependent information in the data for prediction. However, both wind power data and meteorological data are data with typical nonlinear and non-stationary

characteristics, and it is difficult to obtain more accurate prediction results for wind power data with nonlinear and non-stationary characteristics. If we hope to further improve the accuracy of wind power prediction, we need to continue to optimize the wind power prediction model.

3) Intelligent learning method

With the in-depth development of computer hardware and software technology, the continuous improvement of machine computing power, and the popular application of artificial intelligence theory, machine intelligence learning methods such as artificial neural networks [145][146], wavelet analysis [147][148], support vector machines [149], etc. have been extended in statistical methods.

The essence of the intelligent learning method is not to describe the relationship between wind power and related influencing factors in the form of mathematical analytic formula, but to establish a nonlinear model by extracting the relationship between input and output variables with artificial intelligence, train the model with labeled data and use the converged model for prediction [150][151][152].

Intelligent learning methods have received a lot of attention from researchers because they are more adaptable and do not require solving complex mathematical equations, and a large number of research results have emerged. However, these learning methods often require a large amount of historical data to train the models [153], and the lack of theoretical guidance makes the model structure and parameters difficult to interpret, resulting in uncertainty and non-reproducibility of the prediction models they construct, and the need to retrain the models in new practical applications, which affects their applicability.

With the further development of deep learning theory and its successful application in various fields, researchers have started to try to use deep learning methods in the field of wind power prediction. Deep learning combines the results of multidisciplinary research in statistics, neurophysiology and mathematics, and often uses Back Propagation Neural Networks (BP) [154], Convolutional Neural Networks (CNN) [155], Recurrent Neural Network (RNN) [156], etc. In the prediction of highly correlated wind power time series, it can rely on its unique model structure to

effectively avoid the gradient disappearance phenomenon and improve the problem of traditional neural networks prone to local optimum, which is more suitable for short-term wind power output power prediction characterized by large amounts of data and many features.

4) Combination method

The combination method is to combine one or more of the above models to give full play to the advantages of each model and weaken the disadvantages of each model, so as to improve the wind power output forecasting accuracy.

Literature [157] used a combined time series and neural network forecasting method, using wind speed time series as input data and wind speed data time series features as input attributes of neural network, using neural network to construct a model and train it, and the prediction accuracy is improved by the combination.

Literature [158] combination of different physical methods using NWP forecasting models outperforms the single NWP model; literature [159] combine physical methods with intelligent computational methods to construct a combined NWP and GPR model with significantly improved prediction accuracy over traditional neural networks; Literature [160] play the respective advantages of statistical models and intelligent learning models to constitute a combined model that is better than time series models and RBF models in terms of prediction effect.

At present, fusing various types of algorithms to construct a combined model to carry out short-term wind power output prediction has received wide attention. The idea of multi-algorithm combination is to select and combine the advantages of each algorithm for wind speed and wind power characteristics, and fuse multiple algorithms for prediction research. The combined approach allows the effective information of each single method to be fully utilized and the accuracy to be improved over the single time series method, which is one of the main directions of wind power prediction development [161][162][163].

3.1.2 Design of predictive Elman neural network

An artificial neural network is an artificially constructed neural network based on the knowledge and understanding of biological neural networks to achieve certain

functions. It is a theoretical mathematical model of the human brain neural network, which is highly nonlinear and can perform complex logical operations.

According to the information flow during the operation of the neural network, the neural network can be divided into two basic types: feedforward and feedback. Feedforward networks have complex nonlinear mapping capabilities by introducing hidden layers and nonlinear transfer functions. But the output of the feedforward network is only determined by the current input and weight matrix, and has nothing to do with the previous output of the network. Feedback neural network is also called recurrent neural network (RNN) [164][165] or regression network. The input of the feedback neural network includes the feedback of delayed input or output data. Since there is a feedback input, it is a feedback dynamic system; the learning process of this system is the change process of its neuron state, this process eventually reaches a steady state in which the neuron state does not change, which also marks the end of the learning process.

The dynamic learning characteristics of the feedback network are mainly determined by the feedback form of the network. The feedback forms of the feedback network are relatively diverse, including input delay, single-layer output feedback, neuron self-feedback, and mutual feedback between two layers. Common feedback neural networks include Elman neural network [166], Hopfield neural network [167] and Boltzmann neural network [168] similar to discrete Hopfield structure.

The neural networks often used for prediction are BP neural network, RBF neural network, fuzzy neural network, genetic neural network, support vector machine, and so on. Neural networks have strong nonlinear approximation ability, self-learning, self-adaptive, data fusion, and other features, which can extract relevant and useful information from a set of historical data and can overcome many problems that cannot be solved by traditional prediction methods. The artificial neural network has a nonlinear mapping function, which can approximate any given nonlinear system with arbitrary accuracy.

The variation in wind direction is highly random, uncertain and unstable, and provides complex non-linear data. It is difficult to obtain an accurate mathematical

model by applying traditional statistical methods to this kind of problem, and therefore it is difficult to meet the desired objectives. The use of neural networks enables the expression of complex nonlinear mappings with arbitrary accuracy without the need to build an accurate mathematical model, which can achieve good prediction results.

The BP neural network is the most widely used method for predicting complex nonlinear data. It has the advantages of a reliable theoretical foundation, rigorous derivation process, high prediction accuracy, and good versatility, but its essence is a static feedforward network. The random nature of the wind direction makes it a real-time dynamic system, therefore, using BP neural network to identify the wind direction and static modeling to predict the wind direction will bring a series of problems from a theoretical point of view. Elman neural network, as a typical dynamic feedback network, can compensate for the shortcomings of the BP neural network.

The Elman neural network was J. L. Elman first put forward the voice processing problem in 1990, which is a typical local regression network. The architecture of the Elman neural network is an extension of a quasi-RBF neural network, which consists of input layer, output layer, hidden layer, and context layer [169][170]. In the neural network, the feedback of the hidden layer comes from the input layer neuron and context layer neuron [171]. Because the connection layer has a memory unit, it can store the output of the previously hidden layer neurons [172].

The Elman neural network has almost all the advantages of the BP neural network, except that the Elman neural network includes a context layer for feedback from the hidden layer to the input layer. The context layer acts as a delay operator in the network, returning the result of the last operation in the hidden layer to the input layer with a delay. It is a dynamic feedback type network, which can internally feedback, store and utilize the output information of past moments, and can realize both the modeling of static systems and the mapping of dynamic systems and directly respond to the dynamic characteristics of the systems, which is superior to BP neural networks in terms of computational power and network stability [173]. **Figure 3.1** shows the Elman neural network model diagram.

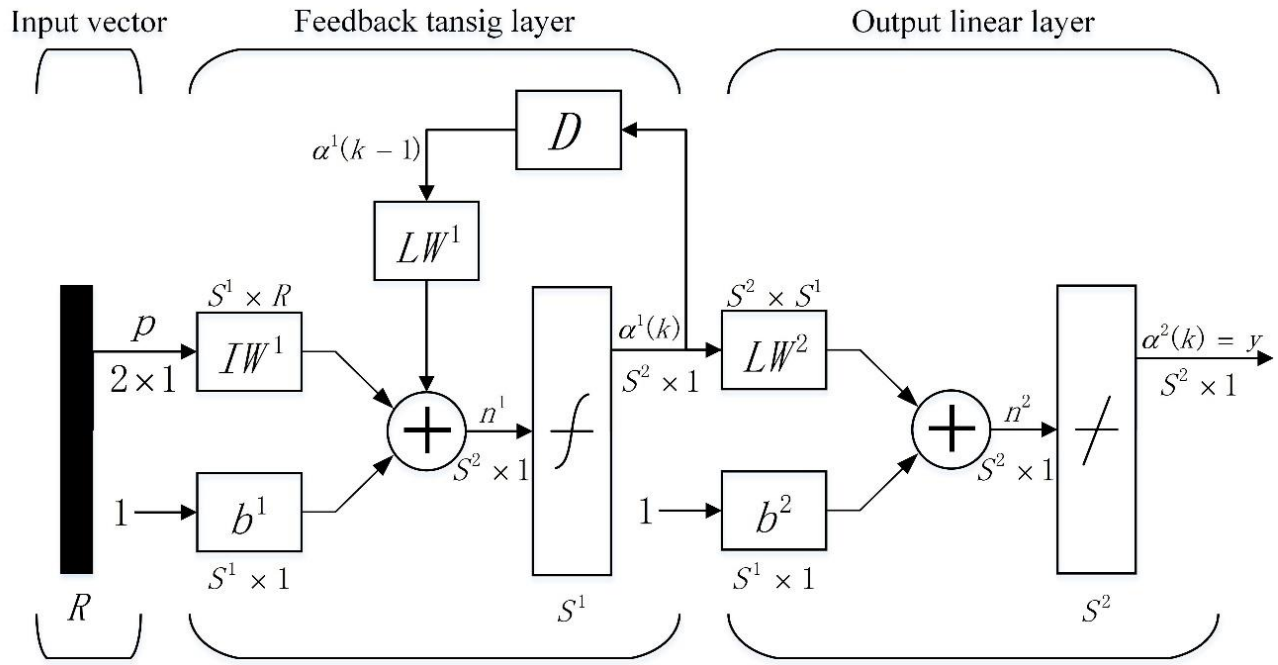

Figure 3.1. Elman neural network model diagram

where：

$$\begin{cases} \alpha^1(k) = \tan sig[LW^1 p + LW^1 \alpha^1(k-1) + b^1] \\ \alpha^2(k) = purelin[LW^2 \alpha^1(k) + b^2] \end{cases} \tag{3.1}$$

The Elman neural network has tansig neurons in the hidden layer (feedback layer) and purelin neurons in the output layer. Such a transfer function can approximate any function with arbitrary accuracy (in continuous finite time) with a special combination of two neural network layers, regarding which only a sufficient number of neurons in the hidden layer is required to achieve. The higher the complexity of the approximating function, the higher the number of neurons in the hidden layer required.

It is worth noting that the Elman neural network differs from the usual two-layer network in that its first network layer has a feedback node whose delayed volume stores the previous moment's value and applies it to the current moment's computation. So even an Elman neural network with the same weights and thresholds may have different outputs at the same moment for the same input vector if its feedback states are different.

Because the Elman neural network is able to store information for future moments, it can learn both time-domain and space-domain patterns; it can be trained to produce both responses to patterns (spatial classification results of patterns) and pattern outputs (time-domain variation relations of patterns).

1) Mathematical model of Elman neural network

In the actual use of this paper, we design the Elman neural network as a typical feedback neural network model, as shown in **Figure 3.2**.

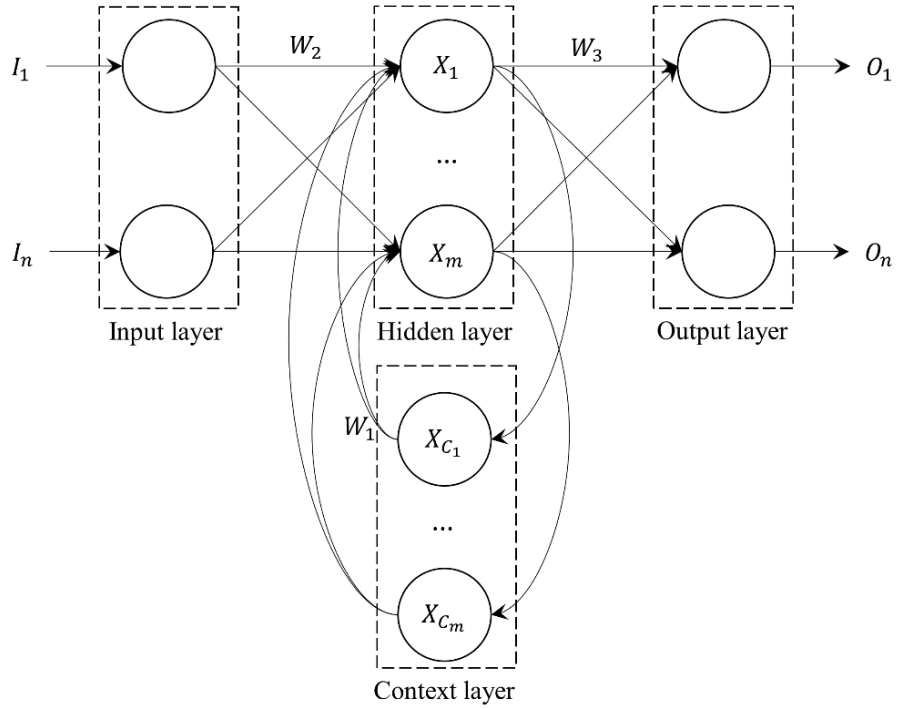

Figure 3.2. The structure of the Elman neural network

The connection of the input layer, hidden layer, and output layer is similar to that of a feed-forward network. The units in the input layer only play the role of signal transmission, and the units in the output layer play the role of weighting. The hidden layers have two types of excitation functions, linear and nonlinear, and usually, the excitation function is taken as a Sigmoid nonlinear function. The context layer is designed for remembering the output value of the previous moment of the hidden layer unit, which can be considered as a delay operator with a one-step delay. The output of the hidden layer is self-linked to the input of the hidden layer through the delay and storage of the context layer [174][175]. This self-linkage makes it sensitive to historical data, and the addition of the internal feedback network increases the ability of the network itself to process dynamic information, thus achieving the purpose of dynamic modeling [176].

For the context layer, there are.

$$\mathrm{X}c_i(k) = X_i(k-1) \tag{3.2}$$

For the hidden layer, there are.

$$\mathrm{X}(k) = f(W_1 Xc(k) + W_2 I) \tag{3.3}$$

For the output layer, there are.

$$\mathrm{O(k)} = \mathrm{f}\big(W_3 \mathrm{X}(k)\big) \tag{3.4}$$

where $\mathrm{f(x)}$ is the excitation function and the Sigmoid function is used.

$$\mathrm{f(x)} = \frac{1}{1+e^{-x}} \tag{3.5}$$

The learning algorithm derivation for Elman neural networks is performed as follows. Define the error function of an Elman neural network as.

$$\mathrm{E} = \frac{1}{2}(D-O)^T(D-O) = \frac{1}{2}\sum_{k=1}^{i}(D_k - O_k)^2 \tag{3.6}$$

The partial derivative of the connection weights W_3 is obtained for E according to the error gradient principle.

$$\frac{\partial E}{\partial W_{3kj}} = -(D_k - O_k) f'\mathrm{O(k)} X_j(k) \tag{3.7}$$

Let $\delta_k^0 = (D_k - O_k) f'\mathrm{O(k)}$,

$$\frac{\partial E}{\partial W_{3kj}} = -\delta_k^0 X_j(k) \tag{3.8}$$

Where k = 1, 2…I; j = 1, 2…, m.

The partial derivative of the connection weights $\mathrm{W_2}$ for E is given by

$$\frac{\partial E}{\partial W_{2ji}} = \frac{\partial E}{\partial X_j(k)}\frac{\partial X_j(k)}{\partial W_{2ji}} = -\sum_{k=1}^{1}\delta_k^0 W_{3kj}\frac{\partial X_j(k)}{\partial W_{2ji}} \tag{3.9}$$

$$\begin{aligned}\frac{\partial X_j(k)}{\partial W_{2ji}} &= \frac{\partial}{\partial W_{2ji}}\left\{f\left[\sum_{i=1}^{m} W_{1ji} Xc(k) + \sum_{i=1}^{n} W_{2ji} I(k)\right]\right\} \\ &= f'\left(X_j(k)\right)\left(I(k) + \sum_{i=1}^{m} W_{1ji}\frac{\partial Xc(k)}{\partial W_{2ji}}\right)\end{aligned} \tag{3.10}$$

Using the same method to derive the partial derivative of the E pair of connection weights $\mathrm{W_1}$, we obtain

$$\frac{\partial E}{\partial W_{1ji}} = -\sum_{k=1}^{1} \delta_k^0 W_{3kj} \frac{\partial X_j(k)}{\partial W_{jji}} \tag{3.11}$$

where k = 1, 2…m; j = 1, 2…, m.

$$\frac{\partial X_j(k)}{\partial W_{1ji}} = \frac{\partial}{\partial W_{1ji}} \left\{ f \left[\sum_{i=1}^{m} W_{1ji} Xc(k) + \sum_{i=1}^{n} W_{2ji} I(k) \right] \right\}$$

$$= f'\left(X_j(k)\right) \left(Xc(k) + \sum_{i=1}^{m} W_{1ji} \frac{\partial Xc(k)}{\partial W_{2ji}} \right) \tag{3.12}$$

2) Learning algorithm for weight correction of Elman neural network

For recurrent neural networks, sometimes a static BP algorithm can be used in correcting the weights for simplicity of computation. However, since the output of a neural network is not only related to the input at moment k, but also to the input signal before k, dynamic learning rules must be used when exact calculation is involved. In BP neural networks, the algorithm of chain rule is used for the derivation of the learning algorithm. In contrast, in the study of recursive algorithms, it is different, and the algorithm of ordered chain rule is generally used [177][178][179]. In addition, there are two methods for computing recurrent neural networks: one is the batch mode and the other is the online mode, where online training rules will be used.

Define the error function for the weight adjustment of the neural network at moment k as:

$$\mathrm{E(k)} = \frac{1}{2} \sum_{i=1}^{r} \left(d_i(k) - y_i(k) \right)^2 \tag{3.13}$$

Where: $d_i(k)$ is the expected output of the i-th output node at moment k.

Let $e_i(k)$ be the error between the expected output and the actual output of the *i-th* output node at moment *k*, i.e.

$$e_i(k) = d_i(k) - y_i(k) \tag{3.14}$$

The weights of the neural network change are

$$w(k+1) = w(k) + \eta \left(-\frac{\partial E(k)}{\partial w} \right) + \alpha \Delta w(k) \tag{3.15}$$

where *w* can represent the weights of input layer, hidden layer or output layer.

For the weights of the output layer, using the ordered chain rule, there are

$$-\frac{\partial \mathrm{E(k)}}{\partial \mathrm{w}_{ij}^{1}} = -\frac{\partial \mathrm{E(k)}}{\partial \mathrm{y_i}(k)} \times \frac{\partial \mathrm{y_i}(k)}{\partial \mathrm{w}_{ij}^{1}}$$

$$= -\frac{\partial \mathrm{E(k)}}{\partial \mathrm{y_i}(k)} \times \frac{\partial \mathrm{y_i}(k)}{\partial \mathrm{s}_{i}^{3}(k)} \times \frac{\partial \mathrm{s}_{i}^{3}(k)}{\partial \mathrm{w}_{ij}^{1}}$$

$$= e_i(k) \times f_2'\left(s_i^3(k)\right) \times s_j^1(k) \tag{3.16}$$

For the weights of the hidden layer, similarly we have

$$-\frac{\partial \mathrm{E(k)}}{\partial \mathrm{w}_{ij}^{0}} = -\sum_{l=1}^{r} \frac{\partial \mathrm{E(k)}}{\partial \mathrm{y_i}(k)} \times \frac{\partial \mathrm{y_i}(k)}{\partial \mathrm{w}_{ij}^{0}}$$

$$= -\sum_{l=1}^{r} \frac{\partial \mathrm{E(k)}}{\partial \mathrm{y_i}(k)} \times \frac{\partial \mathrm{y_i}(k)}{\partial \mathrm{s}_{i}^{3}(k)} \times \frac{\partial \mathrm{s}_{i}^{3}(k)}{\partial \mathrm{x}_{i}^{1}(k)} \times \frac{\partial \mathrm{x}_{i}^{1}(k)}{\partial \mathrm{w}_{ij}^{0}}$$

$$= \sum_{l=1}^{r} e_l(k) \times f_2'\left(s_i^3(k)\right) \times w_{li}^1(k) \times \frac{\partial \mathrm{x}_{i}^{1}(k)}{\partial \mathrm{w}_{ij}^{0}} \tag{3.17}$$

If we let $\beta_{\mathrm{ij}}^{i}(k) = \frac{\partial \mathrm{x}_{i}^{1}(k)}{\partial \mathrm{w}_{ij}^{0}}$, then we have

$$\beta_{\mathrm{ij}}^{i}(k) = \frac{\partial \mathrm{x}_{i}^{1}(k)}{\partial \mathrm{w}_{ij}^{0}} = \frac{\partial \mathrm{x_i^1(k)}}{\partial \mathrm{s_i^1}(k)} \times \frac{\partial \mathrm{s_i^1}(k)}{\partial \mathrm{w}_{ij}^{0}}$$

$$= f_1'\left(s_i^1(k)\right) \times \left(x_j^0(k) + \sum_{m=1}^{n^1} w_{im}^2 \times \frac{\partial c_m(k)}{\partial \mathrm{w}_{ij}^{0}}\right)$$

$$= f_1'\left(s_i^1(k)\right) \times \left(x_j^0(k) + \sum_{m=1}^{n^1} w_{im}^2 \times \frac{\partial x_m^1(k-1)}{\partial \mathrm{w}_{ij}^{0}}\right)$$

$$= f_1'\left(s_i^1(k)\right) \times \left(x_j^0(k) + \sum_{m=1}^{n^1} w_{im}^2 \times \beta_{ij}^m(k-1)\right) \tag{3.18}$$

Then we can get

$$\begin{cases} -\dfrac{\partial \mathrm{E(k)}}{\partial \mathrm{w}_{ij}^{0}} = \sum_{l=1}^{r} e_l(k) \times f_1'\left(s_i^3(k)\right) \times w_{li}^1(k) \times \beta_{\mathrm{ij}}^i(k) \\ \beta_{\mathrm{ij}}^i(k) = f_1'\left(s_i^1(k)\right) \times \left(x_j^0(k) + \sum_{m=1}^{n^1} w_{im}^2 \times \beta_{ij}^m(k-1) \right) \end{cases} \tag{3.19}$$

Where: $\beta_{\mathrm{ij}}^m = 0; m, i, j = 1,2,\cdots, n.$

Similarly, the weights for the context layer are

$$\begin{cases} -\dfrac{\partial \mathrm{E(k)}}{\partial \mathrm{w}_{ij}^{0}} = \sum_{l=1}^{r} e_l(k) \times f_2'\left(s_i^3(k)\right) \times w_{li}^1(k) \times \delta_{\mathrm{ij}}^i(k) \\ \delta_{\mathrm{ij}}^i(k) = f_1'\left(s_i^1(k)\right) \times \left(x_j^1(k-1) + \sum_{m=1}^{n^1} w_{im}^2 \times \delta_{ij}^m(k-1) \right) \end{cases} \tag{3.20}$$

Where: $\delta_{\mathrm{ij}}^m = 0; m, i, j = 1,2,\cdots, n.$

3) Elman neural network weight stability

We use Lyapunov stability theory to analyze the stability of the studied Elman neural network [180][181] [182]. The defined **Eq. (3.14)** of the global error function is used as the Lyapunov function, and by bringing **Eq. (3.14)** into **Eq. (3.13)**, we have

$$\mathrm{E(k)} = \frac{1}{2}\sum_{i=1}^{r} e_i^2(k) \tag{3.21}$$

To ensure the stability of the system, it is necessary to have

$$\Delta E(k+1) = E(k+1) - E(k) < 0 \tag{3.22}$$

That is

$$\frac{1}{2}\sum_{i=1}^{r}\left(e_l^2(k+1) - e_i^2(k)\right) \tag{3.23}$$

When the neural network weights vary less, a Taylor expansion of $\mathrm{e_i}(k+1)$ is

$$\mathrm{e_i}(k+1) = e_i(k) + \frac{\partial \mathrm{e_i}(k)}{\partial w}\Delta w + \cdots \approx e_i(k) + \frac{\partial \mathrm{e_i}(k)}{\partial w}\Delta w \tag{3.24}$$

Substituting **Eq. (3.24)** into **Eq. (3.23)**, we get

$$\Delta \mathrm{E}(\mathrm{k}+1)$$

$$= \frac{1}{2}\sum_{i=1}^{r}\left(e_i^2(k) + 2\frac{\partial e_i(k)}{\partial w}\Delta w \times e_i(k) + \left(\frac{\partial e_i(k)}{\partial w}\Delta w\right)^2 - e_i^2(k)\right)$$

$$= \frac{1}{2}\sum_{i=1}^{r}\frac{\partial e_i(k)}{\partial w}\Delta w\left(2e_i(k) + \frac{\partial e_i(k)}{\partial w}\Delta w\right) \quad (3.25)$$

With small changes in the weights, **Eq. (3.15)** can be approximated as

$$\Delta \mathrm{w} \approx \eta\left(-\frac{\partial E(k)}{\partial w}\right) = -\eta\sum_{i=1}^{r}\frac{\partial E(k)}{\partial e_j(j)} \times \frac{\partial e_j(k)}{\partial w} = -\eta\sum_{j=1}^{r} e_j(k) \times \frac{\partial e_j(k)}{\partial w} \quad (3.26)$$

Substituting **Eq. (3.26)** into **Eq. (3.25)**, we get

$$\Delta \mathrm{E}(\mathrm{k})$$

$$= -\frac{1}{2}\sum_{i=1}^{r}\frac{\partial e_i(k)}{\partial w} \times \Delta w\left(2e_i(k) + \frac{\partial e_i(k)}{\partial w}\left(-\eta\sum_{j=1}^{r} e_j(k) \times \frac{\partial e_j(k)}{\partial w}\right)\right)$$

$$= -\frac{1}{2}\sum_{i=1}^{r}\frac{\partial e_i(k)}{\partial w}$$

$$\times\left(-\eta\sum_{j=1}^{r} e_j(k) \times \frac{\partial e_j(k)}{\partial w}\right)\left(2e_i(k) + \frac{\partial e_i(k)}{\partial w}\left(-\eta \times \frac{\partial e_j(k)}{\partial w}\right)\right)$$

$$= \frac{1}{2}\sum_{i=1}^{r}\sum_{j=1}^{r} e_j(k) \times \frac{\partial e_i(k)}{\partial w} \times \frac{\partial e_j(k)}{\partial w}\left(2e_i(k)\right.$$

$$\left.-\eta\left(\sum_{j=1}^{r} e_j(k) \times \frac{\partial e_i(k)}{\partial w} \times \frac{\partial e_j(k)}{\partial w}\right)\right)$$

$$= -\frac{1}{2}\eta\left(\eta\sum_{i=1}^{r}\sum_{j=1}^{r} e_j(k) \times \frac{\partial e_i(k)}{\partial w} \times \frac{\partial e_j(k)}{\partial w}\right)^2$$

$$-2\sum_{i=1}^{r}\sum_{j=1}^{r} e_i(k) \times e_j(k) \times \frac{\partial e_i(k)}{\partial w} \times \frac{\partial e_j(k)}{\partial w} \quad (3.27)$$

According to **Eq. (3.23)** and **Eq. (3.27)**, we get

$$0 < \eta < \frac{2\sum_{i=1}^{r}\sum_{j=1}^{r} e_i(k) \times e_j(k) \times \frac{\partial e_i(k)}{\partial w} \times \frac{\partial e_j(k)}{\partial w}}{\sum_{i=1}^{r}\sum_{j=1}^{r}\left(e_i(k) \times \frac{\partial e_i(k)}{\partial w} \times \frac{\partial e_j(k)}{\partial w}\right)^2} \tag{3.28}$$

let

$$g_{\max} = \left\| \frac{\sum_{i=1}^{r}\sum_{j=1}^{r}\left(e_i(k) \times \frac{\partial e_i(k) \times e_j(k)}{\partial w}\right)^2}{\sum_{i=1}^{r}\sum_{j=1}^{r} e_i(k) \times e_j(k) \times \frac{\partial e_i(k)}{\partial w} \times \frac{\partial e_j(k)}{\partial w}} \right\| \tag{3.29}$$

Then we get

$$0 < \eta < \frac{2}{g_{max}} \tag{3.30}$$

Eq. (3.29) or **Eq. (3.30)** is the convergence range that guarantees a stable learning rate for the Elman neural network.

4) Determination of learning rate at stabilization of diagonal recurrent neural networks

According to **Eq. (3.28)**, the diagonal neural network is to take the case of i=1 and j=1, at this time, the range of values of the learning rate of the neural network stable can be obtained as

$$0 < \eta < \frac{2}{\left(\frac{\partial e(k)}{\partial w}\right)^2} \tag{3.31}$$

If we set $g_{\max}^{D} = \max_{k} \left\| \frac{\partial e(k)}{\partial w} \right\|$, then we get

$$0 < \eta < \frac{2}{(g_{\max}^{D})^2} \tag{3.32}$$

If $f_1(x) = \frac{1-e^{-x}}{1+e^{-x}}$, $f_2(x) = x$, the learning of output layer, association layer and hidden layer can be obtained The range of rate values are:

$$\begin{cases} 0 < \eta^{O} < \dfrac{2}{n^1} \\ 0 < \eta^{D} < \dfrac{2}{n^1 (w_{max}^1)^2} \\ 0 < \eta^{I} < \dfrac{2}{n^1 (w_{max}^1 x_{max}^0)^2} \end{cases} \tag{3.33}$$

This result is obtained because it is related to the value of $\frac{\partial e(k)}{\partial w}$. In practice, the optimal value of the learning rate of each layer is taken as

$$\begin{cases} \eta_{\text{opt}}^{O} = \dfrac{2}{n^1} \\ \eta_{\text{opt}}^{D} = \dfrac{2}{n^1 (w_{max}^1)^2} \\ \eta_{\text{opt}}^{I} = \dfrac{2}{n^1 (w_{max}^1 x_{max}^0)^2} \end{cases} \tag{3.34}$$

Figure 3.3 shows the process of the Elman neural network for wind direction prediction: initialize the network weights; perform network output calculations on the normalized wind direction data, and perform network weighting through the error gradient method. The value is revised until the training accuracy meets the requirements before prediction [183][184].

5) Prediction performance analysis

The prediction performance analysis in the prediction model is the key to optimize the model performance, and the mean squared error (MSE) along with the correlation coefficient R, generally used to evaluate the prediction performance index of the neural network model [185]. Mean squared error is a metric used to describe the systematic error, it represents the sum of the quadratic differences among the detected values and the predicted values divided by the number of observed values. The closer the MSE to 0, the smaller the deviation among the detected values and the predicted values of the two variables, i.e., the better the performance of the neural network. The correlation coefficient (R) is a statistical indicator that reflects the closeness of the correlation between the variables. The correlation coefficient varies between [-1, 1]. The value of |R| is closer to 1, and the degree of linear correlation between the variables is higher. This state is described as the formulas:

$$\mathrm{MSE} = \frac{1}{\mathrm{n}}\sum_{i=1}^{n}(y_i - \hat{y}_i)^2 \tag{3.35}$$

$$\mathrm{R} = \frac{\sum_{i=1}^{n}(\hat{y}_i - \bar{\hat{y}}_i)(y_i - \bar{y})}{\sqrt{\sum_{i=1}^{n}\left(\hat{y}_i - \bar{\hat{y}}_i\right)^2 \sum_{i=1}^{n}(y_i - \bar{y})^2}} \tag{3.36}$$

Where:

y_i - the input sample data;

$\hat{y}_i$ - the predicted value;

$\bar{\hat{y}}_i$ - the mean of the predicted value;

$\bar{y}$ - the mean of the sample input data.

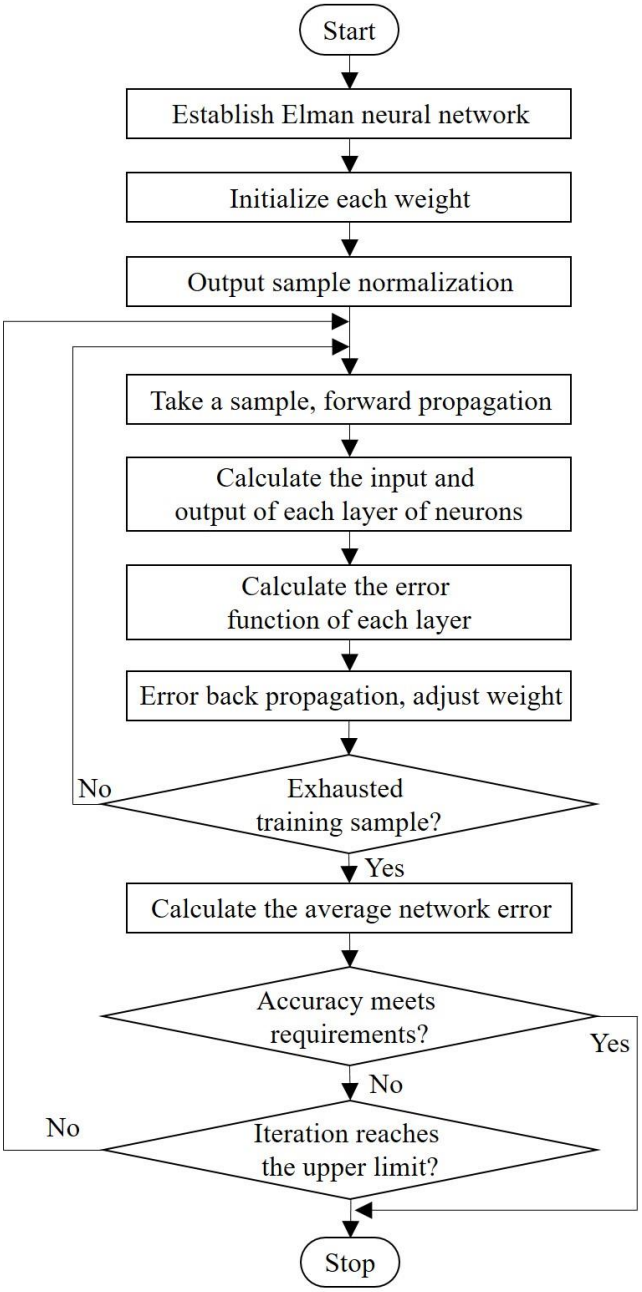

Figure 3.3. The process of the Elman neural network

3.1.3 Improved automatic yaw based on predicted wind direction

Normally the yaw controller sends 4 signals to the yaw motor, which depends on the wind direction and nacelle position [186]. The signal can be called "ASS", the meaning is shown in **Figure 3.4**.

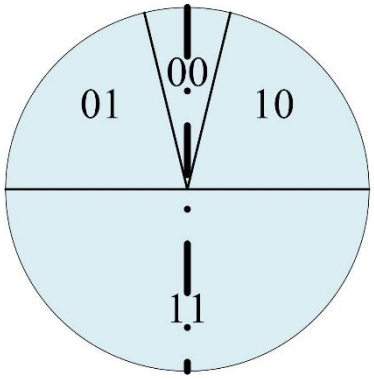

Figure 3.4. Meanings of ASS signal

When ASS=00, it means that there is no yaw error, and the unit does not need to make yaw action (ASS=00 does not mean that the wind direction is exactly right with the axial direction of the blade, but that the error is within the tolerance range).

When ASS=01, the nacelle drives the left yaw of the blade, i.e., the yaw motor forward.

When ASS=10, the nacelle drives the right yaw of the blade, i.e., the yaw motor reverses.

When ASS=11, it means that the unit needs to perform obtuse angle yawing, and in order to avoid the winding of cables, the direction of this obtuse angle yawing should be opposite to the direction of the last obtuse angle yawing, and the yaw controller records the direction of this obtuse angle yawing at the same time.

In the existing automatic yaw control, the yaw action is executed based on the average wind direction of the first 30s without considering the future wind direction, and this execution process will have certain blindness and lag, which increases the number of yaw actions to a certain extent and also causes yaw errors. To solve this problem, we propose an improved automatic yaw control method that combines the predicted wind direction with the first 10min wind direction as the basis for executing yaw action. The workflow diagram of the improved auto-yaw is shown in **Figure 3.5**.

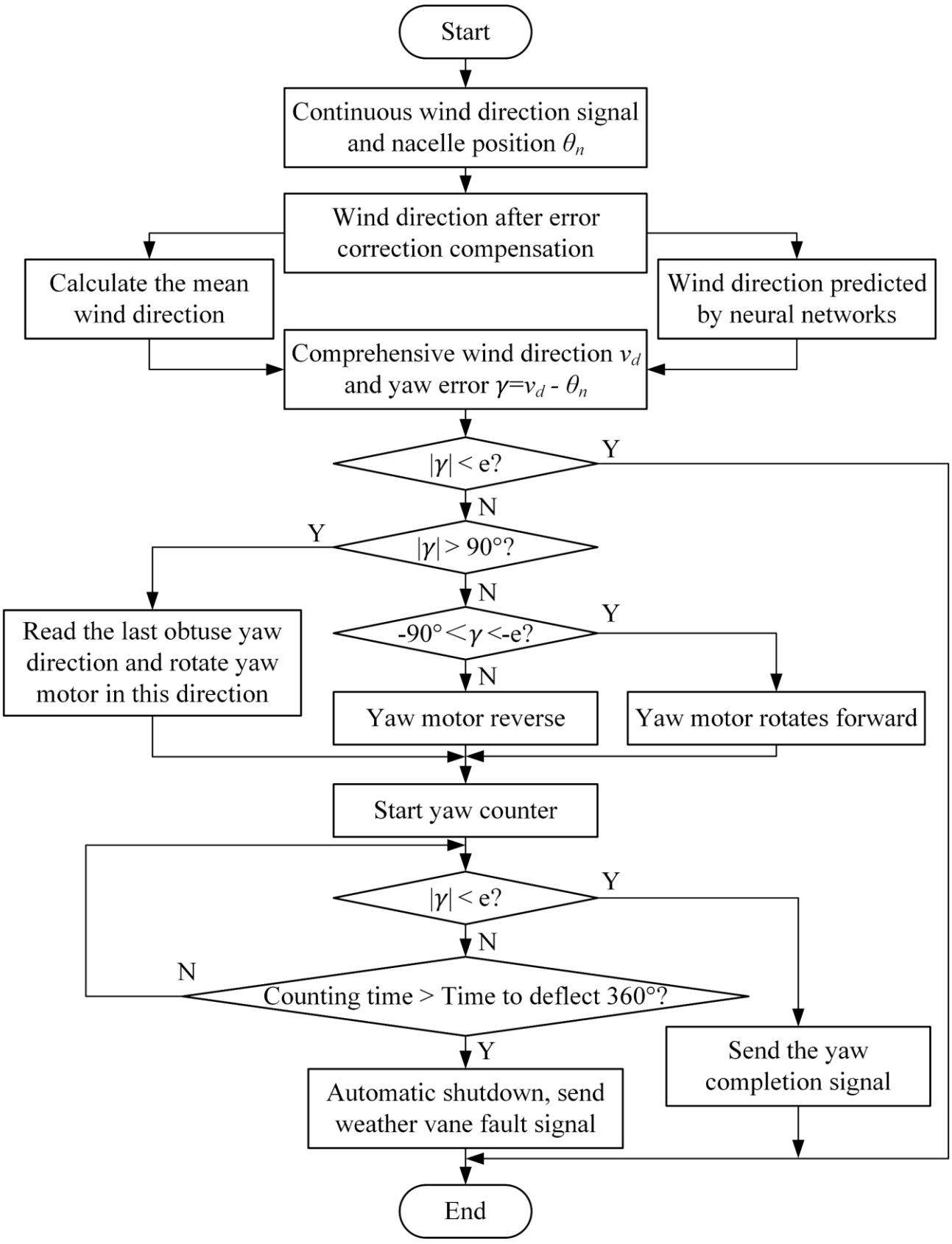

Figure 3.5. Flow chart of the improved auto-yaw

The specific process of the improved automatic yaw control of the wind turbine yaw system is as follows: take the wind direction measured by the weather vane for 10 min continuously before a certain time point, compensate for the error in this wind

direction data, calculate the average wind direction of the corrected wind direction during this period, and predict the wind direction after 10min based on the corrected wind direction by neural network; sum the corrected average wind direction and the predicted wind direction to obtain the integrated wind direction v_d. The modified average wind direction and the predicted wind direction are summed and averaged to obtain the integrated wind direction, and the yaw controller issues the signal for yaw control according to the integrated wind direction. The wind direction data used in the improved automatic yaw control are the error-corrected wind direction data, so the tolerance angle is set to 9°, while the other execution processes related to the signal are still consistent with the existing automatic yaw control process.

3.2 Power control algorithm based on hill climbing search

3.2.1 The basic principle of hill climbing search algorithm

Hill climbing search (HCS), also known as hill climbing algorithm [187][188][189], is an artificial intelligence control algorithm mainly used to find the extreme value point of an unknown function. The specific idea of this algorithm is to continuously apply a series of rules and constraints to the controlled object, while checking its output, i.e., using recursive calls to gradually increase the output value to ensure that the output is gradually approaching the maximum value, and finally making the output value infinitely close to the maximum output value.

1) Fixed-step hill climbing search algorithm

The traditional hill climbing search algorithm uses fixed-step optimization search [190][191][192], and when the wind speed or wind direction changes during the experiment, it will cause the system output power to change. Let the power change at the *k-th* sampling be ΔP and the wind direction change be $\Delta\theta$. The direction of the command signal change of the wind regulator is shown in **Table 3.1**:

If the power sampling time is comparable to the period of the wind regulator, wrong information about the power variation ΔP will be obtained, leading to oscillation of the system at the operating point due to the fluctuation of the generator torque. Therefore, the period of power sampling should be larger than the period of the yaw wind direction control loop. In this system, the operating period of power sampling is

4 times larger than the adjustment period of the yaw wind control loop.

Table 3.1 Disturbance discriminant table

Judgment Conditions	$\Delta P_k > 0$	$\Delta P_k < 0$
$\Delta\theta(k-1) = 0$	$\Delta\theta(k) > 0$	$\Delta\theta(k) < 0$
$\Delta\theta(k-1) > 0$	$\Delta\theta(k) > 0$	$\Delta\theta(k) < 0$
$\Delta\theta(k-1) < 0$	$\Delta\theta(k) < 0$	$\Delta\theta(k) > 0$

For wind power generation, the fixed-step hill climbing search algorithm has many disadvantages: the fixed yaw perturbation is slow to track the rapidly changing wind direction; the torque pulsation caused by the dead zone of the inverter affects the observation and comparison of the wind turbine output power in the yaw control; the stepped variation of the wind turbine yaw command value generated by the fixed speed perturbation makes the output power of the wind turbine always varying from one step to another.

2) Variable step length hill climbing search algorithm

The variable step length hill climbing search algorithm improves the step length on the basis of the traditional hill climbing search algorithm by using the perturbation value of variable step length [193][194][195][196][197]. Specifically, $\Delta\theta$ should be increased appropriately when the wind direction changes rapidly. The wind turbine yaw perturbation can be determined by **Eq. (3.35)**:

$$\Delta\theta = \mathrm{K}_\theta \left(\frac{dP_r}{d\theta_r}\right) \tag{3.35}$$

K_θ: coefficient to adjust the wind turbine yaw perturbation, which can be determined experimentally to obtain stable tracking control. The farther away from the optimal operating point, the larger $\frac{dP_r}{d\theta_r}$ is, thus making the wind turbine yaw system track faster, and when the extreme point is reached, $\frac{dP_r}{d\theta_r}$ tends to 0, making the wind turbine have a smoother power output in stable wind direction.

The lower limit of the yaw perturbation $\Delta\theta_{\min}$ is set appropriately to avoid overflow when calculating the power slope, and the calculated wind turbine

perturbation value will be limited between its upper and lower limit values. In each yaw control cycle, there is a wind turbine yaw perturbation value that causes the wind turbine position to change, so that the wind turbine position is always different in the two control cycles that are separated, and therefore the calculation of the wind turbine power slope is always valid (the denominator is not too small). Only the yaw control with variable step perturbation can get a larger yaw perturbation when the wind direction is changing rapidly, so that the wind turbine maximum power point can be tracked faster, and a smaller yaw perturbation can be obtained when the wind direction is changing less or constant, so that the wind turbine has a smoother power output in a stable wind direction.

For variable-step yaw control, the algorithm generates step-change yaw commands that cause dramatic fluctuations in the position of the wind turbine. To obtain fast yaw control, a relatively large value of yaw perturbation is used, but using a large control factor K_θ, the position of the wind turbine becomes very unstable. To make the yaw control smooth, a low-pass filter is used at the output of the yaw controller to smooth the yaw command, and the cut-off frequency of the filter is just a little lower than the frequency band of the yaw control loop. In digital control, this low-pass filter can be implemented with a first-order difference equation. The purpose of this low-pass filter is to make the wind tracking control of the wind turbine both fast and smooth.

3) Intelligent hill climbing search algorithm

Although the hill climbing search algorithm can be used to constantly adjust the wind turbine position to eliminate yaw errors, in large WECS, the wind direction usually changes immediately when the hill climbing search algorithm is searching for the position of a certain wind direction. Hill climbing search algorithm can only work well when the turbine inertia is very small, so that the response of the turbine yaw speed to the wind direction is almost instantaneous [198]. For large inertia turbines, the system output power is interleaved with the mechanical power of the turbine and the rate of change of mechanical stored energy, resulting in a hill climbing search method that is not very effective.

In order to make the hill climbing search method applicable to WECS with different levels of wind turbine inertia values, the advanced hill climbing search algorithm is thus proposed [199][200]. The principle is shown in **Figure 3.6**.

The intelligent hill climbing search algorithm uses a direct current-driven control method that combines the intelligent hill climbing search algorithm with direct current-driven control to form a complete search-memory-apply yaw control algorithm. The principle behind this algorithm is the "search- memory-apply" process. The algorithm starts with an empty smart memory with relatively low initial performance, and during operation, the training mode gradually trains the smart memory with the data searched by the advanced hill climbing search algorithm, continuously recording the training data. The algorithm reuses the recorded data in application mode for fast execution, and this "search-memory-apply" will keep repeating itself until an accurate memory of system characteristics is established. Thus, after the algorithm has been trained enough, its performance in tracking wind direction will be optimized.

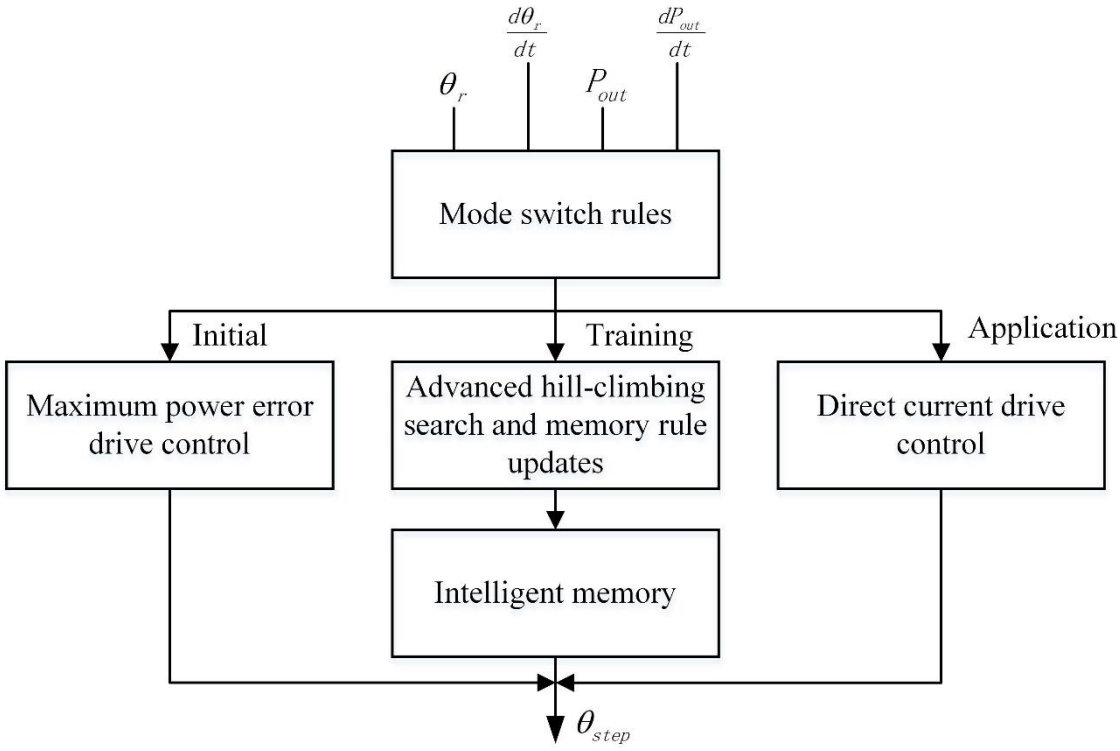

Figure 3.6. Intelligent hill climbing search algorithm

3.2.2 Design of hill climbing search algorithm

Aiming at the problems of weather vane measurement error (about ±5°) and neural network prediction wind direction error, a hill climbing search algorithm is

proposed to control the yaw mechanism and accurately adjust the position of the nacelle when the yaw error occurs, so that the normal direction of the wind turbine rotor is always consistent with the changing wind direction, and the control strategy of capturing the maximum wind energy is realized.

The yaw system of the wind turbine has been discussed in detail in **Section 1.3**. The wind measuring device uses anemometers and weather vanes. The weather vane can rotate freely with the wind, and its direction is consistent with the wind direction, and the anemometer is used to measure the wind speed. The anemometer and the weather vane are usually installed above the nacelle, and their reference direction is consistent with the normal direction of the blade plane, so that the angle between the direction of the weather vane and the reference direction of the sensor base is the angle between the wind direction and the normal direction of the blade plane. Usually the wind direction sensor sends the wind direction signal to the controller through the angle-to-electrical signal converter. When the wind direction changes and exceeds the allowable error range, the controller sends out an automatic yaw command, and the yaw system composed of the transmission mechanism and the yaw motor performs corrective actions to make the nacelle track the wind accurately.

Because the wind turbine blade turbulence has a large disturbance to the wind direction sensor, and due to the discreteness and turbulence of the wind direction, the weather vane will swing continuously due to its influence, which will greatly shorten the life of the angle-to-electrical signal converter. The accuracy of the weather vane on the wind turbine is usually relatively low. It can only measure the approximate angle between the nacelle and the direction of the incoming wind, but cannot detect the actual direction of the wind. It is easily damaged in strong winds such as typhoons. Moreover, the cost of wind turbines has always been an open issue.

In order to effectively control the yaw system, the industrial development and application of Kalman filter, PI control, fuzzy control, optimal control and other controllers. The yaw control signals of these controllers are all derived from weather vane. Because it is located in the downwind direction, it is affected by various unfavorable factors such as turbulence, and its own direction finding accuracy is also

insufficient, so that the control signal is not ideal, which leads to low accuracy. When the wind changes within the range of ±15°, the weather vane cannot accurately measure the wind direction. So a control algorithm without the use of the weather vane to find the direction of wind is proposed. The hill climbing search algorithm is used to detect the generated power, and according to the change of the power, cooperate with the corresponding algorithm to control the steering of the yaw motor and find the maximum power value point. This algorithm can eliminate the weather vane and find the wind direction by comparing the power output.

The hill climbing search algorithm is introduced into the power control to optimize the yaw control system. The algorithm can shorten the time of the wind turbine tracking the wind, improve the wind energy utilization rate of the generator set and prolong the service life of the wind turbine [201][202][203].

The specific control strategy is: set V_d as the wind direction, P* as the power given value, P^*_{max} as the maximum value of the power given, P as the intermediate variable, P_f as the detected instantaneous power feedback value, ΔP_1 as the wind speed or wind direction The power change value when changing, $\Delta P_1 = P^*_{max} - P$; ΔP_2 is the power change value when the wind speed or wind direction changes, $\Delta P_2 = P_f - P$, Δp^* is the power difference given value, Δ is the assignment to Δp^* a constant value of *, θ is the rotation angle of the yaw motor [204][205][206].

(1) When the wind speed is constant and the wind direction is deflected. Set $p(\theta) = P_{max} \cdot \cos(\theta)$, as can be seen from **Figure 3.7**, at this time $\Delta p_1 = P^*_{max} - p(\theta) = P^*_{max} \cdot (1 - \cos(\theta))$, among them, define y-axis is the power axis; the x-axis is the positioning axis of the yaw motor; the curves V_1 and V_2 are the curves of different wind directions. Since at θ_1, $\Delta p_1 > \Delta p^*$, the yaw motor rotates towards the wind direction of V_2, then continue to perform yaw control in the original direction, at θ_2, $\Delta p_2 = p_f - p$, $\Delta p = \Delta p_1 - \Delta p_2$, $\Delta p > \Delta p^*$, therefore, the yaw motor still rotates in the original direction, and the sampling is compared until it reaches the vicinity of θ_3.

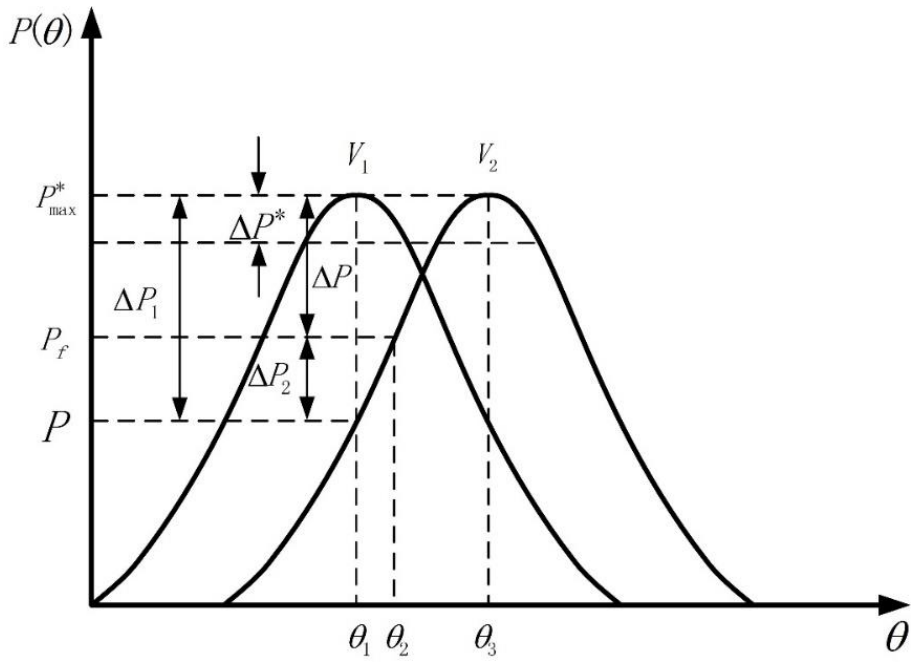

Figure 3.7. Hill climbing search algorithm when wind direction changes

(2) When the wind direction remains unchanged, the wind speed V_{s1} changes from V_{s2}. As can be seen from **Figure 3.8**, $\Delta p_1 = P^*_{1max} - P^*_{2max}$, $\Delta p_1 > \Delta p^*$, the yaw motor is started, counterclockwise from θ_2 to θ_1, sampling comparison, $\Delta p = \Delta p_1 - \Delta p_2 > \Delta p_1$, indicating that the yaw direction is wrong , clockwise from θ_1 to θ_3, there is still $\Delta p = \Delta p_1 - \Delta p_2 > \Delta p_1$, which means that the wind direction has not changed, but the wind speed has changed, and the yaw motor has returned to its original position.

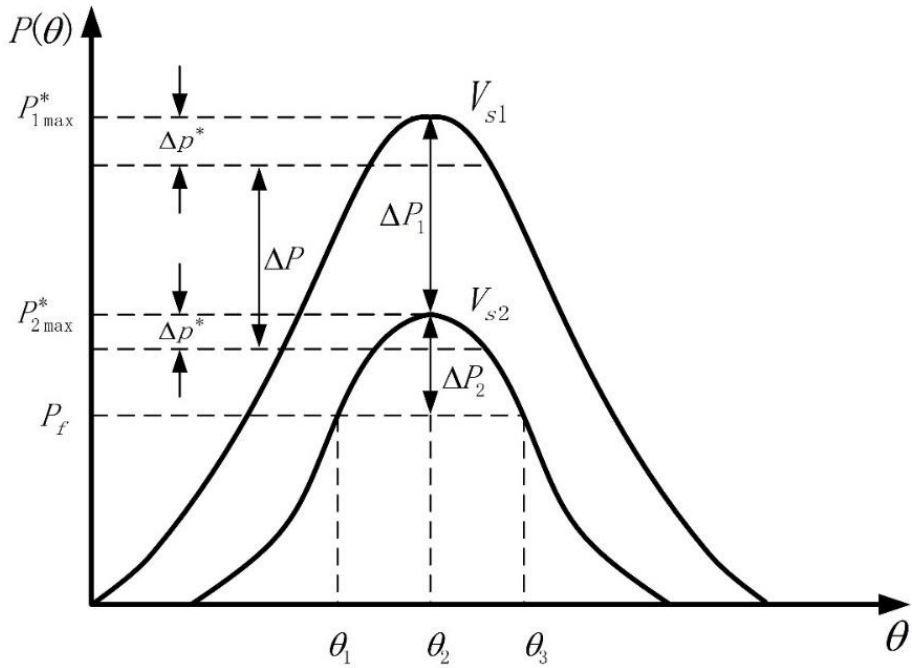

Figure 3.8. Hill climbing search algorithm when wind speed changes

Feedback control design: after the yaw process is over, due to unfavorable factors such as the mechanism itself and the natural environment, it cannot be guaranteed whether the wind turbine nacelle reaches the correct position. Therefore, feedback detection should be performed when yawing the nacelle. As shown in **Figure 3.9**, the detected signal is transmitted to the yaw system through the input/output interface, and the yaw system is compared according to the rotation angle transmitted in the overall control area. Any deviations will be compensated immediately.

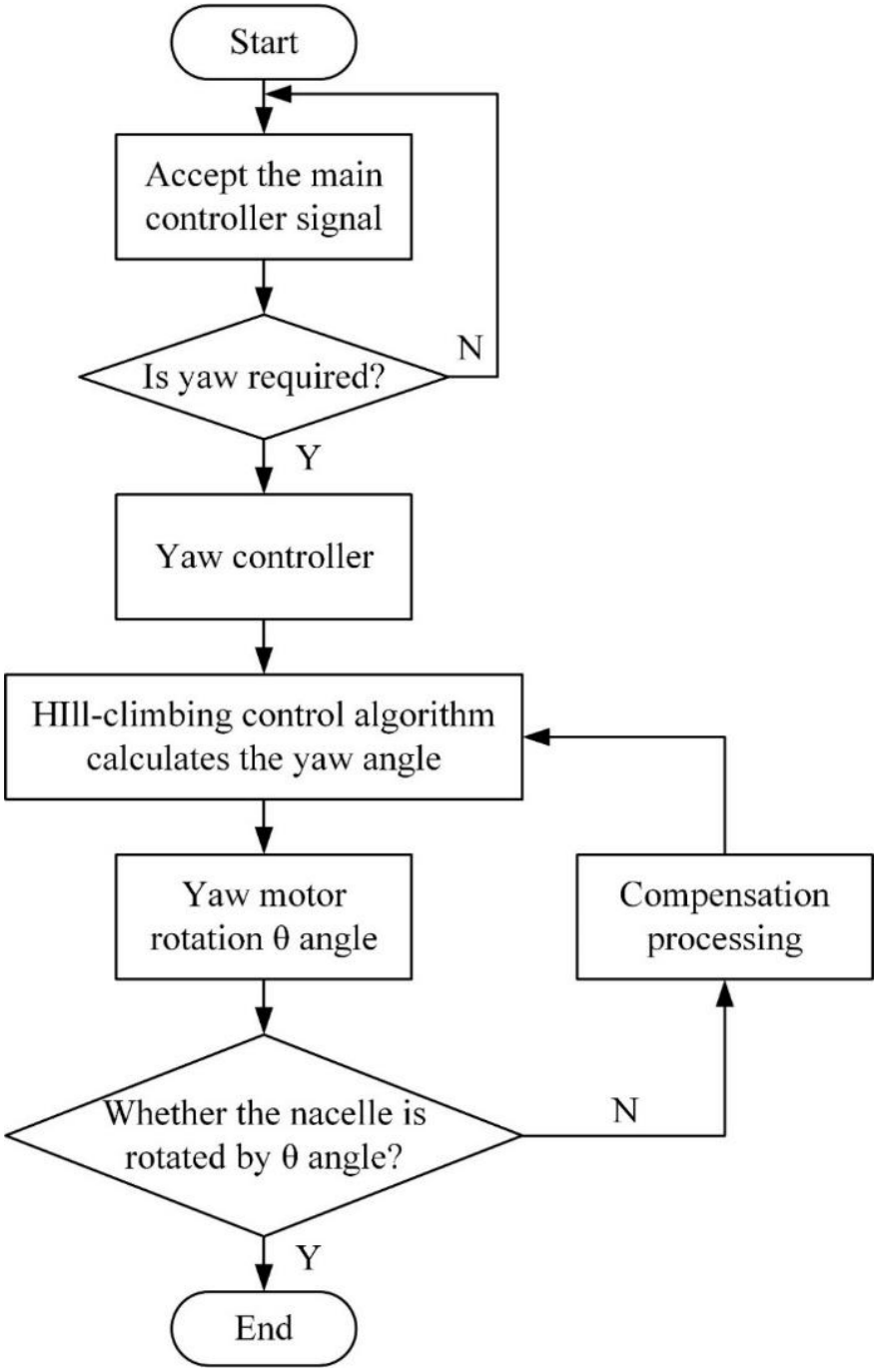

Figure 3.9. Yaw system feedback control flow chart

When applying the hill climbing search algorithm for yaw control, issues such as generator output power detection, power value calculation, and yaw control parameters need to be considered and handled [207]. **Figure 3.10** shows the block diagram of the source departure for detecting the generator output power.

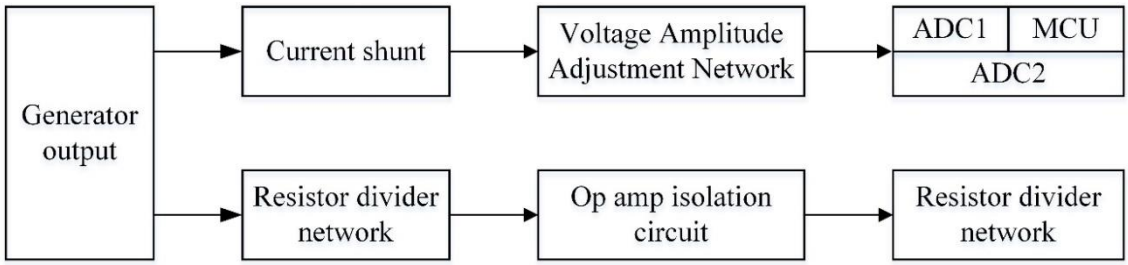

Figure 3.10. DC power measurement principle block diagram

The output power of the generator can be calculated from the voltage $\mathrm{U_{DC}}$ and current $\mathrm{I_{DC}}$ after the microprocessor sampling transformation, that is, $\mathrm{P = U_{DC} \cdot I_{DC}}$.

For the generator, there are many ways to measure its output power, one of the easier methods is to measure the single-phase power, but this method will produce a relatively large error when the three-phase power is not balanced. Using two wattmeter method to measure the AC power, the results are more accurate, the calculation formula is **Eq. (3.36)**.

$$\mathrm{P} = \frac{1}{\mathrm{T}}\int_0^T [u_{AC}(t)i_A(t) + u_{BC}(t)i_B(t)]dt \tag{3.36}$$

where $\mathrm{u_{AC}(t)}$ and $\mathrm{u_{BC}(t)}$ are the line voltages; $\mathrm{i_A(t)}$ and $\mathrm{i_B(t)}$ are the phase currents.

In a cycle, the voltage and current should be sampled several times at equal intervals according to Nyquist's sampling theorem [208], and the highest resonant wave number of voltage and current should be taken into account when taking values. Let the number of samples per cycle be N, and use $\mathrm{u_{AC}(n)}$, $\mathrm{u_{BC}(n)}$, $\mathrm{i_A(n)}$, $\mathrm{i_B(n)}$ to denote the *n-th* sample value, so that $\mathrm{P(n) = u_{AC}(n)i_A(n) + u_{BC}(n)i_B(n)}$. When an even number is used to equalize the integration interval, the integral of **Eq. (3.36)** can be approximated using Simpson's method, i.e. where $u_{AC}(t)$, $u_{BC}(t)$ are line voltages; $i_A(t)$, $i_B(t)$ are phase currents.

$$\mathrm{P} = \frac{2}{3}\left[\sum_{n=1}^{N} P(n) + \sum_{n=2k}^{N} P(n)\right] \tag{3.37}$$

where k is a natural number.

The main features of this method are:

1. the calculation results are more accurate.

2. the power can be calculated for any cycle

3. the amount of computational data is relatively large, so a high-speed processor or DSP should be used to improve the real-time performance of power detection.

The output power of the generator is not stable due to the randomness of the wind, and if the jittering frequent instant power is used for calculation in the hill climbing search algorithm, it will affect the stability and accuracy of the yaw control, so it is necessary to calculate the average value of the instant power, which can be calculated using **Eq. (3.38)**.

$$\bar{P} = \sum_{i=1}^{m}\left(\frac{P_i}{m}\right) \tag{3.38}$$

where $\bar{P}$ is the average power value, $\mathrm{P_i}$ is the instantaneous power value, and m is the number of power samples.

3.2.3 Improved automatic yaw based on predicted wind direction

When the wind direction changes, there will be a difference angle between the wind direction and the wind turbine axis, and this difference angle is called yaw angle or yaw error angle θ_e, which is related to the wind angle θ_w, the wind turbine axis angle θ_t, and the generator output power as shown in the **Figure 3.11**.

Then the output power of the generator can be expressed as

$$\mathrm{P_E} = \mathrm{P_{max}} \cdot cos\theta_e = P_{max} \cdot \cos(\theta_w - \theta_t) \tag{3.39}$$

where $\mathrm{P_{max}}$ is the output power of the generator at the highest wind energy utilization.

From **Eq. (3.39)**, it can be seen that the generator output power will change when the wind direction changes. The larger the yaw angle is, the smaller the generator output power is. The generator output power is maximum only when $\theta_e = 0$.

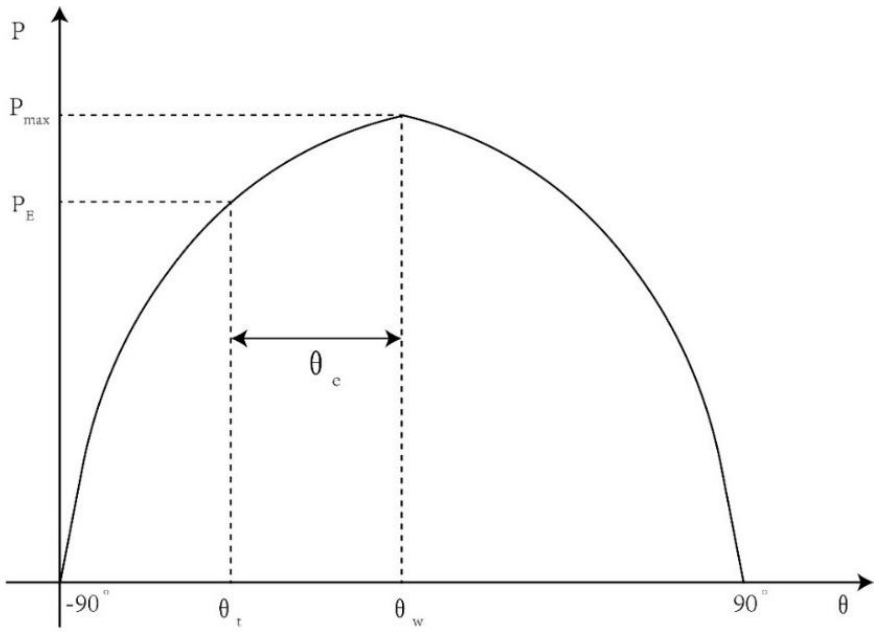

Figure 3.11. The relationship between generator output power and yaw angle

In order to achieve the purpose of accurate control of wind turbine yaw, the hill climbing search algorithm can be used to first find the great value of its output power, and then control the yaw action of the yaw motor according to the relationship between θ_e and generator power. The schematic diagram of hill climbing search algorithm is shown in **Figure 3.12**.

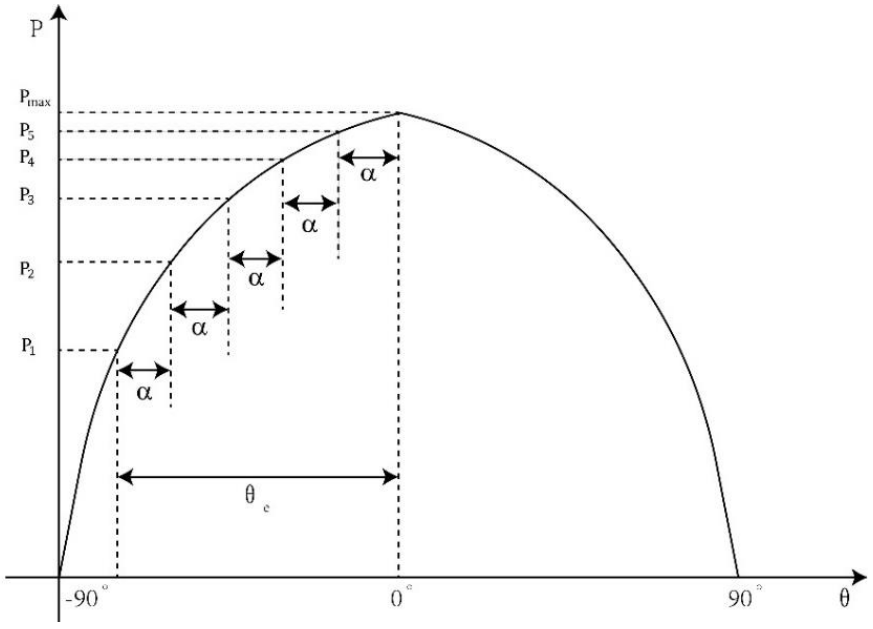

Figure 3.12. Schematic diagram of HCC algorithm

The variables involved in the power detection based hill climbing search algorithm are: the current cycle power detection value P_{new}, the next preceding cycle power detection value P_{old}, the difference between two adjacent power detections

$\Delta P = P_{new} - P_{old}$, the maximum allowable error in power P_{e1}, P_{e2}, the given power value P_{max}, the initial yaw angle θ_e, P_1, P_2, P_3, P_4 are the power values of the generator at different yaw moments, and α is the yaw angle of the wind turbine between the two power detections.

Let the wind speed be fixed and the wind energy captured by the wind turbine decreases in the case of a change in wind direction. The yaw controller obtains the current detected power value as $P_{new} = P_1$ and compares the magnitude of $|P_{new} - P_{max}|$ with that of P_{e1} to determine the magnitude of $|P_{new} - P_{max}|$ and P_{e1}. Only when $|P_{new} - P_{max}| > P_{e1}$, the yaw motor starts rotating in the counterclockwise direction (a random direction of rotation needs to be determined at the first start, and here the direction is fixed as counterclockwise).

Assign P_{new} to P_{old}, i.e., $P_{old} = P_{new}$. The yaw controller again obtains the currently detected power value $P_{new} = P_2$, at which point the wind turbine has rotated by an angle of α, if $\Delta P > 0$ and $|\Delta P| > P_{e2}$, then the yaw motor is rotating correctly in the counterclockwise direction, but the yaw effect is not at an acceptable level for the design requirements and the yaw motor needs to continue to rotate in this steering direction. In this way, the detected power value is continuously obtained and the size of $|P_{new} - P_{max}|$ is judged, and the operation status of the yaw motor is controlled according to the judgment result. When $P_{new} = P_4$ and $P_{old} = P_3$, the turbine has yawed by $\theta_e = 4\alpha$ angle, then $|\Delta P| < P_{e2}$, which indicates that the yawing effect has reached the design requirement, and the yawing motor can stop running. After ending this yaw, make $P_{max} = P_{new}$ for the next yaw control.

When the wind turbine yaws for the first time and its yaw direction is opposite to the direction of wind change, $\Delta P<0$, then the yaw controller gives the judgment that the yaw motor is turned in the wrong direction and it controls the yaw motor to rotate in the opposite direction.

In the actual operation of WECS, wind speed is not fixed, and changes in wind speed can interfere with the normal operation of the yaw control system. For wind speed changes, the HCC method based on power detection can quickly determine them. The output power of the generator will also change significantly when the wind speed

changes. When $|P_{new} - P_{max}| > P_{e1}$, the yaw control process will be initiated and the yaw motor will rotate in the initial direction. When the wind turbine yaws past α angle, if ΔP<0, it can be determined that the yaw motor rotates in the initially set direction is wrong and the yaw motor will rotate in the opposite direction under the control of the controller. When the wind turbine reverses the yaw -α angle, still ΔP<0, in this case it can be determined that it is the wind speed change rather than the wind direction change, and no yaw is needed, then the wind turbine is turned back to its original initial position and the current detected value of power is assigned to P_{max}. Therefore, when the wind speed changes, the generator will reduce its output power regardless of which direction the wind turbine rotates to under the control of the yaw control system.

Determination of control parameters: to meet the requirements of accurate and reliable operation of the yaw control system, its control parameters must be reasonable. The maximum power error P_{e1} means that the system is allowed to have a certain wind speed fluctuation and a small yaw error. In order to avoid frequent starting of the yaw motor to reduce the sensitivity of the yaw controller to the output power change, the value of P_{e1} must be determined reasonably. To get a better yaw control effect, the parameter P_{e1} must be determined reasonably.

Figure 3.13 shows the schematic diagram of the starting conditions of the yaw control motor. It can be seen that: before the t_e moment, the power P lies between $[P_{max} - P_{e1}, P_{max} + P_{e1}]$, the yaw motor does not meet the start condition, so it does not start; after the t_0 moment, the average power value exceeds the range of $[P_{max} - P_{e1}, P_{max} + P_{e1}]$ and meets the start condition of $|P_{new} - P_{max}| > P_{e1}$, the yaw motor will start only when the start condition is satisfied. After the start of yaw, the wind turbine axis turns through an angle of α between the two power detections. The microprocessor gets a new average power value for each power detection and calculates ΔP. Only when the condition $|\Delta P| < P_{e2}$ is satisfied, the yaw motor is stopped and this yaw is finished. Otherwise, the power P is obtained continuously and the comparison of the magnitude of $|\Delta P| < P_{e2}$ continues until the condition $|\Delta P| < P_{e2}$ is satisfied.

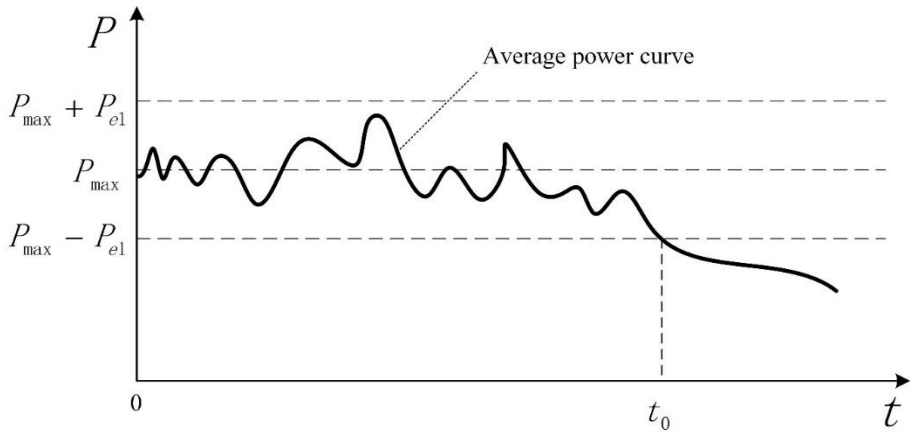

Figure 3.13. Yaw motor start condition

After the yaw motor is turned on, the windward direction of the wind turbine will gradually tend to the wind direction, and according to **Figure 3.13**, the power difference ΔP will gradually decrease in the last two cycles. Near the end of the yaw, it can be considered that:

$$\Delta \mathrm{P} = \mathrm{P}_{\mathrm{new}}(t) - P_{old}(t) = \mathrm{P}_{\mathrm{e2}} \tag{3.40}$$

Therefore, P_{e1} determines how often the yaw motor is turned on, while the parameter P_{e2} affects the control effect of the yaw system. If P_{e1} is chosen to be large, the control system will be more tolerant to the change of wind direction, but at the same time, a certain power loss will be generated. If P_{e2} is selected small, near the point of early maximum power value, the yaw motor will move back and forth in forward and reverse directions after starting, which reduces the control effect. According to the actual situation and experience of wind farm, $P_{e1} > 0.0152P_{max}$, $\mathrm{P}_{\mathrm{e2}} > 0.0603P_{max}$ can be selected.

The program flow of the microprocessor in the yaw controller is designed according to the principle of hill climbing search algorithm, and its program block diagram is shown in **Figure 3.14**. This flowchart has three main parts: in the A wireframe is the part to obtain relevant data and calculate the average power; in the B wireframe is the part to determine whether the yaw motor needs to be turned on; and in the C wireframe is the part to determine whether the yaw motor needs to be turned off. In the flow chart, P_{S} is the accumulated power value; k is the current accumulated power count; m is the total accumulated power count; $\mathrm{P}_{\mathrm{new}}(t)$、$P_{old}(t)$ these powers are the power values that have been averaged.

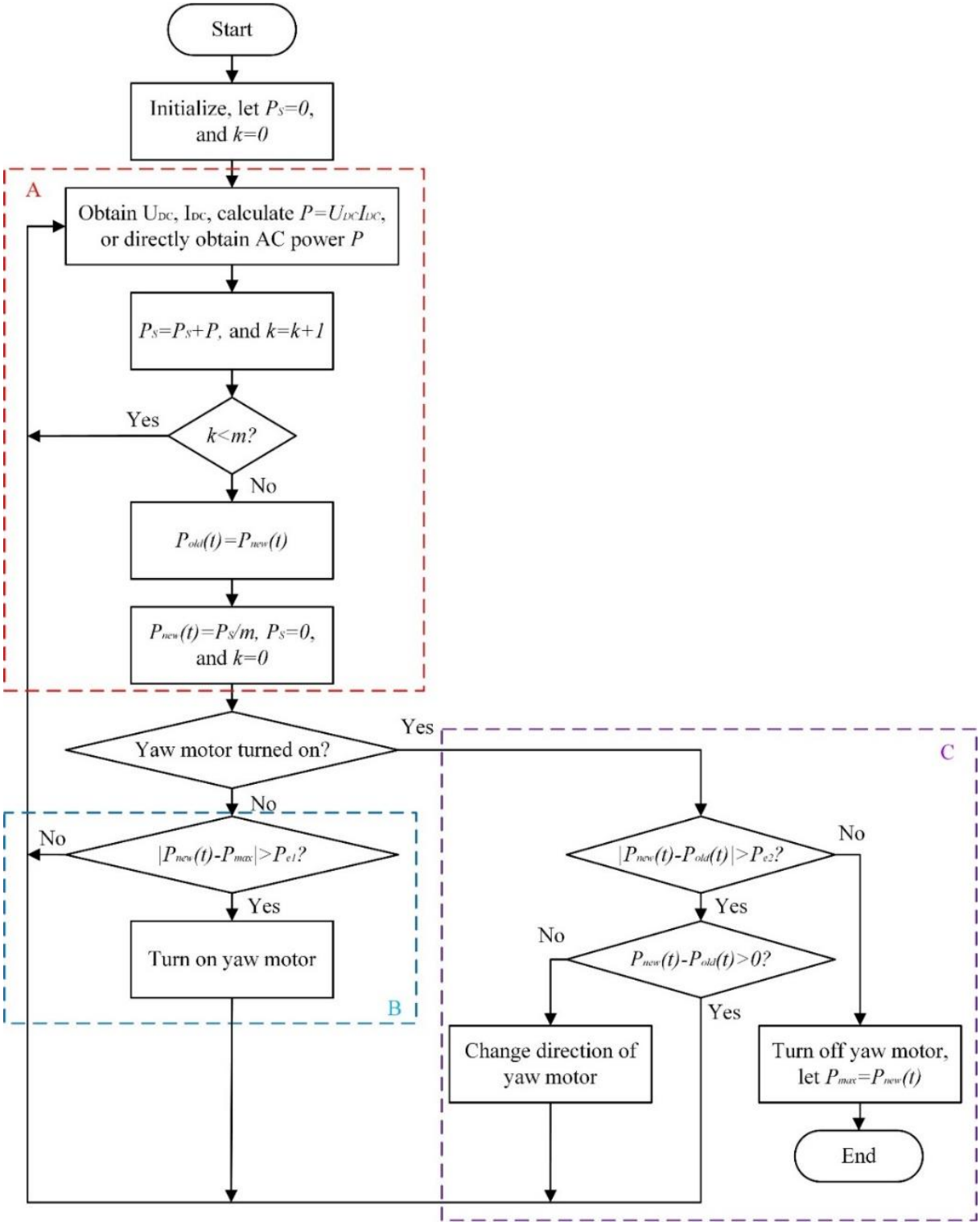

Figure 3.14. HCC algorithm program flow chart of yaw controller MCU

3.3 Combined yaw control strategy

The block diagram of a WECS with an active yaw system is illustrated in **Figure 3.15**. The rotational power of the turbine is transferred to the generator through a gearbox to set up the rotor speed. The variable-frequency, variable voltage power produced by the electrical generator is converted to fixed-frequency, fixed voltage by

the use of two back-to-back converters by applying space vector control technique. A capacitance filter is inserted between the inverter and the grid in order to enhance the quality of generated power that is injected to the grid, by reducing the voltage and current harmonics.

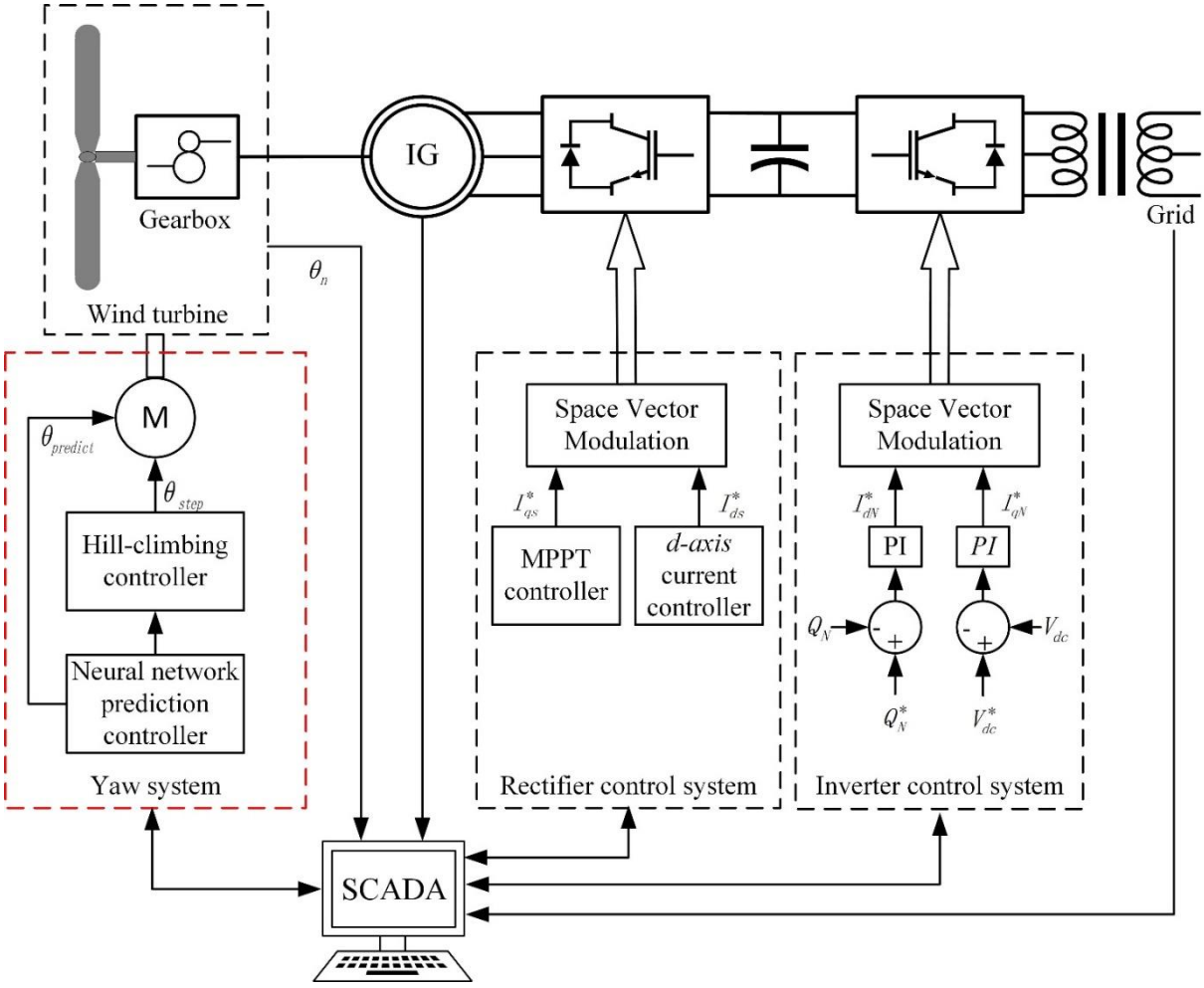

Figure 3.15. Overall control diagram of wind turbine

For the active yaw control system, a composite yaw control strategy combining neural network predictive control algorithm and hill climbing search algorithm is adopted. In this way, the yaw motor can be started in advance by predicting the wind direction and position through the neural network, so as to achieve the goal of tracking the wind direction in real time, and when there is a deviation in the prediction result, the hill climbing search algorithm can be used to make up for it, so as to achieve the goal of accurate yaw, thereby maximizing the reduce yaw error.

The yaw control of wind turbine adopts two methods: neural network predictive control and hill climbing search. According to the wind direction data recorded by the

SCADA system, the neural network is used to predict the wind direction, and the yaw system is activated to track the wind direction changes according to the predicted wind direction data. Since the prediction result of the neural network will have an error (about 2°), this angle is difficult to use the weather vane to measure and process, so it is necessary to use power control (hill climbing search algorithm) to eliminate this error. The output power of the generator changes, and the power detector measures the output power of the generator. Among them, adopting the hill climbing search algorithm in power control can shorten the yaw process time of the wind turbine, improve the tracking accuracy of the wind turbine and the wind energy utilization efficiency of the generator set, and prolong the service life of the wind turbine.

Figure 3.16 is a flow chart of the specific implementation of yaw control. The specific implementation process is as follows:

(1) When the wind turbine is connected to the grid, initialize the yaw control system and start to detect the nacelle position θ_n and wind direction v_d.

(2) After detecting the nacelle position θ_n and the wind direction v_d, first enter the A control part.

If the nacelle position θ_n is not equal to the wind direction v_d, it indicates that there is a yaw error at this time, which requires the control algorithm of part A of the neural network to be executed first. By analyzing the wind direction data recorded by the SCADA system, and then using the neural network to predict the wind direction, the future wind direction data can be obtained (10 minutes or 20 minutes as a cycle). According to the predicted wind direction result, the yaw motor is started by the controller, the coaxially connected reduction gear is driven by the yaw motor, and the slewing bearing between the nacelle and the tower is driven by the deceleration large gear to drive the nacelle to rotate, and the wind direction is tracked in advance to make the nacelle rotate. The nacelle is always in the position on the largest windward side.

If the nacelle position θn is equal to the wind direction vd, it means that there is no yaw error at this time, or the yaw error is too small to be detected, so skip part A and enter the part using the hill climbing search algorithm based on power feedback.

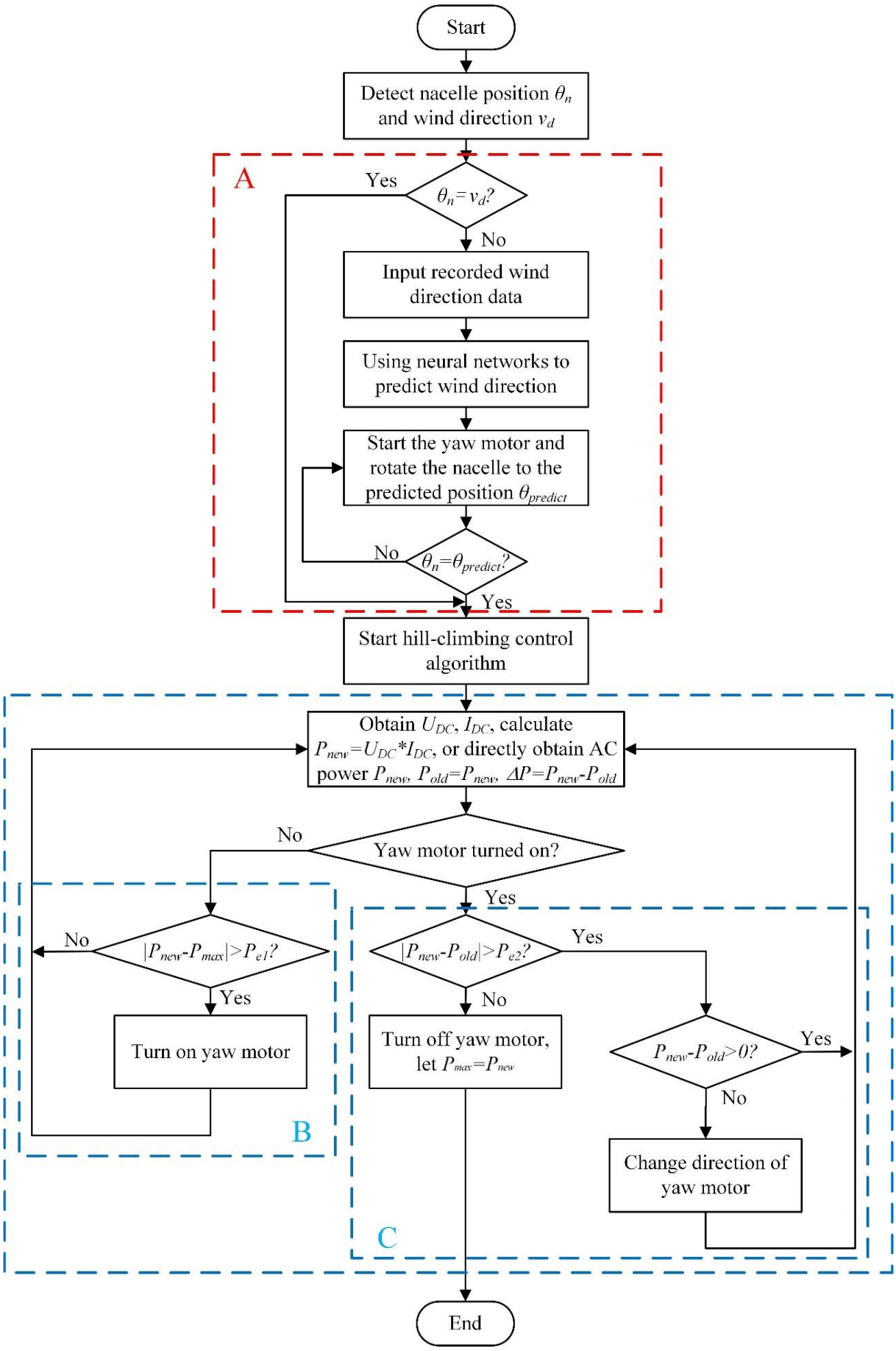

Figure 3.16. Combined yaw control strategy

(3) When the wind direction prediction yaw control algorithm in Part A is completed, it means that the nacelle has reached the predicted position at this time. However, since the results predicted by the neural network may have errors, and the prediction is the average wind direction in a period, the hill climbing search algorithm is used to eliminate the error caused by the fluctuation of the wind direction in the remaining time of the period.

(4) If the yaw motor is not turned on at this time, enter the B part of the hill climbing search algorithm. If the difference between the output power $\mathrm{P_{new}}$ at the current moment and the maximum output power $\mathrm{P_{max}}$ is greater than $\mathrm{P_{e1}}$, return to the starting position of the hill climbing search algorithm to detect the output power of the next measurement cycle; otherwise, turn on the yaw motor, and then return to the start of the hill climbing search algorithm to detect the output power of the next measurement cycle.

(5) When the yaw motor has been turned on, go to part C of the hill climbing search algorithm. If the difference between the output power at the current moment $\mathrm{P_{new}}$ and the output power at the previous moment $\mathrm{P_{old}}$ is less than P_{e2}, $|\mathrm{P_{new}} - \mathrm{P_{old}}| < P_{e2}$, turn off the yaw motor, and assign the value of $\mathrm{P_{new}}$ to $\mathrm{P_{old}}$ to end the yaw in this cycle. When $|\mathrm{P_{new}} - \mathrm{P_{old}}| > P_{e2}$, and $\mathrm{P_{new}} - \mathrm{P_{old}} > 0$, return to the starting position of the hill climbing search algorithm to detect the output power of the next measurement cycle; if $\mathrm{P_{new}} - \mathrm{P_{old}} < 0$, change the direction of the yaw motor, and then return to the starting position of the hill climbing search algorithm to detect the output power of the next measurement cycle.

Figure 3.17 shows the operation of the proposed combined yaw control system. When measuring the wind direction, the average value is usually taken within 10 minutes. Therefore, when designing the combined yaw control system, the control cycle is also set to 10 minutes. At the beginning of each control cycle, the yaw motor is first activated to reach the position predicted by the NN, and then the nacelle is adjusted according to the HCS-based power control algorithm, and the yaw action stops when the tolerance (small) error is reached.

To observe the specific change in the position of the nacelle during one control

cycle of the combined yaw control system, one cycle (from 20 min to 30 min) was locally increased (from 20 min to 22 min), as shown on the minor axis. At the beginning of the control cycle (20 min), the nacelle must reach the position predicted by the NN (45°) from the previous position (45.5°), so the yaw motor drives the nacelle to rotate from the position at the end of the previous cycle to the predicted position (the process is shown by the magenta ellipse). Since there is an error (1°) in the predicted value of the NN when the nacelle reaches the predicted position, the HCS algorithm controls the yaw motor to gradually rotate the nacelle until the error between the nacelle and the wind direction is satisfied (the process is shown by the blue rectangle).

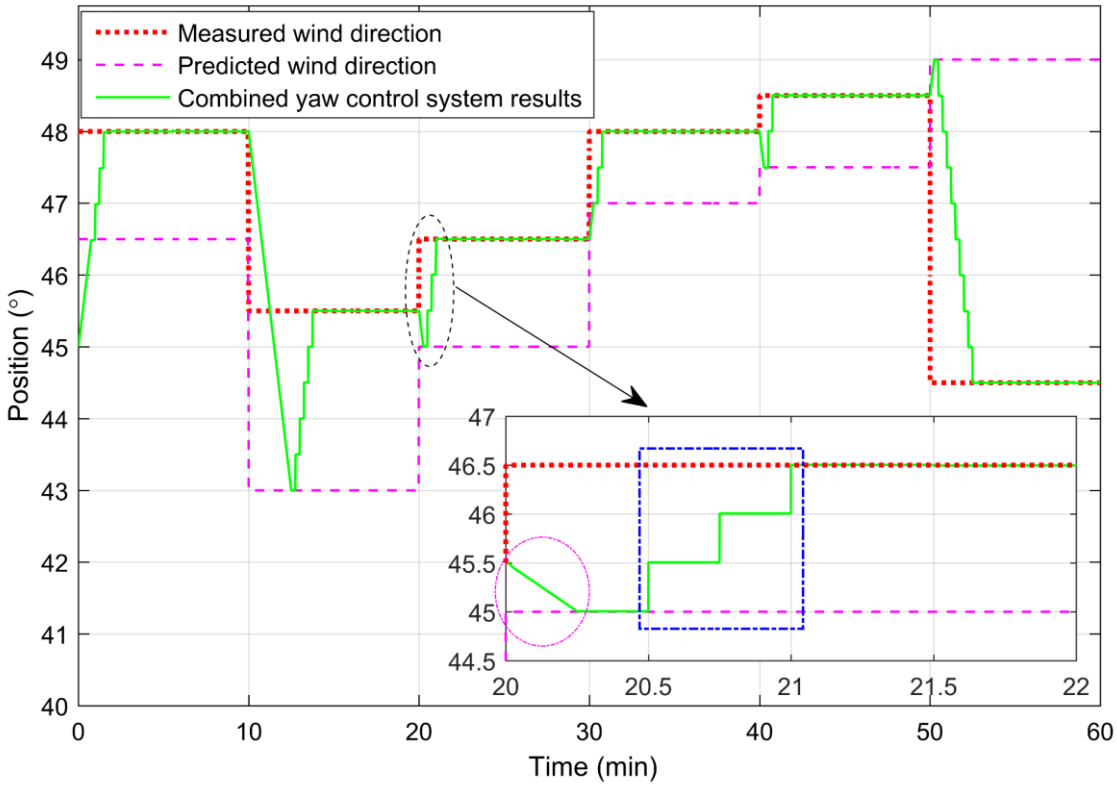

Figure 3.17. Demonstration of the proposed combined yaw control strategy

3.4 Conclusion of chapter 3

This chapter is based on the purpose of tracking wind direction in time and accuracy, the neural network predictive control algorithm and the hill climbing search algorithm that meet the requirements are designed. Finally, according to the operation period of these two control algorithms and the connection with other control systems, a compound yaw control system that meets the requirements is designed.

CHAPTER 4: VERIFICATION OF WIND TURBINE YAW CONTROL STRATEGY

Aiming at the problem of simulating the operation of wind turbine yaw control system, two models are proposed: MATLAB/Simulink mathematical simulation model and simplified physical wind turbine yaw control model. Among them, the mathematical simulation model verifies the efficiency of the designed yaw control algorithm according to the actual operation data of SWT-3.6-120. The wind direction and wind speed data are more complicated and more in line with the actual situation; the simplified physical model is because there is no complete wind power generation. For the control system, when testing the proposed yaw control algorithm, the wind direction and wind speed data used are relatively simple.

4.1 Visual interface of wind turbine yaw control system

In order to control the wind turbine more conveniently and observe the changes of various parameters during the simulation operation of the wind turbine more intuitively, a visual interface for wind turbine yaw control was developed using MATLAB/GUI, as shown in **Figure 4.1**.

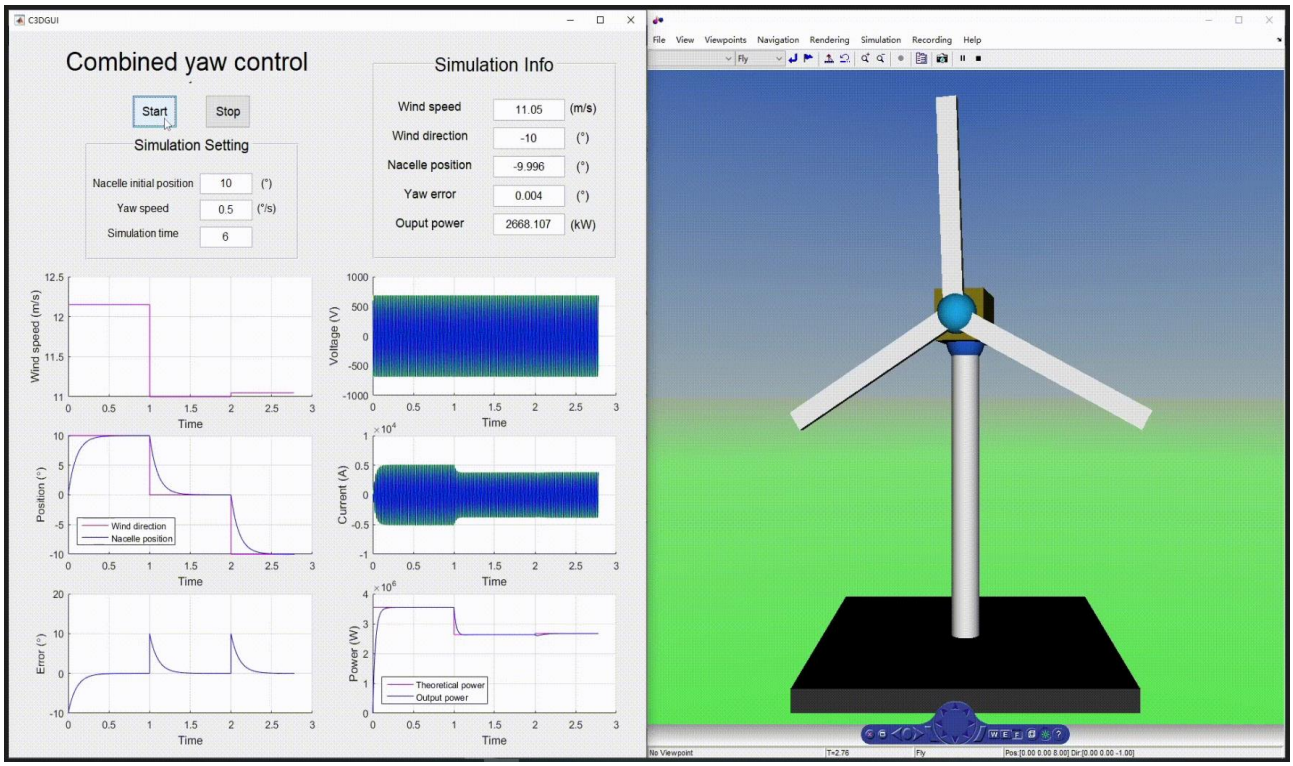

Figure 4.1. Visual interface of wind turbine yaw control system

The visual interface consists of two parts: the visual interface and the 3D model of the wind turbine. Through the visual interface, the parameters of the wind turbine model in Simulink can be directly changed to adapt to the test in different situations; at the same time, the wind turbine 3D also changes with the operation of the simulation model, which can reflect the real operating state of the wind turbine in real time.

4.2 Simulation results of predictive control strategy based on neural networks

For the wind turbine operating in Yalova, Turkey, data such as time, wind speed, wind direction, theoretical output power and actual output power are collected and saved every 10 minutes through the SCADA system of the wind turbine, the data set collected in 2018 has a total of 50530 rows. The wind rose figure in this year is shown in **Figure 4.2**.

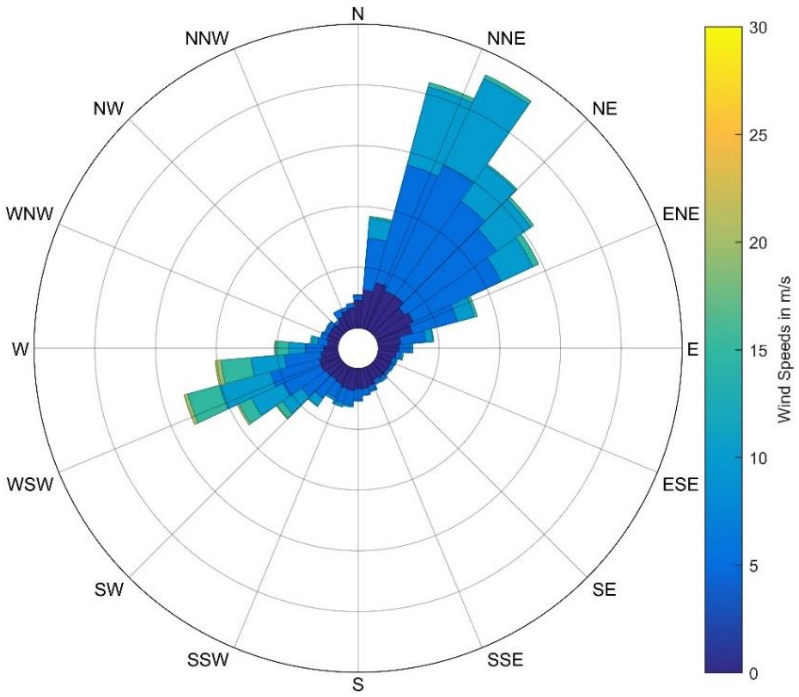

Figure 4.2. Wind rose from the SCADA data

It can be seen from the wind rose figure that the dominant wind direction in this area in 2018 is the northeasterly wind, and the wind speed is concentrated in the range of 5 m/s ~ 15 m/s, with almost no phenomenon exceeding the cut-out wind speed. This shows that the area is very suitable for wind power generation, which is why wind farms are built in the area.

Figure 4.3 depicts the on-site measurement of the SCADA system, and the corresponding output power for different wind speeds in one year. As can be seen from

the figure, most points are concentrated around the theoretical output power curve shown in red. But there are still some abnormal points that deviate from the theoretical output power curve. By analyzing the original data set, the abnormal data types can be classified into abnormal wind speed and abnormal power. When the wind speed sensor fails, the measured wind speed may be too high or too low, and the wind speed point may be shifted to the right or left. When the power sensor fails, the measured power may be too high or too low, and the output power point may be shifted upward or downward. In addition to sensor failures, abnormal power values may also be caused by turbine shutdowns (due to faults or to avoid damage to turbine caused by excessive wind speed) and artificially actively abandoning wind. Specifically, it can be divided into: (a) output power is 0, caused by turbine shutdown; (b) manual active wind abandonment, that is, output power is artificially limited; (c) randomly distributed around the curve, usually caused by sensor failure or noise during signal processing.

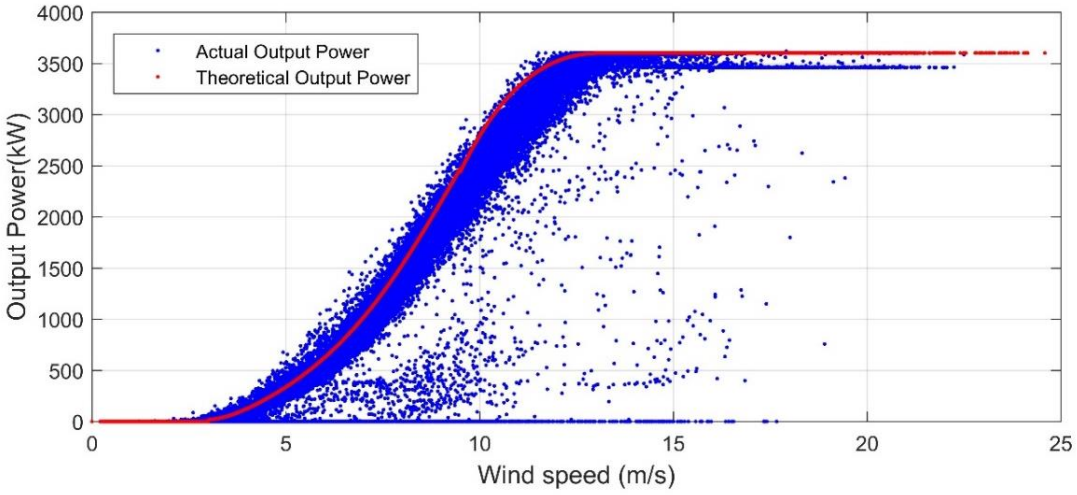

Figure 4.3. Comparison of actual output power and theoretical output power in the SCADA data set

It can also be seen from **Figure 4.3** that under any wind speed value, the output power generated by the wind turbine is not unique, but corresponds to multiple values, which are distributed in scattered points. The reasons for the scattered distribution of output power are mainly divided into two points; the first point is that the wind speed is not the only factor affecting the output power of WECS, and the wake effect of the air and the turbine should also be considered; the second point is that adjust the direction of the nacelle so that the blades are always facing the incoming wind in order

to maintain the maximum wind force, so there will be a time lag in the adjustment process, so even under the same wind speed conditions, the generated output power is not unique value, but fluctuates within a range.

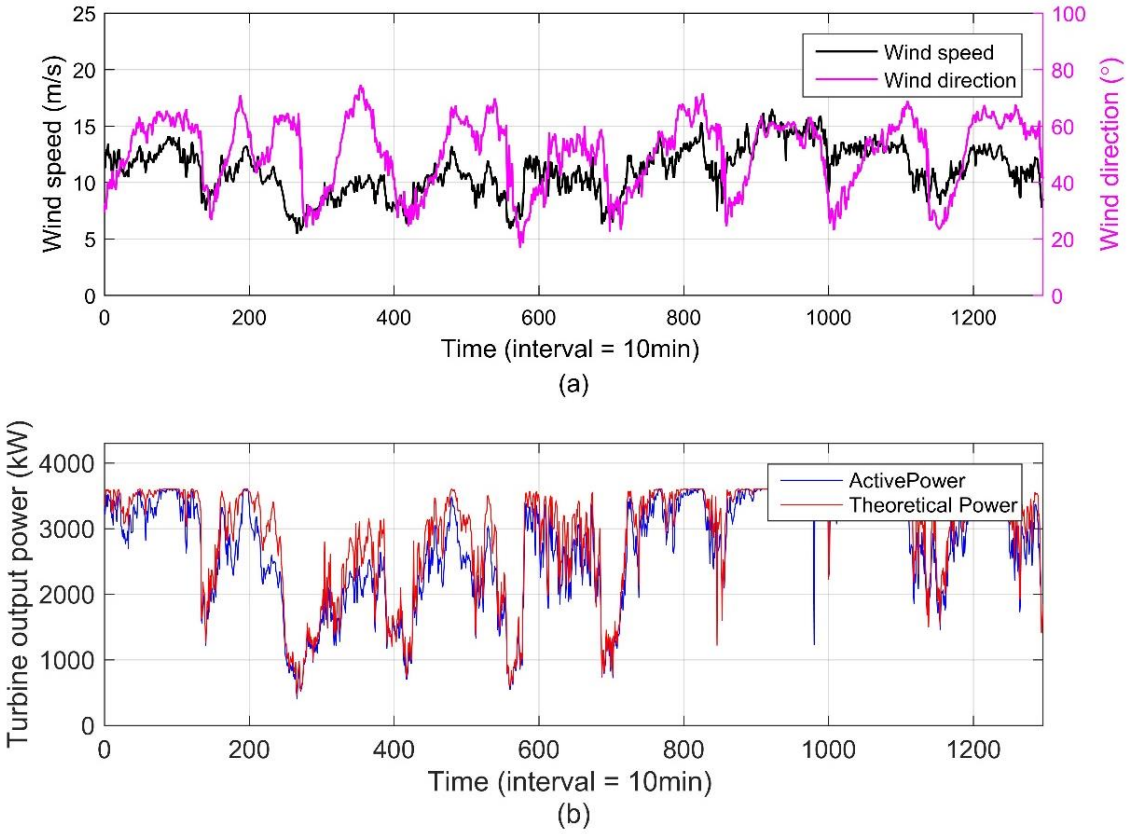

Figure 4.4. (a) Wind speed and direction from SCADA system (b) Power from SCADA system

Figure 4.4 represents the 9 days' SCADA data from the wind turbine which is in a wind farm in Yalova. By analyzing the data recorded by the wind farm SCADA system and combining the nonlinear mapping capability of neural networks, and then realize the wind direction prediction.

It can be seen from **Figure 4.4** that during these 9 days, the wind speed is higher than the WT rated cut-in speed, which indicates that the WT has been working and no shutdown has occurred. The wind direction variation range is within 16.7797° to 74.5948°, which is relatively stable and is beneficial for the WT to obtain maximum energy from wind. Then there is the comparison between the theoretical output power and real active power. It can be found that the actual active power is only 91.576% of the theoretical output power, which means that about 9% of the wind energy is not

utilized by the WT. This is the main reason – why we should use neural networks to predict wind direction, improve yaw efficiency and increase output power.

In order to obtain the optimal parameters of Elman neural network. We use the control variable method to conduct experiments under different conditions for the two parameters that affect Elman neural network, namely hidden sizes and layer delays.

First of all, hidden sizes are considered, which requires setting layer delays to a constant (set to 2 in this experiment). By changing the hidden sizes, we can obtain the prediction result, which is displayed in **Figure 4.5**. When the hidden sizes are greater than 35, the performance has become stable. At the same time, considering the problem of training time, 35 is determined as the optimal hidden sizes for this experiment.

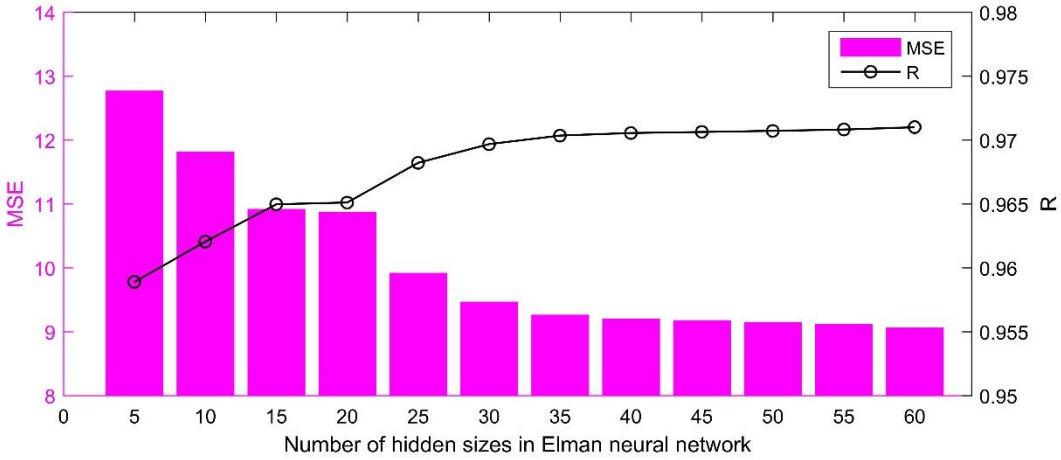

Figure 4.5. Performance with different numbers of hidden sizes in Elman neural networks

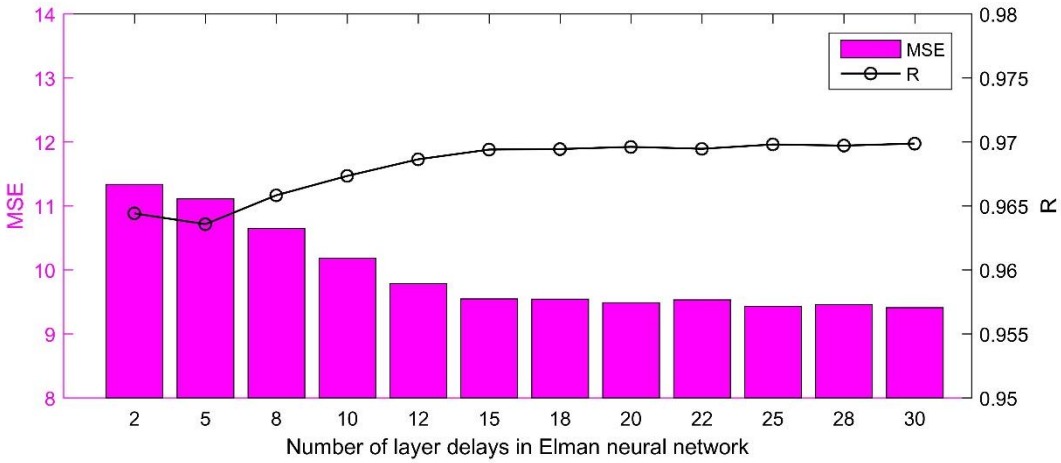

Figure 4.6. Performance with different numbers of layer delays in Elman neural networks

Then, the layer delays need to be determined. Here, the hidden sizes are set to a constant (here is 10), and observe the Elman neural network's prediction results by way of adjusting layer delays. **Figure 4.6** shows these results. When layer delays are greater than 15, the performance of the Elman neural network tends to be stable. Obviously, the increase of delays in the layer is able to increase the prediction precision and impact the training time. In this experiment the optimal value of the layer delay is 25.

In this experiment, the hidden sizes of Elman neural network are set to 35, layer delays are set to 25, thus the Elman neural network can be trained and used for the yaw system. In **Figure 4.7**, the comparison between actually measured wind direction and Elman neural network predictive value is presented. And the predicted error is presented in **Figure 4.8**.

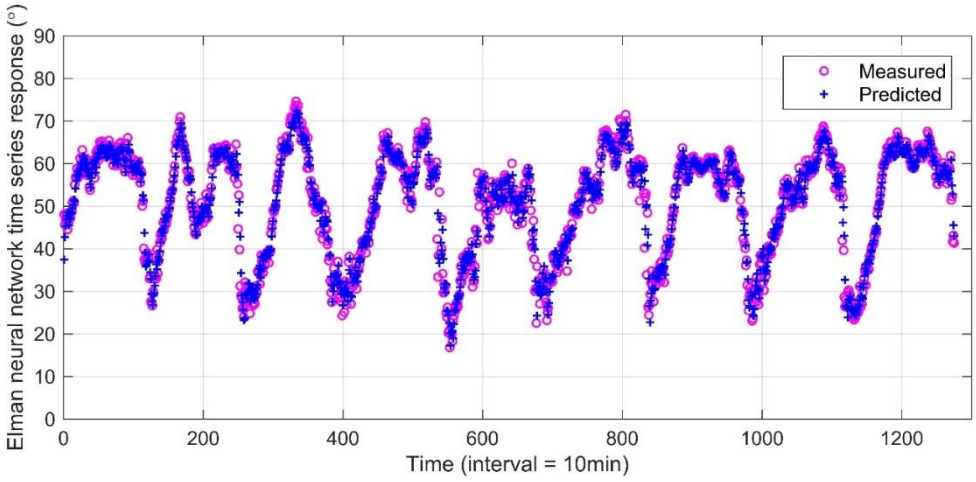

Figure 4.7. Comparison of measured wind direction with predicted wind direction with Elman neural networks

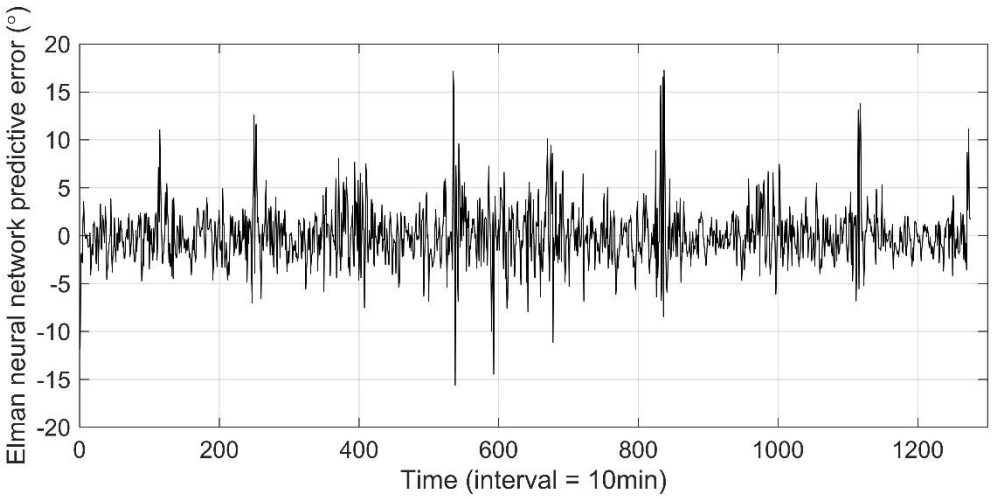

Figure 4.8. Predicted error of Elman neural networks

It shows that the predictive wind direction is quite accurate. The prediction value has errors in the specific value of the wind direction change at certain moments, but the prediction of the time when the wind direction changes, is still quite accurate. Although some points have big errors, the tendency and general prediction are perfect. After analysis and calculation, the MSE is 9.4064, R is 0.9701, the average error is 2.1514°, the number of prediction data with an error greater than 5° is 98, which means that the prediction data with an error range within 5° can reach 92.31%.

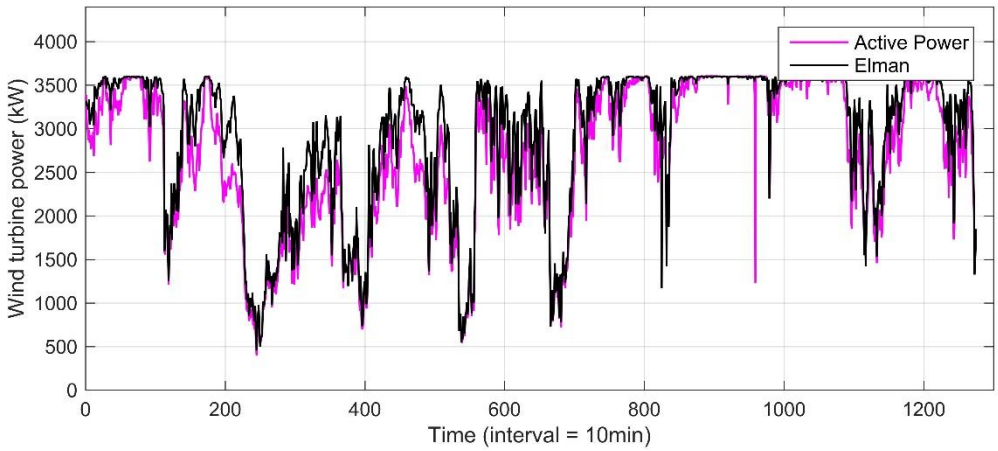

Figure 4.9. Comparison of wind turbine active power with Elman neural network's predictive power

The **Figure 4.9** shows the comparison of wind turbine active power with Elman predictive power. The yaw system that uses Elman neural network to predict the wind direction can improve the turbine output power to a certain extent. After calculation, the predicted average output power is 97.5884% of the theoretical output power, which is about 6.0124% higher than the actual active power before.

4.3 Simulation results of HCS control strategy

For the yaw system simulation based on the HCS algorithm, the algorithm first drives the nacelle to rotate a yaw step, and then judges the next yaw direction according to the feedback output power.

To better observe the performance of the hill climbing search algorithm in the simulation experiment, it is necessary to set the wind speed as a constant and the wind direction as a variable. This input setting ensures that there is just one variable (wind direction) during the simulation, making it easier to analyze the experimental results

and judge the performance of the hill climbing search algorithm.

In this simulation, the input wind speed was 9 m/s, the wind direction changed 4 times. When the simulation started, the wind direction was 0°; at 5 sec, it changed to 10°; at 10 sec, it changed to 15°; at 15 sec, it changed to 5°. The input wind source is shown in **Figure 4.10**.

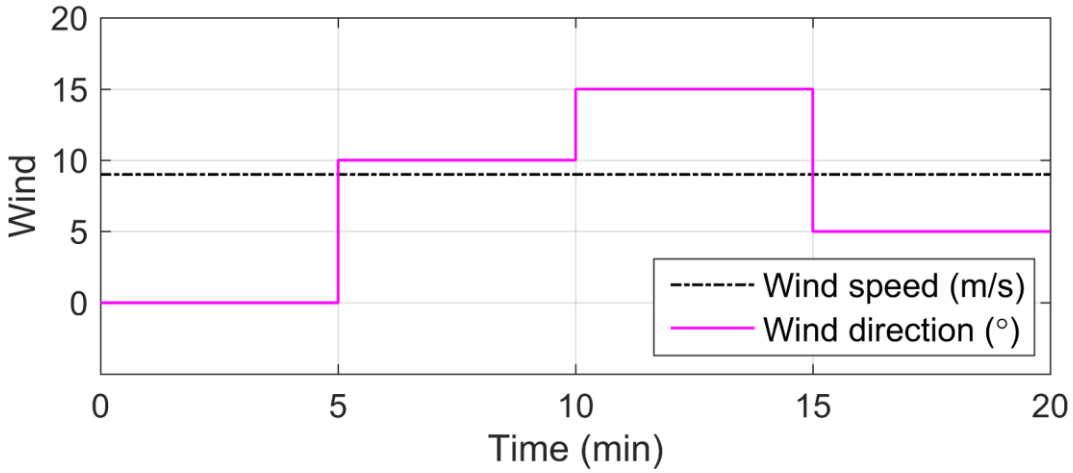

Figure 4.10. Information of input wind source

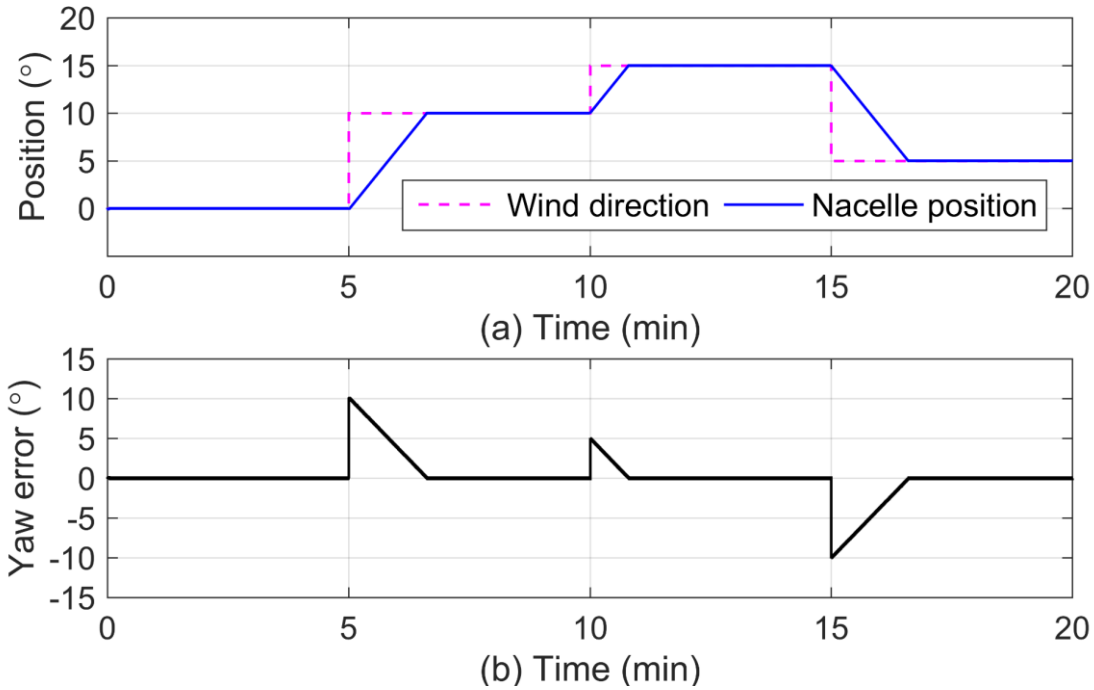

Figure 4.11. Information of yaw system

When the simulation finished, all the information about the yaw system and turbine were collected. **Figure 4.11** shows the process of the yaw system.

In the beginning, the wind direction was 0°, which means the wind turbine was oriented to wind direction, the yaw error was 0. But the turbine rotated from 0 to the maximum rotation speed, during this period, the yaw system was trying to eliminate

the yaw error, that's why the yaw error was not 0°. After regulation, the turbine reached the optimal rotation speed, the output power also reached the maximum value, and the yaw error oscillated around 0°. Because this yaw system used the fixed step hill climbing search algorithm when it found the maximum value, it wouldn't stop working, it would oscillate around the maximum value.

At 5 sec, 10 sec, and 15sec, the wind direction changed in different values and directions, but the yaw system could easily track the wind direction, eliminating the yaw error. It can be seen that if the set yaw speed is appropriate, the yaw system based on the HCC algorithm can still track the wind direction changes quickly and accurately.

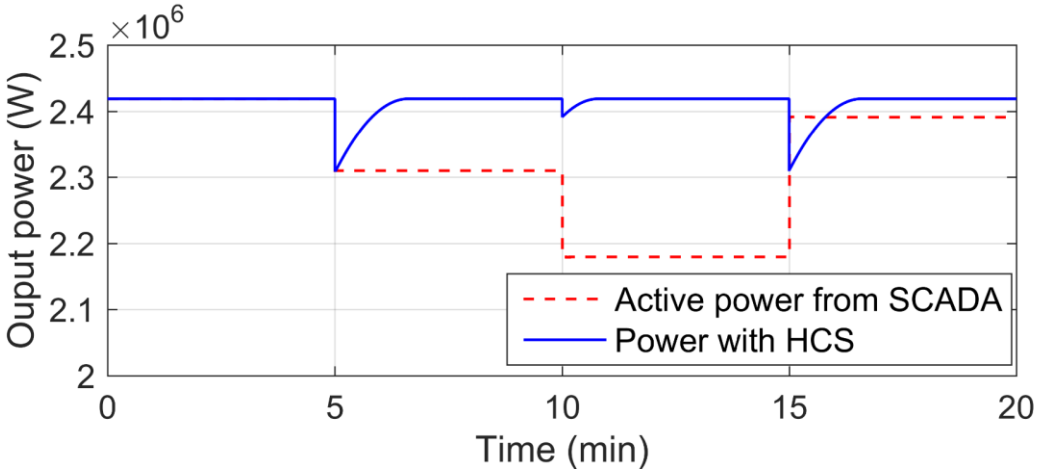

Figure 4.12. Wind turbine output power

Figure 4.12 shows the wind turbine output power. It is obvious that when the wind direction changed, the output power was decreased, but after regulation, the yaw system tracked the wind direction and eliminate the saw error, the output power went back to the maximum value. Besides, compared to the wind energy conversion system without a yaw system, it improved lots of output power.

4.4 Simulation results of combined control strategy

When the wind turbine operates under the control of a yaw control system with a combination of NN and a HCS-based power control algorithm, the impact of frequent changes in wind direction is minimized. This conclusion is extremely important. **Figure 4.13** shows the performance of the wind turbine with the built-in yaw control system in operation. It can be seen that the combined yaw control system can predict and track wind direction changes well and improve power output.

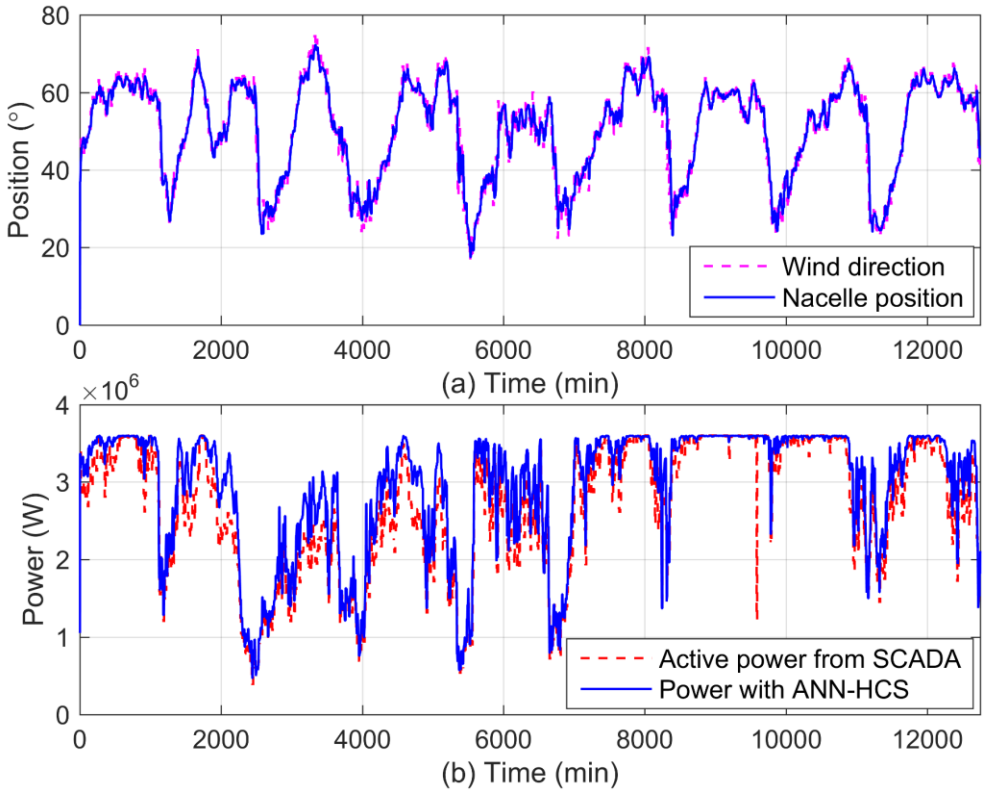

Figure 4.13. Performance of the orientation system based on the combined ENN-HCS control strategy

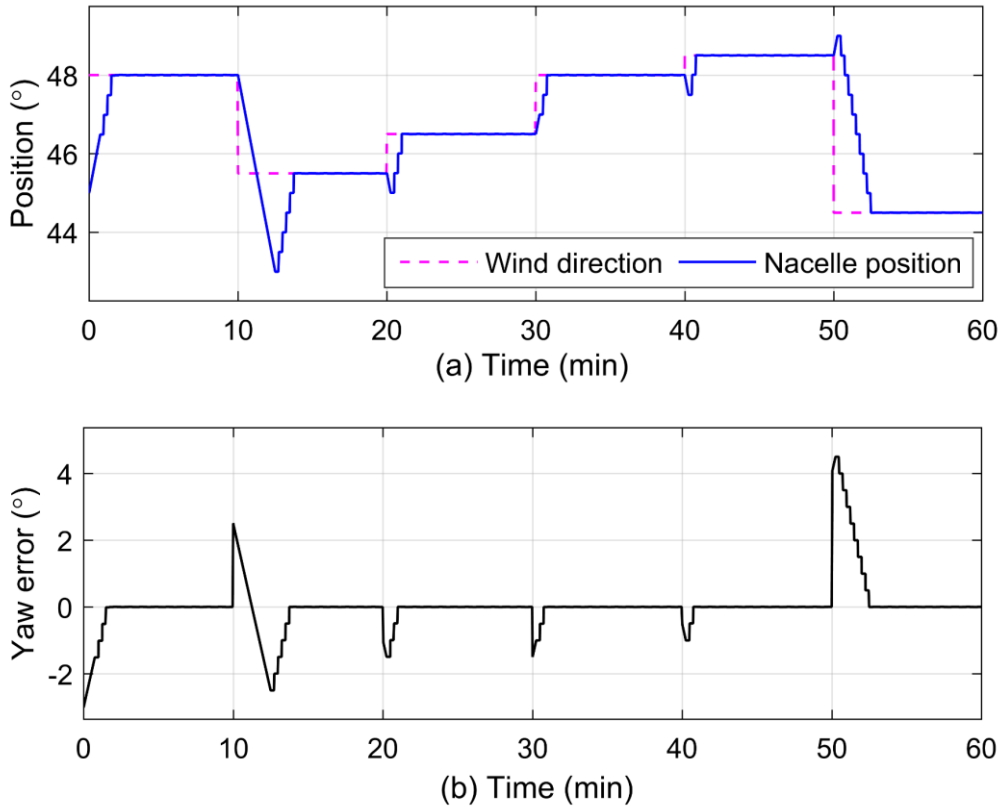

Figure 4.14. (a) Comparison of wind direction and nacelle position (b) Orientation error during operation of the combined orientation control system

Figure 4.14 shows the change in the position of the nacelle and yaw errors during the operation of the combined yaw control system. **Figure 4.14 (a)** details the comparison between actual wind direction and nacelle position. For example, after 20 minutes, the wind direction is predicted by the ANN neural network based on the wind direction data recorded by the SCADA system and drives the yaw motor from the previous position (45.5°), turning to the predicted position (45°). Since there is an error in the NN prediction results, which means that there is a yaw error after the nacelle reaches the predicted position (the wind direction at this time is 46.5°, the error is 1.5°), then a HCS-based power control algorithm is applied to eliminate the yaw. After 20.25 min, the HCS-based power control algorithm first makes the nacelle rotate clockwise (or counterclockwise) one step, and if the power increases, it means that the yaw error decreases, and then the nacelle continues to rotate in this direction; if the power decreases, this means that the yaw error increases and it is necessary to rotate the nacelle in the opposite direction. This is repeated until 21 minutes, when the change in WT output power becomes negligible, which means that the yaw error has been eliminated.

Figure 4.14 (b) shows the change in yaw error during WT operation. When the nacelle turns to the forecast position, it can pass the position of the actual wind direction without stopping until it reaches the forecast position. Thus, in some cases, the yaw error will decrease to 0° and then increase. It can be seen from the figure that the maximum error predicted by the ANN is 4.5° and the minimum error is 1°, and the orientation error finally converges to 0 after optimization by the HCS-based power control algorithm.

Figure 4.15 shows the variation of the output power during the operation of the WT. Since both the Elman NN prediction and the HCS-based power control algorithm run with errors, there is a loss of output power during this period. However, the yaw error eventually converges to 0, so the output power eventually converges to the theoretical output power, and improves the output power by 6%.

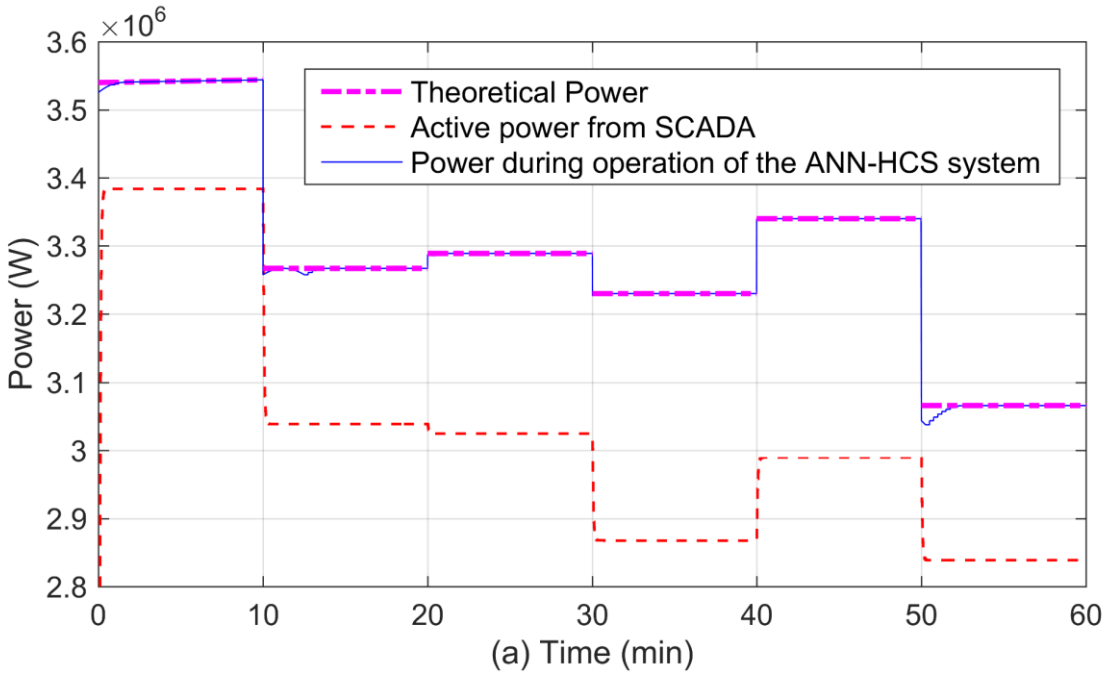

Figure 4.15. Comparison of different capacities during operation of the combined orientation control system

Table 4.1 Comparison of the performance of different orientation systems

	Mean yaw error	C_p ($C_{pmax} = 0.44$)	$\frac{\text{Output power}}{\text{Theoretical power}} \times 100\%$
Traditional yaw system	10°	0.4029	91.57%
Elman NN	2°	0.4294	97.58%
NN-HCS	<1°	0.4312	98.45%

Table 4.1 shows the performance when applying various algorithms to the yaw system. The first is the yaw error, which is usually about 10° for a conventional yaw system using a weather vane and up to 2° for an Elman NN prediction, and less than 1° for a yaw system with a combined NN-HCS control algorithm. When the error is less than 2°, the power loss can be negligible, but the wind direction changes in real time, and the Elman NN predicts the average wind direction for a certain period of time, not the real-time wind direction. The combined NN-HCS control algorithm is designed to solve the problem of real-time wind direction change, which can effectively reduce

real-time error and improve output efficiency. Secondly, from the point of view of the $C_p$value, the combined yaw algorithm of NN-HCS has a value of 0.4312, which is already very close to the maximum designed value of 0.44, which indicates high yaw accuracy. Finally, in terms of output efficiency, the output efficiency of the combined yaw algorithm of NN-HCS is 98.45%, which is 6.88% more than the traditional orientation system, which is a very significant improvement for a megawatt class WT.

According to the statistics data of the global wind turbine, by the end of 2022, the power of the wind turbine connected to the power grid was 906 GW. Assuming that all wind turbines operate at rated power for an average of 6 hours a day for 365 days a year, after using the combined yaw control algorithm, the output power will increase by 6.88%, that is, electricity generation can increase by:

$$365\ \text{days} \times 6\ \text{hours} \times 906\ \text{kW} \times 6.88\% = 1.37 \times 10^{11}\ \text{k} \cdot \text{Wh}$$

At a price of $ 0.15 per k•Wh, the annual energy savings due to the reduction of the orientation error is：

$$1.37 \times 10^{11}\text{k} \cdot \text{Wh} \times 0.15\ \text{dollars} = 2.05 \times 10^{10}\ \text{dollars. USA or}$$
$$\approx 2\ \text{trillion rubles. RU}$$

4.5 Conclusion of chapter 4

1. A number of simulation iterations were carried out in order to study various operating modes of a wind power plant with specific technical characteristics of electrical equipment under conditions of dynamic changes in wind speed and direction.

2. A synthesis of neural networks and hill climbing search algorithms was carried out to ensure minimization of the orientation error with a corresponding increase in the power of the wind turbine by 6%.

3. The effectiveness of wind turbine operation control based on the developed algorithms was carried out in a wide range of variable components of wind speed and direction, which demonstrates the independence of algorithms from wind behavior.

Conclusion

The paper considers the possibility of decreasing the yaw error and increasing the output power of the wind turbine.

In conclusion, the main results and conclusions based on modeling, theoretical calculations and virtual experiments are given:

1. Research and analysis of experimental SCADA data obtained from operating wind turbines were carried out in the dissertation work. Statistical processing of wind speed and direction data, rotor position and output power under various weather conditions has been carried out.

2. For the first time in the MATLAB/Simulink package, a computer simulation model of the SWT-3.6-120 WPP with a virtual controller was built and verified. Based on an intelligent algorithm, it allows to control the orientation and power control systems of WTs according to parameters predicted by an artificial neural network.

3. 3. A study of the influence of yaw error on the performance characteristics of WTs has been conducted, as a result of which a number of shortcomings of the sensor and software of WPPs have been identified. Taking into account the identified problems, a new combined algorithm for controlling the yaw of the wind turbine rotor was developed based on the results predicted by the ANN based on SCADA data. A method has also been developed for controlling the power of wind turbines based on PVNK in real time with forecasting the upcoming change in wind direction.

4. 4. The testing results of the simulation model based on the developed control algorithm show that the angle of yaw error can be reduced to 1°, and the use of wind energy can be increased by more than 6.88%.

Prospects for further development of the research topic and recommendations:

1. To continue work in terms of implementing the developed software solutions into existing wind turbine yaw control systems in Russia (at Rosatom Group wind farms) and China with subsequent commercialization.

2. To investigate the possibility of applying the developed algorithm and method to large wind farms, taking into account the mutual influence of neighboring WTs.

References

[1] P. McKay, R. Carriveau, and D. S.-K. Ting, "Wake impacts on downstream wind turbine performance and yaw alignment," *Wind Energy*, vol. 16, no. 2, pp. 221–234, Mar. 2013, doi: 10.1002/we.544.

[2] W. Chen, H. Liu, Y. Lin, W. Li, Y. Sun, and D. Zhang, "LSTM-NN Yaw Control of Wind Turbines Based on Upstream Wind Information," *Energies*, vol. 13, no. 6, p. 1482, Mar. 2020, doi: 10.3390/en13061482.

[3] M. Z. M. Z. Jacobson, "Review of solutions to global warming, air pollution, and energy security," *Energy Environ. Sci.*, vol. 2, no. 2, pp. 148–173, 2009, doi: 10.1039/B809990C.

[4] X. Xia and J. Xia, "Evaluation of Potential for Developing Renewable Sources of Energy to Facilitate Development in Developing Countries," in *2010 Asia-Pacific Power and Energy Engineering Conference*, Mar. 2010, pp. 1–3, doi: 10.1109/APPEEC.2010.5449477.

[5] F. Krupp, M. Horn, F. Karupp, and M. Horn, *Earth, the sequel: the race to reinvent energy and stop global warming*. WW Norton & Company, 2008.

[6] International Energy Agency(IEA), "World Energy Outlook 2022," Paris, 2022.

[7] International Renewable Energy Agency(IREA), "Renewable Energy Capacity Statistics 2022," 2022.

[8] GWEC, "Global Wind Energy Outlook (GWEO) 2014," *Glob. Wind Energy Counc.*, 2014.

[9] N. Goudarzi and W. D. Zhu, "A review on the development of wind turbine generators across the world," *Int. J. Dyn. Control*, vol. 1, no. 2, pp. 192–202, Jun. 2013, doi: 10.1007/s40435-013-0016-y.

[10] EWEA, "Pure Power - Wind energy targets for 2020 and 2030," Brussels, Belgium, 2011.

[11] GWEC, "Global Wind Report 2022," Brussels, Belgium, 2022.

[12] J. Ribrant and L. M. Bertling, "Survey of Failures in Wind Power Systems With Focus on Swedish Wind Power Plants During 1997–2005," *IEEE Trans. Energy*

Convers., vol. 22, no. 1, pp. 167–173, Mar. 2007, doi: 10.1109/TEC.2006.889614.

[13] J. M. Pinar Pérez, F. P. García Márquez, A. Tobias, and M. Papaelias, "Wind turbine reliability analysis," *Renew. Sustain. Energy Rev.*, vol. 23, pp. 463–472, Jul. 2013, doi: 10.1016/j.rser.2013.03.018.

[14] J. Yang *et al.*, "Review of control strategy of large horizontal-axis wind turbines yaw system," *Wind Energy*, vol. 24, no. 2, pp. 97–115, Feb. 2021, doi: 10.1002/we.2564.

[15] A. Turnbull, C. McKinnon, J. Carrol, and A. McDonald, "On the Development of Offshore Wind Turbine Technology: An Assessment of Reliability Rates and Fault Detection Methods in a Changing Market," *Energies*, vol. 15, no. 9, p. 3180, Apr. 2022, doi: 10.3390/en15093180.

[16] H. Piao and Z. Wang, "A new control algorithm for yaw control system of wind turbine," *Acta Energiae Solaris Sin.*, vol. 29, no. 8, pp. 1028–1033, 2008.

[17] F. Bu, W. Huang, Y. Hu, Y. Xu, K. Shi, and Q. Wang, "Study and implementation of a control algorithm for wind turbine yaw control system," in *2009 World Non-Grid-Connected Wind Power and Energy Conference*, Sep. 2009, pp. 1–5, doi: 10.1109/WNWEC.2009.5335830.

[18] Kung Chris Wu, R. K. Joseph, and N. K. Thupili, "Evaluation of Classical and Fuzzy Logic Controllers for Wind Turbine Yaw Control," in *Proceedings. The First IEEE Regional Conference on Aerospace Control Systems,* 1993, pp. 254–258, doi: 10.1109/AEROCS.1993.720937.

[19] F. Chen and J. Yang, "Fuzzy PID controller used in yaw system of wind turbine," in *IEEE International Conference on Power Electronics Systems and Applications*, 2009, pp. 1–4.

[20] E. V. Solomin *et al.*, "Horizontal axis wind turbine yaw differential error reduction approach," *Energy Convers. Manag.*, vol. 254, no. December 2021, p. 115255, Feb. 2022, doi: 10.1016/j.enconman.2022.115255.

[21] R. Bakhshi and P. Sandborn, "Maximizing the returns of LIDAR systems in wind farms for yaw error correction applications," *Wind Energy*, vol. 23, no. 6, pp. 1408–1421, Jun. 2020, doi: 10.1002/we.2493.

[22] T. Ouyang, A. Kusiak, and Y. He, “Predictive model of yaw error in a wind turbine,” *Energy*, vol. 123, pp. 119–130, Mar. 2017, doi: 10.1016/j.energy.2017.01.150.

[23] N. Hure, R. Turnar, M. Vašak, G. Benčić, M. Vasak, and G. Bencic, “Optimal wind turbine yaw control supported with very short-term wind predictions,” in *2015 IEEE International Conference on Industrial Technology (ICIT)*, Mar. 2015, vol. 2015-June, no. June, pp. 385–391, doi: 10.1109/ICIT.2015.7125129.

[24] X. Wu, Y. Liu, and W. Teng, “Modified hill climbing method for active yaw control in wind turbine,” in *IEEE Control Conference*, 2012, pp. 6677–6680.

[25] N. Karakasis, A. Mesemanolis, T. Nalmpantis, and C. Mademlis, “Active yaw control in a horizontal axis wind system without requiring wind direction measurement,” *IET Renew. Power Gener.*, vol. 10, no. 9, pp. 1441–1449, Oct. 2016, doi: 10.1049/iet-rpg.2016.0005.

[26] A. Mesemanolis and C. Mademlis, “Combined maximum power point and yaw control strategy for a horizontal axis wind turbine,” in *2014 International Conference on Electrical Machines (ICEM)*, Sep. 2014, pp. 1704–1710, doi: 10.1109/ICELMACH.2014.6960412.

[27] T. Pedersen, U. Paulsen, S. Petersen, and P. Enevoldsen, “Operational experience and analysis of a spinner anemometer on a MW size wind turbine,” 2008.

[28] M.-S. Jeong, S.-W. Kim, I. Lee, S.-J. Yoo, and K. C. Park, “The impact of yaw error on aeroelastic characteristics of a horizontal axis wind turbine blade,” *Renew. Energy*, vol. 60, pp. 256–268, Dec. 2013, doi: 10.1016/j.renene.2013.05.014.

[29] S. Ke, W. Yu, L. Xu, W. Yu, and Q. Yang, “Flow fields and aerodynamic loads of wind turbine considering yaw effect under wind and rain interaction,” *J. ZheJiang Univ. (Engineering Sci.*, vol. 53, no. 10, pp. 1936–1945, 2019, doi: 10.3785/j.issn.1008-973X.2019.10.011.

[30] T. Ahmad *et al.*, “Implementation and Analyses of Yaw Based Coordinated Control of Wind Farms,” *Energies*, vol. 12, no. 7, p. 1266, Apr. 2019, doi: 10.3390/en12071266.

[31] R. Barthelmie *et al.*, “Flow and wakes in large wind farms in complex terrain and offshore,” in *European Wind Energy Conference & Exhibition*, 2008, pp. 1–10.

[32] P. A. Fleming *et al.*, “Evaluating techniques for redirecting turbine wakes using SOWFA,” *Renew. Energy*, vol. 70, pp. 211–218, Oct. 2014, doi: 10.1016/j.renene.2014.02.015.

[33] T. Ahmad, A. Basit, J. Anwar, O. Coupiac, B. Kazemtabrizi, and P. Matthews, “Fast Processing Intelligent Wind Farm Controller for Production Maximisation,” *Energies*, vol. 12, no. 3, p. 544, Feb. 2019, doi: 10.3390/en12030544.

[34] D. S. Zalkind and L. Y. Pao, “The fatigue loading effects of yaw control for wind plants,” in *2016 American Control Conference (ACC)*, Jul. 2016, pp. 537–542, doi: 10.1109/ACC.2016.7524969.

[35] T. Burton, N. Jenkins, D. Sharpe, and E. Bossanyi, *Wind Energy Handbook, Second Edition*. 2011.

[36] X. Shen, X. Zhu, and Z. Du, “Wind turbine aerodynamics and loads control in wind shear flow,” *Energy*, vol. 36, no. 3, pp. 1424–1434, Mar. 2011, doi: 10.1016/j.energy.2011.01.028.

[37] J. D. M. De Kooning, T. L. Vandoorn, J. Van de Vyver, B. Meersman, and L. Vandevelde, “Shaft speed ripples in wind turbines caused by tower shadow and wind shear,” *IET Renew. Power Gener.*, vol. 8, no. 2, pp. 195–202, Mar. 2014, doi: 10.1049/iet-rpg.2013.0008.

[38] H.-S. Choi, J.-G. Kim, J.-H. Cho, and Y. Nam, “Active yaw control of MW class wind turbine,” in *ICCAS 2010*, Oct. 2010, pp. 1075–1078, doi: 10.1109/ICCAS.2010.5669699.

[39] K. A. Kragh, P. A. Fleming, and A. K. Scholbrock, “Increased Power Capture by Rotor Speed–Dependent Yaw Control of Wind Turbines,” *J. Sol. Energy Eng.*, vol. 135, no. 3, pp. 1–7, Aug. 2013, doi: 10.1115/1.4023971.

[40] K. Fischer, F. Besnard, and L. Bertling, “Reliability-Centered Maintenance for Wind Turbines Based on Statistical Analysis and Practical Experience,” *IEEE Trans. Energy Convers.*, vol. 27, no. 1, pp. 184–195, Mar. 2012, doi: 10.1109/TEC.2011.2176129.

[41] H. Guo, S. Watson, P. Tavner, and J. Xiang, “Reliability analysis for wind turbines with incomplete failure data collected from after the date of initial installation,” *Reliab. Eng. Syst. Saf.*, vol. 94, no. 6, pp. 1057–1063, Jun. 2009, doi: 10.1016/j.ress.2008.12.004.

[42] Z. Chen and F. Blaabjerg, “Wind farm—A power source in future power systems,” *Renew. Sustain. Energy Rev.*, vol. 13, no. 6–7, pp. 1288–1300, Aug. 2009, doi: 10.1016/j.rser.2008.09.010.

[43] N. S. F. . Murad, M. N. Kamarudin, S. . Rozali, and M. Shaharudin, “Review on Wind Turbine Technology and Control,” *J. Adv. Manuf. Technol.*, vol. 11, no. (2), pp. 87–100, 2017.

[44] J. Wu, Z. X. Wang, and G. Q. Wang, “The key technologies and development of offshore wind farm in China,” *Renewable and Sustainable Energy Reviews*, vol. 34. Elsevier, pp. 453–462, 2014, doi: 10.1016/j.rser.2014.03.023.

[45] J. E. Sierra-García and M. Santos, *Wind Turbine Pitch Control with an RBF Neural Network*, vol. 1268 AISC. Springer International Publishing, 2021.

[46] M. Q. Duong, F. Grimaccia, S. Leva, M. Mussetta, and E. Ogliari, “Pitch angle control using hybrid controller for all operating regions of SCIG wind turbine system,” *Renew. Energy*, vol. 70, pp. 197–203, 2014, doi: 10.1016/j.renene.2014.03.072.

[47] P. Guo, S. Chen, J. Chu, and D. Infield, “Wind direction fluctuation analysis for wind turbines,” *Renew. Energy*, vol. 162, pp. 1026–1035, 2020, doi: 10.1016/j.renene.2020.07.137.

[48] Z. Dong, “Research on control strategy of wind turbine yaw system,” 2018.

[49] M. Cheng and Y. Zhu, “The state of the art of wind energy conversion systems and technologies: A review,” *Energy Convers. Manag.*, vol. 88, pp. 332–347, Dec. 2014, doi: 10.1016/J.ENCONMAN.2014.08.037.

[50] K. Nagendra, K. Chandan, P. N. Gowri, M. S. Prathika, and D. Kavyashree, “Modeling and Simulation of Wind Turbine Coupled with a Permanent Magnet Synchronous Generator under Grid Connected System,” *Int. J. Res. Granthaalayah*, vol. 5, no. 4, pp. 29–35, 2017.

[51] M. Kesraoui, N. Korichi, and A. Belkadi, “Maximum power point tracker of wind energy conversion system,” *Renew. Energy*, vol. 36, no. 10, pp. 2655–2662, 2011, doi: 10.1016/j.renene.2010.04.028.

[52] E. Guan and X. Dong, “Study on the SHE modulation of a 5 MW offshore wind three-level converter prototype,” in *2018 13th IEEE Conference on Industrial Electronics and Applications (ICIEA)*, May 2018, pp. 571–576, doi: 10.1109/ICIEA.2018.8397781.

[53] “https://www.br-automation.com/ru/o-nas/korporativnyi-zhurnal/2016/20169/substantial-potential-for-optimizing-azimuth-control.” .

[54] “https://www.ifm.com/us/en/applications/060/wind-energy.html#!/content/documents/en-us/shared/applications/060/1020/1020.” .

[55] M.-G. Kim and P. H. Dalhoff, “Yaw Systems for wind turbines – Overview of concepts, current challenges and design methods,” *J. Phys. Conf. Ser.*, vol. 524, no. 1, p. 012086, Jun. 2014, doi: 10.1088/1742-6596/524/1/012086.

[56] G. Li, “Design of Yaw Control System of Wind Turbine Based on HCC Algorithm,” 2015.

[57] X. Ma, “Optimization and Simulation of MW-Level Doubly-fed Wind Turbine Yaw Control System,” 2010.

[58] D. Qi, “Study on Wind Turbine Bionic Yaw Control System,” 2015.

[59] R. Bharani and A. Sivaprakasam, “Application of fuzzy logic method in wind turbine yaw control system to obtain maximum energy: a methodological and prototype approach,” *Electr. Eng.*, vol. 104, no. 3, pp. 1373–1387, Jun. 2022, doi: 10.1007/s00202-021-01396-1.

[60] Y. Xiao, Z. Feng, Z. Yu, and X. Yang, “A novel yaw control method for wind turbines based onpredicted wind directions,” *Acta Energiae Solaris Sin.*, vol. 42, no. 2, pp. 144–149, 2021, doi: 10.19912/j.0254-0096.tynxb.2018-0918.

[61] M. F. Howland, “Wind farm yaw control set-point optimization under model parameter uncertainty,” *J. Renew. Sustain. Energy*, vol. 13, no. 4, p. 043303, Jul. 2021, doi: 10.1063/5.0051071.

[62] E. Yatiyana, S. Rajakaruna, and A. Ghosh, “Wind speed and direction forecasting

for wind power generation using ARIMA model," *2017 Australas. Univ. Power Eng. Conf. AUPEC 2017*, vol. 2017-Novem, pp. 1–6, 2018, doi: 10.1109/AUPEC.2017.8282494.

[63] A. Saenz-Aguirre, E. Zulueta, U. Fernandez-Gamiz, J. A. Ramos-Hernanz, and J. M. Lopez-Guede, *Self-tuning Yaw Control Strategy of a Horizontal Axis Wind Turbine Based on Machine Learning*. 2021.

[64] Y. Yang and E. Solomin, "Hill-Climbing Algorithm for the Wind Turbine Yaw System," in *2021 International Ural Conference on Electrical Power Engineering (UralCon)*, Sep. 2021, pp. 561–565, doi: 10.1109/UralCon52005.2021.9559498.

[65] D. Zhang, "Research on Control Strategy for Yaw System of Wind Turbine," 2018.

[66] H. Zhang, P. Sun, and Z. Zhang, "Research on Yaw Control System for Wind Turbine based on Optimized Kalman Filter," *Microcomput. Inf.*, vol. 26, no. 028, pp. 42–43, 2010.

[67] A. Torabi, E. Tarsaii, and S. K. M. Mashhadi, "Fuzzy Controller Used In Yaw System Of Wind Turbine Noisy," *J. Math. Comput. Sci.*, vol. 08, no. 02, pp. 105–112, Jan. 2014, doi: 10.22436/jmcs.08.02.02.

[68] D. Choi, W. Shin, K. Ko, and W. Rhee, "Static and Dynamic Yaw Misalignments of Wind Turbines and Machine Learning Based Correction Methods Using LiDAR Data," *IEEE Trans. Sustain. Energy*, vol. 10, no. 2, pp. 971–982, 2019, doi: 10.1109/TSTE.2018.2856919.

[69] H. Piao and Z. Wang, "Control strategy of CPSO-based PID neural network and a yaw motor," *Electr. Mach. Control*, vol. 14, no. 09, pp. 55–62, 2010.

[70] D. Song, J. Yang, Y. Liu, M. Su, A. Liu, and Y. H. Joo, "Wind direction prediction for yaw control of wind turbines," *Int. J. Control. Autom. Syst.*, vol. 15, no. 4, pp. 1720–1728, Aug. 2017, doi: 10.1007/s12555-017-0289-6.

[71] Y. Zhang, P. Han, D. Wang, and S. Wang, "Short-term wind speed prediction of wind farms based on variational modal decomposition and LSSVM," *Acta Energiae Solaris Sin.*, vol. 38, no. 01, pp. 194–202, 2018.

[72] J. K. Kaldellis, *Stand-Alone and Hybrid Wind Energy Systems: Technology, Energy Storage and Applications*. Elsevier Science, 2010.

[73] D. Zhang, "Study on Wind Turbine Yaw System Based on Wind Direction Forecast."

[74] M. Hansen, *Aerodynamics of wind turbines*. Earthscan, 2015.

[75] A. C. Hansen, C. P. Butterfield, and X. Cui, "Yaw Loads and Motions of a Horizontal Axis Wind Turbine," *J. Sol. Energy Eng.*, vol. 112, no. 4, pp. 310–314, Nov. 1990, doi: 10.1115/1.2929939.

[76] D. Micallef and T. Sant, "A Review of Wind Turbine Yaw Aerodynamics," in *Wind Turbines - Design, Control and Applications*, InTech, 2016.

[77] S. Schmitz, *Aerodynamics of wind turbines: a physical basis for analysis and design*. John Wiley & Sons, 2020.

[78] J. F. J. F. Manwell, J. G. J. G. McGowan, and A. L. A. L. Rogers, *Wind energy explained: theory, design and application*. John Wiley & Sons, 2010.

[79] C. J. Bai and W. C. Wang, "Review of computational and experimental approaches to analysis of aerodynamic performance in horizontal-axis wind turbines (HAWTs)," *Renew. Sustain. Energy Rev.*, vol. 63, pp. 506–519, 2016, doi: 10.1016/j.rser.2016.05.078.

[80] L. Wang, "Study on Systematic Dynamic Model and Simulation for Offshore Wind Turbine," 2011.

[81] K. Xu, "Research on Yaw Error Generation Mechanism and Adjustment Strategy of Wind Turbine," 2021.

[82] R. Gasch and J. Twele, *Wind power plants: fundamentals, design, construction and operation*. Berlin, Heidelberg: Springer Science & Business Media, 2011.

[83] X. Yao, "Wind turbine Generator System Theory and Design," 2012.

[84] K. A. Kragh and M. H. Hansen, "Load alleviation of wind turbines by yaw misalignment," *Wind Energy*, vol. 17, no. 7, pp. 971–982, Jul. 2014, doi: 10.1002/we.1612.

[85] F. Porté-Agel, M. Bastankhah, and S. Shamsoddin, "Wind-Turbine and Wind-Farm Flows: A Review," *Boundary-Layer Meteorol.*, vol. 174, no. 1, pp. 1–59,

Jan. 2020, doi: 10.1007/s10546-019-00473-0.

[86] B. Dou, M. Guala, L. Lei, and P. Zeng, “Wake model for horizontal-axis wind and hydrokinetic turbines in yawed conditions,” *Appl. Energy*, vol. 242, pp. 1383–1395, May 2019, doi: 10.1016/j.apenergy.2019.03.164.

[87] M. F. Howland, J. Bossuyt, L. A. Martínez-Tossas, J. Meyers, and C. Meneveau, “Wake structure in actuator disk models of wind turbines in yaw under uniform inflow conditions,” *J. Renew. Sustain. Energy*, vol. 8, no. 4, p. 043301, Jul. 2016, doi: 10.1063/1.4955091.

[88] Á. Jiménez, A. Crespo, and E. Migoya, “Application of a LES technique to characterize the wake deflection of a wind turbine in yaw,” *Wind Energy*, vol. 13, no. 6, pp. 559–572, Dec. 2009, doi: 10.1002/we.380.

[89] J. Liew, A. M. Urbán, and S. J. Andersen, “Analytical model for the power-yaw sensitivity of wind turbines operating in full wake,” *Wind Energy Sci.*, vol. 5, no. 1, pp. 427–437, 2020, doi: 10.5194/wes-5-427-2020.

[90] T. Sant, “Improving BEM-based Aerodynamic Models in Wind Turbine Design Codes,” 2007.

[91] B. Dou, M. Guala, L. Lei, and P. Zeng, “Experimental investigation of the performance and wake effect of a small-scale wind turbine in a wind tunnel,” *Energy*, vol. 166, pp. 819–833, Jan. 2019, Accessed: Aug. 21, 2022. [Online]. Available: https://linkinghub.elsevier.com/retrieve/pii/S0360544218320930.

[92] M. Bastankhah and F. Porté-Agel, “Experimental and theoretical study of wind turbine wakes in yawed conditions,” *J. Fluid Mech.*, vol. 806, pp. 506–541, Nov. 2016, doi: 10.1017/jfm.2016.595.

[93] X. Li, Y. Qiu, Y. Feng, and Z. Wang, “Wind turbine power prediction considering wake effects with dual laser beam LiDAR measured yaw misalignment,” *Appl. Energy*, vol. 299, p. 117308, Oct. 2021, doi: 10.1016/j.apenergy.2021.117308.

[94] G. Wanke, M. H. Hansen, and T. J. Larsen, “Qualitative yaw stability analysis of free-yawing downwind turbines,” *Wind Energy Sci.*, vol. 4, no. 2, pp. 233–250, May 2019, doi: 10.5194/wes-4-233-2019.

[95] R. Damiani *et al.*, “Assessment of wind turbine component loads under yaw-

offset conditions," *Wind Energy Sci.*, vol. 3, no. 1, pp. 173–189, Apr. 2018, doi: 10.5194/wes-3-173-2018.

[96] P. Wang, "Design and Study on Yaw Control System for Wind Turbine," 2012.

[97] X. Liu, R. Goodall, and S. Iwnicki, "Yaw compensation and yaw relaxation controls for active steering of railway wheelsets via electromechanical actuators," *Proc. Inst. Mech. Eng. Part F J. Rail Rapid Transit*, vol. 236, no. 1, pp. 70–79, Jan. 2022, doi: 10.1177/09544097211004322.

[98] C. Qu *et al.*, "Improved Data-Driven Yaw Misalignment Calibration of Wind Turbine via LiDAR Verification," *Proc. - 2020 Chinese Autom. Congr. CAC 2020*, pp. 5611–5616, Nov. 2020, doi: 10.1109/CAC51589.2020.9326891.

[99] P. Fleming *et al.*, "Investigation into the shape of a wake of a yawed full-scale turbine," in *Journal of Physics: Conference Series*, 2018, vol. 1037, no. 3, doi: 10.1088/1742-6596/1037/3/032010.

[100] S. Wan, L. Cheng, and X. Sheng, "Numerical analysis of the spatial distribution of equivalent wind speeds in large-scale wind turbines," *J. Mech. Sci. Technol.*, vol. 31, no. 2, pp. 965–974, 2017, doi: 10.1007/s12206-017-0149-6.

[101] M. R. Patel, *Wind and Solar Power Systems-Design, Analysis and Operation, Second Edition*, vol. 35, no. 2. Taylor & Francis, 2006.

[102] M. Garcia-Sanz and C. H. Houpis, *Wind Energy Systems: Control Engineering Design*. Taylor \& Francis, 2012.

[103] I. Delgado and M. Fahim, "Wind Turbine Data Analysis and LSTM-Based Prediction in SCADA System," *Energies*, vol. 14, no. 1, p. 125, Dec. 2020, doi: 10.3390/en14010125.

[104] F. Blaabjerg and D. M. Ionel, *Renewable Energy Devices and Systems with Simulations in MATLAB®and ANSYS®*. CRC Press, 2017.

[105] U. Eminoglu and S. Ayasun, "Modeling and Design Optimization of Variable-Speed Wind Turbine Systems," *Energies*, vol. 7, no. 1, pp. 402–419, Jan. 2014, doi: 10.3390/en7010402.

[106] I. Abdulrahman, "An open-source Simulink-based program for simulating power systems integrated with renewable energy sources," *Electr. Eng.*, vol. 102, no. 4,

pp. 2181–2192, Dec. 2020, doi: 10.1007/s00202-020-01022-6.

[107] M. Benchagra, M. Hilal, Y. Errami, M. Ouassaid, and M. Maaroufi, “Modeling and control of SCIG based variable-speed with power factor control,” *Int. Rev. Model. Simulations*, vol. 4, no. 3, pp. 1007–1014, 2011.

[108] N. Singh and M. T. Scholar, “Design and Modeling of Wind Energy Conversion System Based on PMSG Using MPPT Technique,” *Int. J. Sci. Res. Eng. Technol.*, vol. 5, no. 2, pp. 96–100, 2016.

[109] A. Rolan, A. Luna, G. Vazquez, D. Aguilar, and G. Azevedo, “Modeling of a variable speed wind turbine with a Permanent Magnet Synchronous Generator,” in *2009 IEEE International Symposium on Industrial Electronics*, Jul. 2009, vol. 7, no. ISlE, pp. 734–739, doi: 10.1109/ISIE.2009.5218120.

[110] B. Boukhezzar and H. Siguerdidjane, “Nonlinear control of a variable-speed wind turbine using a two-mass model,” *IEEE Trans. Energy Convers.*, vol. 26, no. 1, pp. 149–162, 2011, doi: 10.1109/TEC.2010.2090155.

[111] P. Anusri and K. C. Sindhu, “Mathematical Modeling of the Squirrel Cage Induction Generator based Wind Farm for Sub-Synchronous Resonance Analysis,” *Indian J. Sci. Technol.*, vol. 9, no. 38, Oct. 2016, doi: 10.17485/ijst/2016/v9i38/101943.

[112] K. M. S. Y. Konara and M. L. Kolhe, “Pitch controller modeling for wind turbine power regulation using feed forward control strategies,” in *2015 IEEE PES Asia-Pacific Power and Energy Engineering Conference (APPEEC)*, Nov. 2015, pp. 1–5, doi: 10.1109/APPEEC.2015.7381018.

[113] S. Muller, M. Deicke, and R. W. De Doncker, “Doubly fed induction generator systems for wind turbines,” *IEEE Ind. Appl. Mag.*, vol. 8, no. 3, pp. 26–33, 2002, doi: 10.1109/2943.999610.

[114] K. Belmokhtar, M. L. Doumbia, and K. Agbossou, “Novel fuzzy logic based sensorless maximum power point tracking strategy for wind turbine systems driven DFIG (doubly-fed induction generator),” *Energy*, vol. 76, pp. 679–693, Nov. 2014, doi: 10.1016/j.energy.2014.08.066.

[115] Y. Ma, J. Yu, G. Wu, and G. Chen, “MPPT Control Strategy for Doubly-Fed Wind

Power Generation," *Trans. China Electrotech. Soc.*, vol. 24, no. 4, pp. 202–208, 2009.

[116] Y. Zhang, L. Zhang, and Y. Liu, "Implementation of Maximum Power Point Tracking Based on Variable Speed Forecasting for Wind Energy Systems," *Processes*, vol. 7, no. 3, p. 158, Mar. 2019, doi: 10.3390/pr7030158.

[117] K. Belmokhtar, M. L. Doumbia, and K. Agbossou, "Modelling and fuzzy logic control of DFIG based Wind Energy Conversion Systems," in *2012 IEEE International Symposium on Industrial Electronics*, May 2012, pp. 1888–1893, doi: 10.1109/ISIE.2012.6237380.

[118] İ. Yazıcı, E. K. Yaylacı, and F. Yalçın, "Modified golden section search based MPPT algorithm for the WECS," *Eng. Sci. Technol. an Int. J.*, vol. 24, no. 5, pp. 1123–1133, Oct. 2021, doi: 10.1016/j.jestch.2021.02.006.

[119] A. Sachan, A. K. Gupta, and P. Samuel, "A Review of MPPT Algorithms Employedin Wind Energy Conversion Systems," *J. Green Eng.*, vol. 6, no. 4, pp. 385–402, 2017, doi: 10.13052/jge1904-4720.643.

[120] S. Marmouh, M. Boutoubat, and L. Mokrani, "MPPT fuzzy logic controller of a wind energy conversion system based on a PMSG," in *2016 8th International Conference on Modelling, Identification and Control (ICMIC)*, Nov. 2016, pp. 296–302, doi: 10.1109/ICMIC.2016.7804126.

[121] J. Li, K. Z. Zhang, S. Q. Li, and C. Liu, "Maximum power point tracking control with active disturbance rejection controller based on the best tip speed ratio," *Electr. Mach. Control*, vol. 19, no. 12, 2015, doi: 10.15938/j.emc.2015.12.014.

[122] J. Singh and M. Ouhrouche, "MPPT Control Methods in Wind Energy Conversion Systems," in *Fundamental and Advanced Topics in Wind Power*, no. June, InTech, 2011, pp. 339–360.

[123] A. W. Manyonge, R. M. Ochieng, F. N. Onyango, and J. M. Shichikha, "Mathematical modelling of wind turbine in a wind energy conversion system: Power coefficient analysis," *Appl. Math. Sci.*, vol. 6, no. 91, pp. 4527–4536, 2012.

[124] E. Mohammadi, R. Fadaeinedjad, and H. R. H. R. Naji, "Flicker emission, voltage fluctuations, and mechanical loads for small-scale stall- and yaw-

controlled wind turbines," *Energy Convers. Manag.*, vol. 165, no. March, pp. 567–577, Jun. 2018, doi: 10.1016/j.enconman.2018.03.094.

[125] A. M. Eltamaly and H. M. Farh, "Maximum power extraction from wind energy system based on fuzzy logic control," *Electr. Power Syst. Res.*, vol. 97, pp. 144–150, Apr. 2013, doi: 10.1016/j.epsr.2013.01.001.

[126] B. Singh and G. K. Kasal, "Voltage and frequency controller for a three-phase four-wire autonomous wind energy conversion system," *IEEE Trans. Energy Convers.*, vol. 23, no. 2, pp. 509–518, 2008, doi: 10.1109/TEC.2008.918620.

[127] P. K. Goel, B. Singh, S. S. Murthy, and N. Kishore, "Isolated wind-hydro hybrid system using cage generators and battery storage," *IEEE Trans. Ind. Electron.*, vol. 58, no. 4, pp. 1141–1153, 2011, doi: 10.1109/TIE.2009.2037646.

[128] A. M. Foley, P. G. Leahy, A. Marvuglia, and E. J. McKeogh, "Current methods and advances in forecasting of wind power generation," *Renew. Energy*, vol. 37, no. 1, pp. 1–8, Jan. 2012, doi: 10.1016/j.renene.2011.05.033.

[129] S. Mishra, C. Bordin, K. Taharaguchi, and I. Palu, "Comparison of deep learning models for multivariate prediction of time series wind power generation and temperature," *Energy Reports*, vol. 6, pp. 273–286, Feb. 2020, doi: 10.1016/j.egyr.2019.11.009.

[130] S. M. Lawan, W. A. W. Z. Abidin, A. M. Lawan, S. L. Bichi, and I. Abba, "The potential of topographical feedforward neural network (T-FFNN) technique in monthly wind speed and direction prediction," *Proc. 2017 6th Int. Conf. Electr. Eng. Informatics Sustain. Soc. Through Digit. Innov. ICEEI 2017*, vol. 2017-Novem, pp. 1–6, 2018, doi: 10.1109/ICEEI.2017.8312407.

[131] Y. Wang, R. Shen, and M. Ma, "Research on ultra-short term forecasting technology of wind power output based on various meteorological factors," *Energy Reports*, vol. 8, pp. 1145–1158, Jul. 2022, doi: 10.1016/J.EGYR.2022.02.058.

[132] M. Yesilbudak, S. Sagiroglu, and I. Colak, "A novel implementation of kNN classifier based on multi-tupled meteorological input data for wind power prediction," *Energy Convers. Manag.*, vol. 135, pp. 434–444, Mar. 2017, doi:

10.1016/J.ENCONMAN.2016.12.094.

[133] L. Wang, Y. Guo, M. Fan, and X. Li, “Wind speed prediction using measurements from neighboring locations and combining the extreme learning machine and the AdaBoost algorithm,” *Energy Reports*, vol. 8, pp. 1508–1518, Nov. 2022, doi: 10.1016/j.egyr.2021.12.062.

[134] V. G. Ochoa, N. J. Alvarez, and V. M. Chamorro, “Data set on wind speed, wind direction and wind probability distributions in Puerto Bolivar - Colombia,” *Data Br.*, vol. 27, p. 104753, Dec. 2019, doi: 10.1016/j.dib.2019.104753.

[135] Y. Zhong, Q. Li, Di. Huang, B. He, L. Sun, and X. Wang, “A Neural Network Approach to Wind Speed Prediction,” *2020 Asia Energy Electr. Eng. Symp. AEEES 2020*, vol. 4, pp. 788–794, 2020, doi: 10.1109/AEEES48850.2020.9121538.

[136] S. Harbola and V. Coors, “One dimensional convolutional neural network architectures for wind prediction,” *Energy Convers. Manag.*, vol. 195, pp. 70–75, Sep. 2019, doi: 10.1016/J.ENCONMAN.2019.05.007.

[137] X.-Y. Xin, J.-W. Wang, and S. Zhao, “Prediction Model of Natural Wind Direction Based on Statistical Method,” *K. Cheng Je Wu Li Hsueh Pao/Journal Eng. Thermophys.*, vol. 42, no. 6, pp. 1438–1445, 2021.

[138] Z. Tian, H. Li, and F. Li, “A combination forecasting model of wind speed based on decomposition,” *Energy Reports*, vol. 7, pp. 1217–1233, Nov. 2021, doi: 10.1016/j.egyr.2021.02.002.

[139] M. A. Rushdi, S. Yoshida, K. Watanabe, and Y. Ohya, “Machine learning approaches for thermal updraft prediction in wind solar tower systems,” *Renew. Energy*, vol. 177, pp. 1001–1013, Nov. 2021, doi: 10.1016/J.RENENE.2021.06.033.

[140] W. Qiao, J. Wang, M. Song, and Y. Wen, “Wind farm micro-siting based on auto-regressive wind prediction,” *2015 IEEE Conf. Control Appl. CCA 2015 - Proc.*, pp. 1853–1855, 2015, doi: 10.1109/CCA.2015.7320879.

[141] S. ho Hur, “Short-term wind speed prediction using Extended Kalman filter and machine learning,” *Energy Reports*, vol. 7, pp. 1046–1054, Nov. 2021, doi:

10.1016/j.egyr.2020.12.020.

[142] A. Stetco *et al.*, "Machine learning methods for wind turbine condition monitoring: A review," *Renew. Energy*, vol. 133, pp. 620–635, Apr. 2019, doi: 10.1016/J.RENENE.2018.10.047.

[143] X.-J. Chen, J. Zhao, X.-Z. Jia, and Z.-L. Li, "Multi-step wind speed forecast based on sample clustering and an optimized hybrid system," *Renew. Energy*, vol. 165, pp. 595–611, Mar. 2021, doi: 10.1016/j.renene.2020.11.038.

[144] D. Astolfi, F. Castellani, M. Becchetti, A. Lombardi, and L. Terzi, "Wind Turbine Systematic Yaw Error: Operation Data Analysis Techniques for Detecting It and Assessing Its Performance Impact," *Energies*, vol. 13, no. 9, p. 2351, May 2020, doi: 10.3390/en13092351.

[145] H. Liu, H. Tian, X. Liang, and Y. Li, "New wind speed forecasting approaches using fast ensemble empirical model decomposition, genetic algorithm, Mind Evolutionary Algorithm and Artificial Neural Networks," *Renew. Energy*, vol. 83, pp. 1066–1075, 2015, doi: 10.1016/j.renene.2015.06.004.

[146] S. Ansari, T. G. Sampath Vinayak Kumar, and J. Dhillon, "Wind Power Forecasting using Artificial Neural Network," in *2021 4th International Conference on Recent Developments in Control, Automation & Power Engineering (RDCAPE)*, Oct. 2021, vol. 3, no. 4, pp. 35–37, doi: 10.1109/RDCAPE52977.2021.9633643.

[147] C. Yu, Y. Li, and M. Zhang, "An improved Wavelet Transform using Singular Spectrum Analysis for wind speed forecasting based on Elman Neural Network," *Energy Convers. Manag.*, vol. 148, pp. 895–904, Sep. 2017, doi: 10.1016/j.enconman.2017.05.063.

[148] N. Ramesh Babu and P. Arulmozhivarman, "Improving Forecast Accuracy of Wind Speed Using Wavelet Transform and Neural Networks," *J. Electr. Eng. Technol.*, vol. 8, no. 3, pp. 559–564, May 2013, doi: 10.5370/JEET.2013.8.3.559.

[149] A. Lahouar and J. Ben Hadj Slama, "Wind speed and direction prediction for wind farms using support vector regression," *IREC 2014 - 5th Int. Renew. Energy Congr.*, 2014, doi: 10.1109/IREC.2014.6826932.

[150] Y. Zhang, G. Pan, Y. Zhao, Q. Li, and F. Wang, “Short-term wind speed interval prediction based on artificial intelligence methods and error probability distribution,” *Energy Convers. Manag.*, vol. 224, no. August, p. 113346, 2020, doi: 10.1016/j.enconman.2020.113346.

[151] J. Maldonado-Correa, M. Valdiviezo, J. Solano, M. Rojas, and C. Samaniego-Ojeda, *Wind Energy Forecasting with Artificial Intelligence Techniques: A Review*, vol. 1194 CCIS. Springer International Publishing, 2020.

[152] W. Dong, H. Sun, J. Tan, Z. Li, J. Zhang, and H. Yang, “Multi-degree-of-freedom high-efficiency wind power generation system and its optimal regulation based on short-term wind forecasting,” *Energy Convers. Manag.*, vol. 249, p. 114829, Dec. 2021, doi: 10.1016/j.enconman.2021.114829.

[153] T. Blanchard and B. Samanta, “Wind speed forecasting using neural networks,” *Wind Eng.*, vol. 44, no. 1, pp. 33–48, Feb. 2020, doi: 10.1177/0309524X19849846.

[154] A. Masoumi, F. Jabari, and B. Mohammadi-Ivatloo, “Wind Speed Forecasting Using Back Propagation Artificial Neural Networks in North of Iran,” *J. Energy Manag. Technol.*, vol. 1, no. 3, pp. 21–25, 2017, doi: 10.22109/JEMT.2017.91014.1026.

[155] B. He *et al.*, “A combined model for short-term wind power forecasting based on the analysis of numerical weather prediction data,” *Energy Reports*, vol. 8, pp. 929–939, Nov. 2022, doi: 10.1016/j.egyr.2021.10.102.

[156] J. Duan, H. Zuo, Y. Bai, J. Duan, M. Chang, and B. Chen, “Short-term wind speed forecasting using recurrent neural networks with error correction,” *Energy*, vol. 217, p. 119397, 2021, doi: 10.1016/j.energy.2020.119397.

[157] K. Zhang, Z. Qu, J. Wang, W. Zhang, and F. Yang, “A novel hybrid approach based on cuckoo search optimization algorithm for short-term wind speed forecasting,” *Environ. Prog. Sustain. Energy*, vol. 36, no. 3, pp. 943–952, May 2017, doi: 10.1002/ep.12533.

[158] S. Alessandrini, L. Delle Monache, S. Sperati, and J. N. Nissen, “A novel application of an analog ensemble for short-term wind power forecasting,” *Renew.*

Energy, vol. 76, pp. 768–781, Apr. 2015, doi: 10.1016/j.renene.2014.11.061.

[159] N. Chen, Z. Qian, I. T. Nabney, and X. Meng, "Wind Power Forecasts Using Gaussian Processes and Numerical Weather Prediction," *IEEE Trans. Power Syst.*, vol. 29, no. 2, pp. 656–665, Mar. 2014, doi: 10.1109/TPWRS.2013.2282366.

[160] S. Chen, L. Ye, G. Zhang, C. Zeng, S. Dong, and C. Dai, "Short-term wind power prediction based on combined grey-Markov model," in *2011 International Conference on Advanced Power System Automation and Protection*, Oct. 2011, pp. 1705–1711, doi: 10.1109/APAP.2011.6180647.

[161] L. Huang, L. Li, X. Wei, and D. Zhang, "Short-term prediction of wind power based on BiLSTM–CNN–WGAN-GP," *Soft Comput.*, Jan. 2022, doi: 10.1007/s00500-021-06725-x.

[162] B. Qu, Z. Xing, Y. Liu, and L. Chen, "Research on short-term output power forecast model of wind farm based on neural network combination algorithm," *Wind Energy*, Jun. 2022, doi: 10.1002/we.2763.

[163] D. Song, X. Fan, J. Yang, A. Liu, S. Chen, and Y. H. Y. H. Joo, "Power extraction efficiency optimization of horizontal-axis wind turbines through optimizing control parameters of yaw control systems using an intelligent method," *Appl. Energy*, vol. 224, no. March, pp. 267–279, Aug. 2018, doi: 10.1016/j.apenergy.2018.04.114.

[164] A. Kisvari, Z. Lin, and X. Liu, "Wind power forecasting – A data-driven method along with gated recurrent neural network," *Renew. Energy*, vol. 163, pp. 1895–1909, Jan. 2021, doi: 10.1016/j.renene.2020.10.119.

[165] M. De Liu, L. Ding, and Y. L. Bai, "Application of hybrid model based on empirical mode decomposition, novel recurrent neural networks and the ARIMA to wind speed prediction," *Energy Convers. Manag.*, vol. 233, p. 113917, Apr. 2021, doi: 10.1016/J.ENCONMAN.2021.113917.

[166] Y. Su, S. Wang, Z. Xiao, M. Tan, and M. Wang, "An Ultra-Short-Term Wind Power Forecasting Approach Based on Wind Speed Decomposition, Wind Direction and Elman Neural Networks," in *2018 2nd IEEE Conference on Energy*

Internet and Energy System Integration (EI2), Oct. 2018, pp. 1–9, doi: 10.1109/EI2.2018.8582514.

[167] A. J. Wood, B. F. Wollenberg, and G. B. Sheblé, *Power generation, operation, and control*. John Wiley & Sons, 2014.

[168] Xiaosheng Peng *et al.*, "A very short term wind power prediction approach based on Multilayer Restricted Boltzmann Machine," in *2016 IEEE PES Asia-Pacific Power and Energy Engineering Conference (APPEEC)*, Oct. 2016, pp. 2409–2413, doi: 10.1109/APPEEC.2016.7779917.

[169] S. Wang *et al.*, "An Improved Model for Power Prediction of PV System Based on Elman Neural Networks," *2020 Asia Energy Electr. Eng. Symp. AEEES 2020*, pp. 902–907, 2020, doi: 10.1109/AEEES48850.2020.9121450.

[170] A. Khan *et al.*, "Forecasting OPEC Electricity Generation Based on Elman Network Trained by Cuckoo Search Algorithm," in *Green Energy and Technology*, 2019, pp. 59–76.

[171] E. Eğrioğlu, C. H. Aladag, and U. Yolcu, "Comparison of Feed Forward and Elman Neural Networks Forecasting Ability: Case Study for IMKB," in *Advances in Time Series Forecasting*, E. Eğrioğlu, C. Hakan Aladag, and U. Yolcu, Eds. BENTHAM SCIENCE PUBLISHERS, 2012, pp. 11–17.

[172] C. Yu, Y. Li, and M. Zhang, "Comparative study on three new hybrid models using Elman Neural Network and Empirical Mode Decomposition based technologies improved by Singular Spectrum Analysis for hour-ahead wind speed forecasting," *Energy Convers. Manag.*, vol. 147, pp. 75–85, Sep. 2017, doi: 10.1016/j.enconman.2017.05.008.

[173] W. Duan, X. Han, L. Ma, S. Liu, and W. Liu, "Fault Prediction of Wind Turbine Wheel Subsystem Based on Elman Neural Network," *Acta Energiae Solaris Sin.*, vol. 42, no. 12, pp. 157–162, 2021.

[174] W. M. Lin, C. M. Hong, and C. H. Chen, "Neural-network-based MPPT control of a stand-alone hybrid power generation system," *IEEE Trans. Power Electron.*, vol. 26, no. 12, pp. 3571–3581, 2011, doi: 10.1109/TPEL.2011.2161775.

[175] T. Shahwan and M. Odening, *Forecasting agricultural commodity prices using*

hybrid neural networks. 2007.

[176] H. Liu, X. wei Mi, and Y. fei Li, "Wind speed forecasting method based on deep learning strategy using empirical wavelet transform, long short term memory neural network and Elman neural network," *Energy Convers. Manag.*, vol. 156, pp. 498–514, Jan. 2018, doi: 10.1016/J.ENCONMAN.2017.11.053.

[177] P. Li, Y. Li, Q. Xiong, Y. Chai, and Y. Zhang, "Application of a hybrid quantized Elman neural network in short-term load forecasting," *Int. J. Electr. Power Energy Syst.*, vol. 55, pp. 749–759, Feb. 2014, doi: 10.1016/j.ijepes.2013.10.020.

[178] K.-H. Lu, C.-M. Hong, and Q. Xu, "Recurrent wavelet-based Elman neural network with modified gravitational search algorithm control for integrated offshore wind and wave power generation systems," *Energy*, vol. 170, pp. 40–52, Mar. 2019, doi: 10.1016/j.energy.2018.12.084.

[179] Y. Zhang, X. Wang, and H. Tang, "An improved Elman neural network with piecewise weighted gradient for time series prediction," *Neurocomputing*, vol. 359, pp. 199–208, Sep. 2019, doi: 10.1016/j.neucom.2019.06.001.

[180] H. Armghan, M. Yang, A. Armghan, and N. Ali, "Double integral action based sliding mode controller design for the back-to-back converters in grid-connected hybrid wind-PV system," *Int. J. Electr. Power Energy Syst.*, vol. 127, 2021, doi: 10.1016/j.ijepes.2020.106655.

[181] S. Saat, S. K. Nguang, and A. Nasiri, *Analysis and Synthesis of Polynomial Discrete-Time Systems*. Elsevier, 2017.

[182] N. T. Nguyen, "Lyapunov Stability Theory," 2018, pp. 47–81.

[183] Y. Li, J. Zhang, and Q. Wu, *Adaptive Sliding Mode Neural Network Control for Nonlinear Systems*. Elsevier, 2019.

[184] K. Xie, H. Yi, G. Hu, L. Li, and Z. Fan, "Short-term power load forecasting based on Elman neural network with particle swarm optimization," *Neurocomputing*, vol. 416, pp. 136–142, Nov. 2020, doi: 10.1016/j.neucom.2019.02.063.

[185] E. A. Pinheiro, J. B. V. L. Júnior, L. C. de Lima, and F. G. de Melo Pinheiro, "Nonlinear Autoregressive Neural Networks for Forecasting Wind Speed Time Series," *Int. J. Dev. Res.*, vol. 10, no. 09, pp. 40336–40343, 2020, doi:

10.37118/ijdr.19845.09.2020.

[186] Y. Liu, S. Liu, L. Zhang, F. Cao, and L. Wang, "Optimization of the Yaw Control Error of Wind Turbine," *Front. Energy Res.*, vol. 9, no. February, pp. 1–10, Feb. 2021, doi: 10.3389/fenrg.2021.626681.

[187] Q. Zou, B. Liu, L. Peng, and J. Wang, "Application of Hill-Climbing Control Algorithm in Yaw Control System for Wind Power Generation Sets," *Power Syst. Technol.*, vol. 34, no. 5, pp. 72–76, 2010, doi: 10.13335/j.1000-3673.pst.2010.05.012.

[188] Y. Huang, G. Li, H. Li, and Y. Bai, "Wind Power Generation System Maximum Power Point Tracking Strategy," *Electr. Meas. Instrum.*, vol. 49, no. 557, pp. 17–20, 2012.

[189] X. Li, H. Xu, and Y. Du, "Maximum power tracking of wind power generation system using the combination of tip speed ratio method and climbing search method," *Power Syst. Prot. Control*, vol. 43, no. 13, pp. 66–71, 2015.

[190] A. Ahmed, Li Ran, and J. Bumby, "Perturbation parameters design for hill climbing MPPT techniques," in *2012 IEEE International Symposium on Industrial Electronics*, May 2012, pp. 1819–1824, doi: 10.1109/ISIE.2012.6237368.

[191] A. S. Badawi, N. F. Hasbullah, S. H. Yusoff, A. Hashim, S. Khan, and A. M. Zyoud, "Power prediction mode technique for Hill Climbing Search algorithm to reach the maximum power point tracking," in *2020 2nd International Conference on Electrical, Control and Instrumentation Engineering (ICECIE)*, Nov. 2020, pp. 1–7, doi: 10.1109/ICECIE50279.2020.9309564.

[192] A. Soetedjo, A. Lomi, and Widodo Puji Mulayanto, "Modeling of wind energy system with MPPT control," in *Proceedings of the 2011 International Conference on Electrical Engineering and Informatics*, Jul. 2011, no. July, pp. 1–6, doi: 10.1109/ICEEI.2011.6021836.

[193] M. Ceretta Moreira, D. Lellis Hoss, M. Jinbo, F. A. Farret, and G. Cardoso Junior, "Fixed and Adaptive Step HCC Algorithms for MPPT of the Cylinders of Magnus Wind Turbines," in *3rd Renewable Power Generation Conference (RPG*

2014), 2014, vol. 2014, no. CP651, pp. 8.36-8.36, doi: 10.1049/cp.2014.0921.

[194] X. Du and H. Yin, "MPPT control strategy of DFIG-based wind turbines using double steps hill climb searching algorithm," in *2015 5th International Conference on Electric Utility Deregulation and Restructuring and Power Technologies (DRPT)*, Nov. 2015, pp. 1910–1914, doi: 10.1109/DRPT.2015.7432585.

[195] Q. Li, "Maximum Power Point Tracking Method of Variable Step Perturbation," *Mod. Archit. Electr.*, vol. 6, no. 5, pp. 50–52, 2015.

[196] J. Li, L. Ben, and L. Ye, "MPPT Strategy Based on Improved Control Method for Small Wind Power System," *Mech. Eng. Autom.*, no. 6, pp. 145–147, 2015.

[197] Y. Jia, B. Cao, and Z. Yang, "A Fast Response MPPT Control Method for Wind Generation," *ACTA ENERGIAE SOLARIS Sin.*, vol. 25, no. 2, pp. 171–176, 2004.

[198] B. Hu, L. Hai, L. Cheng, Y. Yuan, L. Xu, and L. Zheng, "Experimental Study on Yaw Control System of Small Wind Turbine," *Micromotors*, vol. 53, no. 6, pp. 64–67, 2020.

[199] I. Ait Ayad, E. Elwarraki, and M. Baghdadi, "Intelligent Perturb and Observe Based MPPT Approach Using Multilevel DC-DC Converter to Improve PV Production System," *J. Electr. Comput. Eng.*, vol. 2021, pp. 1–13, Feb. 2021, doi: 10.1155/2021/6673022.

[200] Y. Mei and P. Sun, "Improvement of hill climbing method based on wind speed prediction," *Technol. Innov. Appl.*, no. 16, pp. 6–9, 2020.

[201] M. Lasheen and M. Abdel-Salam, "Maximum power point tracking using Hill Climbing and ANFIS techniques for PV applications: A review and a novel hybrid approach," *Energy Convers. Manag.*, vol. 171, pp. 1002–1019, Sep. 2018, doi: 10.1016/j.enconman.2018.06.003.

[202] H. Li, Q. Li, X. Jiang, Y. Ruan, and W. Huang, "The Application of Improved Hill-Climb Search Algorithm in Wind Power Generation," *IFAC Proc. Vol.*, vol. 46, no. 20, pp. 263–267, 2013, doi: 10.3182/20130902-3-CN-3020.00004.

[203] X.-S. Yang, *Nature-Inspired Optimization Algorithms*. Elsevier, 2014.

[204] Ю. Ян, Е. В. Соломин, Ж. Сюе, А. А. Ковалев, Г. Н. Рявкин, and А. А.

Мирошниченко, “ИССЛЕДОВАНИЕ МРРТ-УПРАВЛЕНИЯ ГОРИЗОНТАЛЬНО-ОСЕВОЙ ВЕТРОЭНЕРГЕТИЧЕСКОЙ УСТАНОВКОЙ,” *Электропитание*, no. 1, pp. 48–61, 2020.

[205] M. J. Khan and L. Mathew, “Artificial neural network-based maximum power point tracking controller for real-time hybrid renewable energy system,” *Soft Comput.*, vol. 25, no. 8, pp. 6557–6575, Apr. 2021, doi: 10.1007/s00500-021-05653-0.

[206] T. A. Kumar and P. G. V Marutheswar, “Maximum Power Point Tracking Algorithms Applied to Wind-Solar Hybrid System,” *Int. J. Adv. Res. Electr. Electron. Instrum. Eng.*, vol. 4, no. 10, pp. 8383–8394, 2015, doi: 10.15662/IJAREEIE.2015.0411096.

[207] Y. Tang, H. He, Z. Ni, J. Wen, and X. Sui, “Reactive power control of grid-connected wind farm based on adaptive dynamic programming,” *Neurocomputing*, vol. 125, pp. 125–133, 2014, doi: 10.1016/j.neucom.2012.07.046.

[208] N. Korprasertsak and T. Leephakpreeda, “Nyquist-based adaptive sampling rate for wind measurement under varying wind conditions,” *Renew. Energy*, vol. 119, pp. 290–298, Apr. 2018, doi: 10.1016/j.renene.2017.12.018.

Appendix 1: List of figures

Appendix 2: List of tables